UNIVERSITÀ DEGLI STUDI DI SIENA

DIPARTIMENTO DI BIOTECNOLOGIE, CHIMICA E FARMACIA

DOTTORATO DI RICERCA IN BIOCHIMICA E BIOLOGIA MOLECOLARE

CICLO 29°

COORDINATORE: Annalisa Santucci

Role of *Neisseria meningitidis* Adhesin A (NadA) in bacteria pathogenesis

SETTORE SCIENTIFICO-DISCIPLINARE: BIO/11

DOTTORANDO

Barbara Benucci

TUTOR AZIENDALE

Marcello Merola

Vega Masignani

TUTOR ACCADEMICO

Emanuele Montomoli

2015/2016

TABLE OF CONTENTS

1 Acknowledgments

I was carrying out my M.sc internship at Imperial College London when my supervisor told me about PhD fellowships at Novartis Vaccines. I decided to submit my application and that was the beginning of three incredible years spent in Siena as a PhD student. I conducted my research work at the Novartis Vaccines, now GlaxoSmithKline Vaccines, Research Centre, thanks to a fellowship sponsored by the University of Siena, represented by my academic supervisor Prof. Emanuele Montomoli.

This thesis is the result of a work that would have not been possible without the excellent and precious supervision of Dr. Marcello Merola, always kind and available for scientific exchange as well as life advices.

I would also acknowledge the MenB project leadership, Dr. Mariagrazia Pizza and Dr. Vega Masignani, for keeping me in track with the "biological meaning" and the "global picture" of all the data produced.

A special thanks to Dr. Xavier Nassif who hosted and carefully supervised me during my three months internship in Paris at INSERM U1151, CNRS UMR 8253, Université Paris Descartes.

Of course these years would have been much more different and harder without all the present and past PhD students of the Research Centre, people who I want to personally thank for their knowledge sharing and experimental support all over my PhD, as well as for all the crazy and happy-go-lucky moments spent together.

My gratitude also goes to all researchers, students and interns I had the chance to meet during this period and that, in different ways, have been essential to the success of this adventure.

In the end, how can I not thank all my family, scattered around Florence, Paris and Siena, for the trust in my choices and capabilities, their daily support and all the useful advices.

2 Publications achieved during the PhD

- **A first author publication** with title "Identification and characterization of Siglec 5 and Siglec 14 as receptors involved in *Neisseria meningitidis* adhesin A (NadA) binding to human monocytes" is in preparation.

- M. Scarselli, **B. Benucci**, M. Mora, L. Fagnocchi, K. L. Seib, M. Comanducci, D. Toneatto and I. Delany "*Neisseria meningitidis adhesin NadA: a key component of meningococcus B vaccine*" Review in preparation.

- M. Giuliani, E. Bartolini, B. Galli, L. Santini, **B. Benucci**, P. Lo Surdo, F. Buricchi, M. Bruttini, R. Cozzi, L. Alleri, I. Peschiera, D. Donnarumma, N. Pacchiani, W. Pansegrau, I. Ferlenghi, D. Maione, N. Norais, S. Savino, A. H. Lucas, M. Giuliani, M. Pizza, O. Finco and V. Masignani "Immunological and functional characterization of the human antibody response to Bexsero® antigens" Manuscript in preparation

- Scietti, L., K. Sampieri, I. Pinzuti, E. Bartolini, **B. Benucci**, A. Liguori, A. F. Haag, P. Lo Surdo, W. Pansegrau, V. Nardi-Dei, L. Santini, S. Arora, X. Leber, S. Rindi, S. Savino, P. Costantino, D. Maione, M. Merola, P. Speziale, M. J. Bottomley, F. Bagnoli, V. Masignani, M. Pizza, M. Scharenberg, J. M. Schlaeppi, M. Nissum, and S. Liberatori. 2016. 'Exploring host-pathogen interactions through genome wide protein microarray analysis', Sci Rep, 6: 27996.

- Calo, S., M. Cortese, C. Ciferri, L. Bruno, R. Gerrein, **B. Benucci**, G. Monda, M. Gentile, T. Kessler, Y. Uematsu, D. Maione, A. E. Lilja, A. Carfi, and M. Merola. 2016. 'The Human Cytomegalovirus UL116 Gene Encodes an Envelope Glycoprotein Forming a Complex with gH Independently from gL', J Virol, 90: 4926-38.

- Bozza, G., M. Capitani, P. Montanari, **B. Benucci**, M. Biancucci, V. Nardi-Dei, E. Caproni, R. Barrile, B. Picciani, S. Savino, B. Arico, R. Rappuoli, M. Pizza, A. Luini, M. Sallese, and M. Merola. 2014. 'Role of ARF6, Rab11 and external Hsp90 in the trafficking and recycling of recombinant-soluble Neisseria meningitidis adhesin A (rNadA) in human epithelial cells', PLoS One, 9: e110047.

3 Introduction

3.1 *N. meningitidis*, a common commensal and a deadly pathogen

3.1.1 Introduction

In 1887, Weichselbaum (Weichselbaum 1887) was the first to identify the meningococcus from the cerebrospinal fluid (CSF) of a patient with meningitis. Epidemics of meningococcal meningitis were first described during the early nineteenth century, in 1805 in Geneva, Switzerland by Vieusseux (Vieusseux 1805), in 1806 in New Bedford, Massachusetts by Danielson and Mann (Danielson 1806) and in the early 1900s in the African meningitis belt (Greenwood 1999). The meningococcus was recognized as a habitant of the nasopharynx of healthy individuals (Kiefer 1896), especially seen in the setting of military recruits camps (Glover 1918) at the beginning of the 20th century. Invasive meningococcal disease results from the interplay of:

a) Microbial factors influencing the virulence of the organism
b) Environmental conditions facilitating exposure and acquisition
c) Host susceptibility factors favouring bacterial acquisition, colonization, invasion, and survival

3.1.2 Classification

N. meningitidis is a gram-negative β proteobacterium and member of the bacterial family of *Neisseriaceae*. It is a spherical or kidney-shaped aerobic diplococcus, non-motile, non-sporulating, and usually encapsulated and piliated. Optimal growth for the bacteria occurs at 35–37 °C with 5–10% (v/v) carbon dioxide and on different media such as blood agar, trypticase soy agar, supplemented chocolate agar, and Mueller-Hinton agar. *N. meningitidis* colonies on blood agar are grayish, nonhemolytic, round, convex, smooth, moist, and glistening with a clearly defined edge. *N. meningitidis,* however, tends to undergo rapid autolysis in stationary phase.

Meningococci are classified according to serological typing (Frasch, Zollinger, and Poolman 1985; Slaterus 1961) and serogrouping is the traditional approach. Further classification into serosubtype, serotype, and immunotype is based on differences in outer membrane proteins (PorA and PorB respectively) and lipo-

oligosaccharide structure(Rosenstein et al. 2001). Based on the immunogenicity and chemical composition of the capsular polysaccharide, *N. meningitidis* strains are classified into 13 different serogroups: A, B, C, E-29, H, I, K, L, W-135, X, Y, Z, and Z' (29E) (Branham 1953).

3.1.3 Epidemiology

Meningococcal infection is a global but not uniform problem occurring as sporadic, hyper-sporadic, and epidemic disease (Fig. 1). There are an estimated 1.2 million cases of meningococcal infection per year, with a death toll of almost 135,000 worldwide. Disease patterns vary widely over time and between geographical areas, age groups, and bacterial serogroups. Most disease is caused by a few genetically defined clonal complexes of *N. meningitidis* that can emerge and spread worldwide (Maiden et al. 1998).

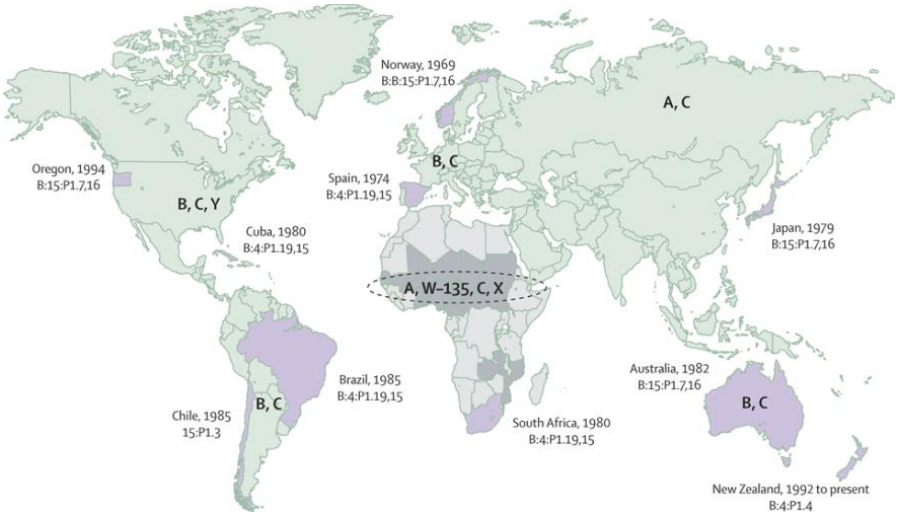

Fig. 1: Worldwide distribution of major meningococcal serogroups and of serogroup B outbreaks by serotype (shaded in purple). The meningitis belt (dotted line) of sub-Saharan Africa and other areas of substantial meningococcal disease in Africa are shown (Stephens, Greenwood, and Brandtzaeg 2007).

Most of the cases of meningococcal disease worldwide are caused by six serogroups (A, B, C, Y, W-135 and recently, in sub-Saharan Africa, X).

- *Serogroup A* has been responsible for the largest and most devastating meningococcal outbreaks in sub-Saharan Africa (Hart and Cuevas 1997). It was the cause of most meningococcal disease in the first part of the twentieth century in developed countries, but is now rare in the US and Europe
- *Serogroup B* is typically associated with a lower incidence of disease when compared to serogroup A or C, but prolonged outbreaks of serogroup B disease cause significant morbidity and mortality.

Currently, serogroup B is the most important cause of endemic disease in developed countries, causing 30–40% of disease in the US and up to 80% in Europe

- *Serogroup C* is responsible for part of the reported endemic disease and localized epidemic outbreaks in developed countries, accounting for 30% of disease in the US and Europe (Jackson et al. 1995). It has occasionally caused large epidemics
- *Serogroup Y* has emerged in the US and caused more than a quarter of the disease due to meningococci in the US in the last decade (Rosenstein et al. 1999).
- *Serogroup W-135* has emerged in the last 20 years as a cause of epidemic disease and like serogroup A previously, it has been also important especially in relationship to the Hajj pilgrimage (Dull et al. 2005).
- *Serogroup X* has recently been found responsible for meningococcal cases and outbreaks in certain African countries such as Kenya (Materu et al. 2007), Niger (Boisier et al. 2007), and Ghana (Gagneux et al. 2002).

3.1.4 Genetics of the Meningococcus

Genome sequences for a number of *N. meningitidis* strains including MC58 (serogroup B, ST-32) (Tettelin et al. 2000) Z2491 (serogroup A, ST-4) (Parkhill et al. 2000) and FAM18 (serogroup C, ST-11) (Bentley et al. 2007) have been reported. Based on these data, the chromosome is between 2.0 and 2.2 megabases in size and contains about 2,000 genes (Schoen et al. 2008). The core meningococcal genome that encodes for essential metabolic functions represents about 70% of the genome. The meningococcus shares about 90% homology at the nucleotide level with either *N. gonorrhoeae* or *N. lactamica*.

3.1.5 Capsule of the Meningococcus

N. meningitidis can be either encapsulated or not. However, *N. meningitidis* strains causing invasive disease and isolated from sterile sites such as the blood or the CSF are almost always encapsulated. The capsule is essential for the survival of the organism in the blood as it provides resistance to

antibody/complement-mediated killing and inhibits phagocytosis (Uria et al. 2008). Antibodies directed at capsule play a major part in protection against meningococcal disease and capsule forms the basis for licensed polysaccharide (Goldschneider, Gotschlich, and Artenstein 1969a, 1969b) and conjugate-polysaccharide meningococcal vaccines (Snape and Pollard 2005), with the exception of vaccines for serogroup B, and for the classification of meningococci into serogroups.

The main meningococcal capsular polysaccharides associated with invasive disease are composed of sialic acid derivatives, except for the serogroup A capsule, which consists of repeating units of N-acetyl-mannosamine-1-phosphate.

In *N. meningitidis* , N-acetylneuraminic acid (Neu5Ac), unlike in mammalian cells, is synthesized from N-acetylmannosamine (ManNAc) and phospoenolpyruvate without phosphorylated intermediates (Blacklow and Warren 1962). Neu5Ac is the most common form of sialic acid in humans and plays an important role in intercellular and/or intermolecular recognition (Varki 1997). The incorporation of Neu5Ac into meningococcal capsules allows the meningococcus to become less visible to the host immune system (Estabrook, Griffiss, and Jarvis 1997; Kahler et al. 1998) because of molecular mimicry. The most striking example is observed in the serogroup B capsule (Hobb et al. 2010), an alpha(2–8)-linked sialic acid homopolymer identical in structure to the human fetal neural cell-adhesion molecule (NCAM). Such identity is responsible for the particularly poor immune response generated against serogroup B capsule by humans (Zimmer and Stephens 2006) and drive the researcher to a different approach for the generation of a MenB vaccine.

In meningococci, capsular genes are clustered within a single chromosomal locus, cps, divided into three regions. Region A encodes enzymes for the biosynthesis and polymerization of the polysaccharide, and regions B and C carry the genes responsible for its translocation from the cytoplasm to the cell surface C (Frosch, Weisgerber, and Meyer 1989).

The capsular polysaccharides of the serogroups B, C, W-135 and Y contain sialic acid [NANA (5-N-acetylneuramic acid); tab. 1], and cps region A of these serogroups harbors a set of the conserved genes siaA, siaB and siaC. These are responsible for the synthesis of sialic acid in the form of CMP-NANA, required for incorporation into the capsular polysaccharide. The fourth gene in this region, siaD, encodes

a serogroup-specific polysialyltransferase involved in capsule polymerization. In serogroup A, the locus contains four mannosamine biosynthesis genes designated mynA–D.

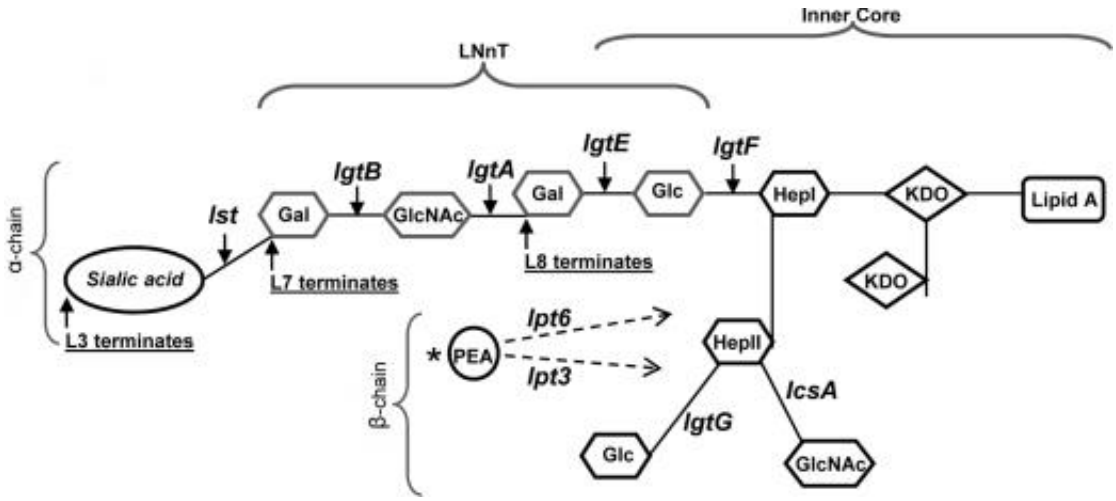

Tab. 1: Schematic diagram showing structural organization of *N. meningitidis* LPS and some important determinants of immunotypes. The membrane-located part of meningococcal LPS comprises lipid A bound to two KDO and two heptose (HepI and HepII) moieties. Extended from the membrane are the structurally variable α- and β-chains of LPS. The different immunotypes of LPS are determined by variations both in the HepI α-chain extensions (Glc, Gal, GlcNAc, Gal and sialic acid) and the HepII β-chain extensions (GlcNAc, PEA and Glc). These arise as a result of phase variation in a number of genes shown and account for the antigenic variation of meningococcal LPS. PEA may be added at position 3 or 6 on HepII by two distinct enzymes encoded by lpt3 and lpt6. The α-chain structures of the L3, L7 and L8 immunotypes are indicated. LNnT and silaylation: the immunotypes L7/L9, L2/L4/L5 contain identical α-chains terminating in LNnT (Gal-GlcNAc-Gal-Glc structure bound to HepI) which can be sialylated. The L7 immunotype, found in serogroup B and C isolates, refers to the immunotype lacking sialic acid, whereas L3 is sialylated. Phase variation of the lgtA gene gives rise to the immunotype L8, which cannot be sialylated (Hill et al. 2010).

3.1.6 Cell Envelope

In gram-negative bacteria, such as *N. meningitidis,* the subcapsular cell envelope consists of an outer membrane (OM), a peptidoglycan layer, and a cytoplasmic or inner membrane (Fig. 2). The OM has an outside layer primarily composed of lipopolysaccharide (LPS), actually a lipooligosaccharide, and proteins and an inside layer composed of phospholipids (Nikaido 1999) that contains proteins primarily responsible for regulating the flow of nutrients and metabolic products. The major phospholipid component of Neisseria membranes consists largely of phosphatidylethanolamine (PE), with varying amounts of phosphatidylglycerol (PG), cardiolipin (CL), and phosphatidate (PA)(Rahman et al. 2000).

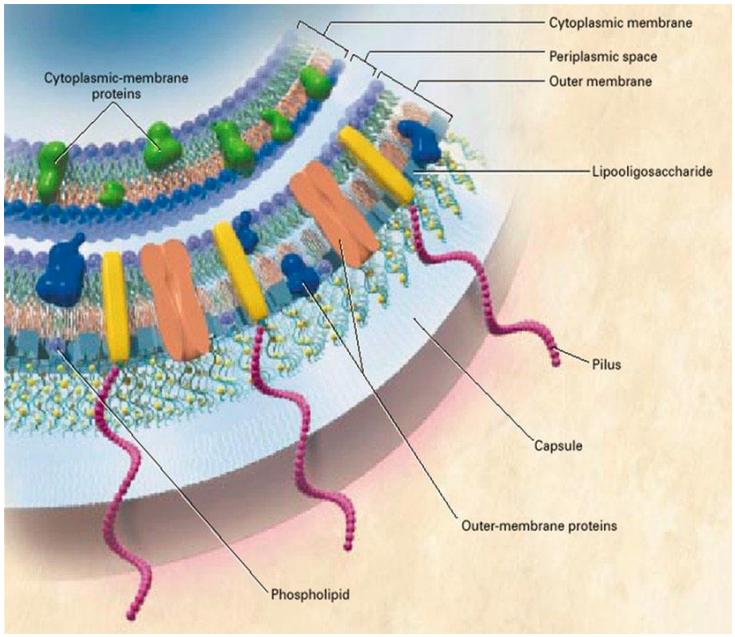

Fig. 2: Cross-sectional view of the meningococcal cell membrane.

3.1.7 Lipopolysaccharide

Meningococcal LPS [also referred to as LOS (lipo-oligosaccharide)] plays a role in the adherence of the meningococcus (Kahler and Stephens 1998) and in activation of the innate immune system (Plant et al. 2006). It comprises an inner and outer oligosaccharide core attached to lipid A. The inner core of meningococcal LPS consists of the diheptose (HepI and HepII) attached to lipid A, via one of the two KDOs (2-keto-3-deoxy-d-manno-2-octulosonic acids). The outer core is heterogeneous, composed of variable numbers of sugars extending from HepI, added by glycosyltransferases encoded by lgt genes (Stephens, Greenwood, and Brandtzaeg 2007).

3.1.8 Adhesins

N. meningitidis strains express a number of surface and secreted proteins that bind to human molecules. Such proteins include, among others, lactoferrin- and transferrin-binding proteins that enable meningococci to acquire iron, a crucial growth factor during colonization and disease.

Neisserial porins, whilst not considered adhesins, interact with numerous human cells and proteins. The *in vitro* defined properties of porins could have implications in pathogenesis and generation of an effective immune response. *N. meningitidis* expresses two distinct porins, PorA (formerly class 1 protein) and PorB (formerly class 2/3 protein). Both porins are β-barrel proteins, which associate as trimers in the bacterial outer membrane through which small hydrophilic nutrients diffuse into the cell. Individual porin vary in molecular mass with PorA (~46 kDa) being expressed in all strains of meningococci with different level of expression regulated via an SSM mechanism. PorB is expressed as one of two mutually exclusive forms: PorB2 (~41kDa) or PorB3 (~38kDa).

Meningococcal adhesins, that enable bacteria to localize on specific host cells, can be divided into major and minor groups. The major adhesins, pili and the opacity proteins, are expressed in abundance on the bacterial surface and have been studied for a considerable period. Genome sequencing has led to the discovery of several other adhesins, which are expressed normally at low levels in vitro; these may be up-regulated *in vivo*, but their potential roles in pathogenesis remain to be fully defined. *In vitro*, several meningococcal adhesive structures have also been shown to lead to cellular entry and can therefore also act as invasins (Hill et al. 2010).

3.1.8.1 Major Adhesins

3.1.8.1.1 Pili

The adhesive properties of capsulate *N. meningitidis* are mediated by pili (Pinner, Spellman, and Stephens 1991), which are long filamentous appendages extending from the bacterial cell surface (Craig et al. 2006). Meningococcal pili belong to the type 4 pilus family, twitching motility generated by pilus retraction is important for passage through the epithelial mucus layer, movement over epithelial surfaces, and microcolonies formation (Merz and So 2000). Piliated meningococci attach to human nasopharyngeal cells (Stephens and McGee 1981) in greater numbers when compared to meningococci devoid of pili. In addition, pili are involved in facilitating the uptake of DNA by meningococci (Proft and Baker 2009) and also enable adherence to endothelial cells and erythrocytes.

Tfp are composed of hetero-multimeric pilin subunits, which are assembled into helical fibers (Craig et al. 2006). PilE, the major pilin subunit, constitutes the fiber scaffold and is a source of antigenic variation. This variation is generated through recombination between the silent loci, designated pilS, and the corresponding portion of the pilE gene (Coureuil et al. 2014). In addition to the major pilin subunit, the pilus fiber contains three other pilin-like proteins known as the minor pilins, designated as ComP, PilV, and PilX, which mediate specific Tfp-dependent functions (Coureuil et al. 2014).

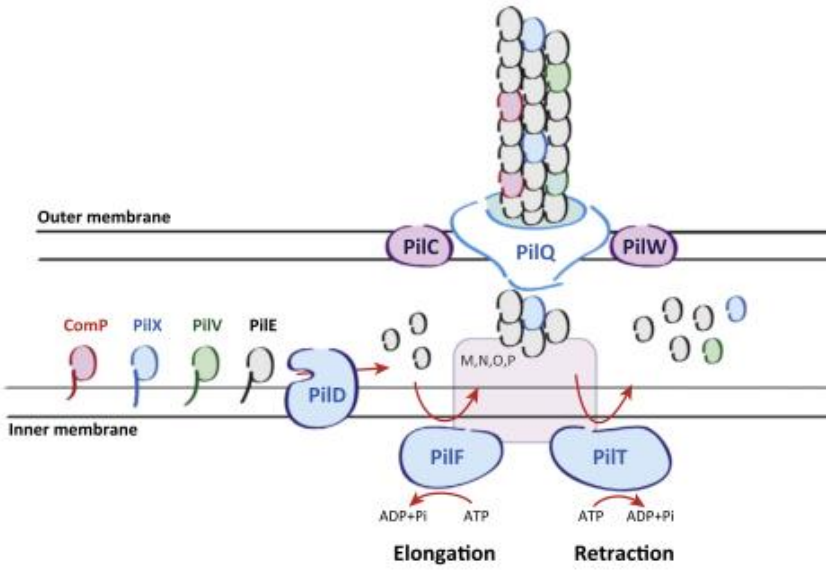

Fig. 3: *Neisseria meningitidis* type IV pilus assembly. The major pilin PilE and the three minor pilins PilX, PilV, and ComP are assembled from a platform complex (comprising PilD, PilF, PilM, PilN, PilO, and PilP) and translocated to the cell surface through a pore formed by the PilQ secretin. The ATPase PilF promotes pilus elongation whereas the ATPase PilT is responsible for pilus retraction via depolymerization of type IV pili (Tfp). PilC proteins (PilC1 and PilC2) are located in the outer membrane where they control pilus retraction. PilC1 is also involved in adhesion to host cells. PilW is an outer membrane protein that is necessary for PilQ stability. (Coureuil et al. 2014)

PilE and PilV are involved in adhesion to host cells and recently shown to activate β2-adrenergic receptor (β2-AR), promoting the endothelial signaling events enabling Neisseria translocation through the brain endothelium (Coureuil and Marullo 2011; Lecuyer, Nassif, and Coureuil 2012). The mechanism of Type IV pili adhesion has been further elucidated by Bernard *et al*. who identified CD147, a member of the immunoglobulin (Ig) superfamily, as receptor for PilE and PilV-mediated adhesion to human brain or peripheral endothelial cells and shown the role of CD147 in vascular colonization by meningococci (Bernard et al. 2014). Tfp promote not only the initial adhesion onto endothelial cells but also the formation of aggregates, which prevents the detachment of bacteria from the colony. The formation of these aggregates is under the control of PilX, a minor pilin component, which connects the pilus fibers of adjacent bacteria. Finally, the cytoplasmic PilT protein controls pilus retraction, a phenomenon that produces a form of movement known as 'twitching motility'. This mechanism enables bacteria to spread over the surface of host cells and form microcolonies. Proliferation of *N. meningitidis* in contact with host cells increases the production of a transferase that adds a phosphoglycerol to the major pilin PilE. This

unusual post-translational modification specifically releases Tfp-dependent contacts between bacteria, favouring their detachment from the colony and bacterial dissemination, a phenomenon that can be reproduced experimentally when bacteria are grown under a liquid flow (Coureuil et al. 2014).

3.1.8.1.2 Opacity proteins

N. meningitidis strains commonly express two types of OM opacity proteins, Opa and Opc, which impart an opaque phenotype to agar-grown colonies. While Opc is only expressed by *N. meningitidis* and encoded by a single gene, Opa proteins are expressed by both meningococci and gonococci, and encoded by multiple genes. Opa and Opc are similar in size (27–31 kDa) and were initially known as Class 5 proteins. Structurally, the Opa proteins are made up of eight transmembrane domains arranged in a β-barrel and presenting four surface-exposed loops. The β-barrel constitutes a highly conserved region of these proteins, whereas three of the four surface loops are variable between different Opa proteins. No crystal structure has been determined for the Opa proteins, but structurally they resemble Neisserial surface protein A. Opa expression is subject to antigenic and phase variation and certain Opa types may predominate in clinical isolates due to their adhesion/virulence properties (Callaghan, Jolley, and Maiden 2006). Opa interacts with multiple members of the CEACAM (carcinoembryonic antigen-related cell-adhesion molecule) family (Virji et al. 1996); during inflammation high levels of CEACAM are expressed, facilitating Opa interactions and therefore cellular attachment and invasion. Both Opa and Opc (Virji et al. 1992) also interact with cell-surface associated HSPGs (heparan sulfate proteoglycans) (Virji et al. 1999).

3.1.8.2 Minor Adhesins

Although Pili, OpC, and Opa represent the most important and the most studied adhesins of meningococcus, additional antigens have been described as having a role in adhesion. Minor adhesins are molecules that are often expressed at low levels *in vitro*, but may be upregulated *in vivo*, and whose potential roles in pathogenesis are not fully defined. Examples of minor adhesins include: NadA (*Neisseria*

meningitidis adhesin A), NhhA (*Neisseria meningitidis* hia/hsf homologue A), App (adhesion and penetration protein) and MspA (meningococcal serine protease A).

3.2 *Neisseria meningitidis* pathogenesis: a multi-step infection

Neisseria meningitidis is a Gram-negative diplococcus considered as an asymptomatic colonizer of the upper respiratory tract in 8-20% of human population. However, under certain conditions, it can become invasive by crossing the mucosal barrier, entering into the bloodstream and disseminating to different organs. Systemic spreading of Nm may eventually lead to rapidly-progressing sepsis or severe meningitidis.

3.2.1 Crossing of the oropharyngeal barrier

Colonization of the upper respiratory mucosal surfaces by *N. meningitidis* is the first step in establishment of a human carrier state and invasive meningococcal disease. Meningococcal transmission among humans occurs largely through respiratory droplets and secretions, but the inoculum size needed for transmission is unknown. Meningococcal disease usually occurs 1–14 days after acquisition of the pathogen and the duration of carriage can vary from days to months (Hill et al. 2010).

The human nasopharyngeal mucosa represents also the first line of organism defence against this bacterium (Trivedi, Tang, and Exley 2011). This physiological barrier consists of highly polarized epithelial cells, characterized by distinct apical and basolateral plasma membrane domains and specialized intracellular trafficking machinery which delivers proteins and lipids to their proper destination (Gibson et al. 1998; Folsch 2008). This peculiar architecture contributes to the preservation of important body nutrients and to the secretion of antimicrobial compounds. Recent studies have postulated that mucosal pathogens may manipulate the host cell machinery to favour acquisition of nutrients, evasion from the immune response and permanence in their preferential niche (Kazmierczak, Mostov, and Engel 2001).

During meningococcal infection Nm is found capable not only to establish an intimate association with the host cell surface, but to invade cells and to eventually localize within intracellular vacuoles (Criss and Seifert 2012; Read et al. 1995; Pujol et al. 1997). In particular, Lécuyer and Sutherland have demonstrated

that Nm crosses the epithelial barrier by an intracellular route that requires a functional microtubular cytoskeleton and occurs without damage of the tight junctions (TJs) (Lecuyer, Nassif, and Coureuil 2012; Sutherland et al. 2010). In addition, Barrile *et al.* suggested that, by reprogramming the host-cell trafficking system, Nm is be able to traverse the cellular monolayer without affecting the epithelial integrity (Barrile et al. 2015).

3.2.2 Interaction with the human immune system

The immune system protects humans from attack by microorganisms such as bacteria, viruses, protozoa, fungi, parasites, and organisms such as helminths. The immune system is very complex and its defensive response is subdivided into innate and adaptive responses. The innate response triggers an immediate, nonspecific, general action and is activated by typical signs of infection. The adaptive response is able to develop a highly specific, extremely accurate action, which is stored in the so-called immune memory (Medzhitov and Janeway 2000).

3.2.2.1 Innate immune system

The complement system plays a major role in innate immune defence against meningococcal disease and subjects with terminal complement deficiencies are more susceptible to invasive meningococcal disease (Figueroa and Densen 1991). There are three main complement pathways: the classical pathway (CP) which is mediated by the binding of the C1 component to the antigen–antibody complex; the lectin pathway which recognizes specific microbial patterns composed of saccharides and related molecules and the alternative pathway (AP) which is mediated by the binding to C3 (Lewis and Ram 2014).

The three pathways involve the cleavage of C3, the central component of the complement cascade. C3b activation allows to reach three goals (Pangburn, Ferreira, and Cortes 2008):

1. Processing antigen, for adaptive cellular and humoral immunity
2. C5b-9 activation, for disruption of bacterium membrane
3. Phagocytosis, for pathogen killing

Thanks to several mechanisms, *N. meningitidis* can escape from the complement system. One of these is its molecular mimicry of human structures (for instance, the meningococcus B polysaccharide capsule is constituted by poly-sialic acid, which is present in many mammalian organs during development), in this way correspondent antibodies do not can be produced and the classical pathway do not can be activated (Finne, Leinonen, and Makela 1983). The capsule is the most important bacterial structure in the prevention of bacterium lysis, mediated by the complement system and by phagocytosis. Further, *N. meningitidis* secerns a lot of blebs, containing outer membrane components, lipopolysaccharide included. In this way the microorganism can steer away from its self the defensive mechanisms, including the complement system (Schneider et al. 2007). In addition, *N. meningitidis* expresses several surface proteins (in particular the factor H binding protein) that capture the factor H, and consequently can block the alternative pathway activation.

In the bloodstream *N. meningitidis* stimulates cytokine release from phagocytic, lymphocytic and endothelial cells. One of the consequences of this release is the damage that leads to clinical symptoms, and, particularly to petechial rash.

3.2.2.2 Adaptive immune system

Antibodies are key effectors in protecting against invasive meningococcal infection. Goldshneider *et al*. demonstrated that age disease incidence was inversely proportional to the prevalence of bactericidal antibodies in the sera (Goldschneider, Gotschlich, and Artenstein 1969a).

Cytokine activation is another important event in the pathogenesis of meningococcal disease (Casey 2000), and has considerable bearing on the clinical course. A fine balance must be achieved, because under activation will result in an inadequate immune response, whereas over activation can be extremely destructive. During the acute phase of meningococcal infection, greatly raised plasma concentrations of tumour necrosis factor α (TNF-α), IL-1, IL-6, and IL-10 can be demonstrated (Waage et al. 1989; Riordan et al. 1996; van Deuren, Brandtzaeg, and van der Meer 2000). Furthermore, cytokine values can be related to clinical severity: high concentrations of TNF-α and IL-6 in severe sepsis are associated with an increased risk of mortality, as are high concentrations of IL-10 (Waage et al. 1989; Riordan et al. 1996; Casey, Balk, and Bone 1993).

3.2.3 N. meningitidis at the blood-brain barrier

N. meningitidis specific interaction with human endothelia enables bacterial access to secondary anatomical sites (meninges, skin, etc), which promote much of the morbidity and mortality associated with neisserial infections (meningitis and thrombotic lesions, respectively). To mediate association with endothelial cells underlying the blood-brain barrier (BBB) and blood-cerebrospinal fluid barrier (BCSFB), meningococci express a variety of adhesins and invasins (Hung and Christodoulides 2013).

The initial binding of fully encapsulated meningococccci to brain endothelial cells is facilitated primarily by type IV pili. Though the outer membrane proteins (Opa and Opc) are partially masked by the polysaccharide capsule, they also efficiently support adhesion and invasion to eukaryotic cells especially on cells of high receptor density (Bradley et al. 2005).

Although studies have shown that pilus expression is crucial for the initial adhesion of pathogenic strains to endothelial cells, the endothelial receptor active in this process has been unclear and a subject of controversial discussion for many years. CD46, an inhibitory complement receptor, was proposed as a host cell receptor for TfP (Kallstrom et al. 1997), whereas other research groups could not reproduce the findings of reduced adhesion/invasion in response to CD46 inhibition. Moreover, analysis of several cell lines with different levels of CD46 expression demonstrated no significant difference in the extent of adhesion of piliated *Neisseriae*, indicating that CD46 is not essential for bacterial adherence and invasion (Kirchner, Heuer, and Meyer 2005; Tobiason and Seifert 2001). Novel data published in recent years has shed new light on possible pilus receptors on brain endothelial cells. Bernard *et al*. showed that *N. meningitidis uses* CD147, (also known as Basigin, or extracellular matrix metalloproteinase inducer), a member of the immunoglobulin superfamily, for pilus dependent adhesion to endothelial cells (Bernard et al. 2014). Interestingly, other pathogens also use this receptor. Earlier studies have shown that CD147 is an essential receptor in infection of erythrocytes by *Plasmodium falciparum*, a causative agent of malaria worldwide (Crosnier et al. 2011). TfP-mediated adhesion to CD147 was shown to involve both PilE and the minor pilin PilV and interference with pilus/CD147 interactions blocked the binding of meningococci to human endothelial cells *in vitro* and, importantly, also prevented colonisation of vessels in human brain tissue explants *ex vivo*. Moreover, *in vivo* PilE- and PilV dependent colonisation of endothelial vessels by *N. meningitidis* was investigated using a mouse model grafted with human skin (Bernard et al. 2014). After

initial binding of *N. meningitidis* to the cell surface, the bacteria start to proliferate and form small aggregates, also known as microcolonies. The formation of microcolonies promotes the development of specific molecular complexes, so-called 'cortical plaques', which are structures containing an accumulation of ezrin, moesin, tyrosine-phosphorylated proteins, ICAM-1/-2, CD44, and epidermal growth factor receptors (EGFR), as well as localised polymerisation of cortical actin underneath the microcolonies resulting in microvilli-like cellular projections which penetrate bacterial colonies and thereby confer resistance to the shear stress elicited by the blood stream (Merz, Enns, and So 1999; Eugene et al. 2002).

In addition, Coureuil *et al*. provided evidence that *N. meningitidis* infection stimulates the β2-adrenoceptor/β-arrestin signalling pathway in endothelial cells. Interaction of PilE and PilV with the β2-adrenoceptor induces activation of the β-arrestin pathway. Amongst others, β-arrestin activates the Src-pathway that mediates the formation of actin-rich cellular protrusions and induces the delocalization of junctional proteins. As result, anatomical gaps are formed and used by bacteria to penetrate into tissues (Coureuil et al. 2010). Interestingly, the activation of the β2-adrenoceptor/β-arrestin pathway by *N. meningitidis* is indeed restricted to endothelial cell lines, and no alteration of the cell-cell junctions can be seen in epithelial monolayers following meningococcal type IV pilus-mediated colonization (Lecuyer, Nassif, and Coureuil 2012).

3.3 4CMenB (Bexsero®) vaccine

Despite successful production of multivalent conjugate vaccines for serogroups A, C, W-135 and Y, MenB has remained an elusive target for immunisation. This is due to the structural homology of the B polysaccharide to the polysialylated form of the neural cell adhesion molecule (PSA-NCAM). Antibodies capable of binding to B polysaccharide could theoretically lead to autoimmunity directed against the PSA-NCAM or cross the placenta and adversely affect the neurological development of the fetus (Finne, Leinonen, and Makela 1983)

To overcome this problem Pizza *et al.* implemented the concept of reverse vaccinology by using the complete genome sequence of a virulent *N. meningitidis* serogroup B strain as input to identify putative vaccine candidates followed by a process of elimination to find those which would be successful in a

vaccine (Pizza et al. 2000). Briefly, from the complete genome of *Neisseria meningitidis* pathogen strain MC58, the authors identified 570 open reading frames using computer algorithms, which encoded potentially novel surface-exposed or exported proteins. Next, by using the polymerase chain reaction, these DNA sequences were amplified and cloned into *Escherichia coli* bacteria. A total of 350 recombinant proteins were successfully expressed, purified and used to immunize mice. The immune sera were then analysed to verify that the novel antigens were expressed on the surface of cells; this resulted in confirmation of 91 surface-exposed proteins. The sera were also tested for the bactericidal activity. Almost one-third (28 proteins) demonstrated the ability to kill the MenB bacteria and 7 of them showed conservation across multiple different MenB strains. This means that they would be expected to be effective against many different types of MenB, including those which have not yet caused epidemics.

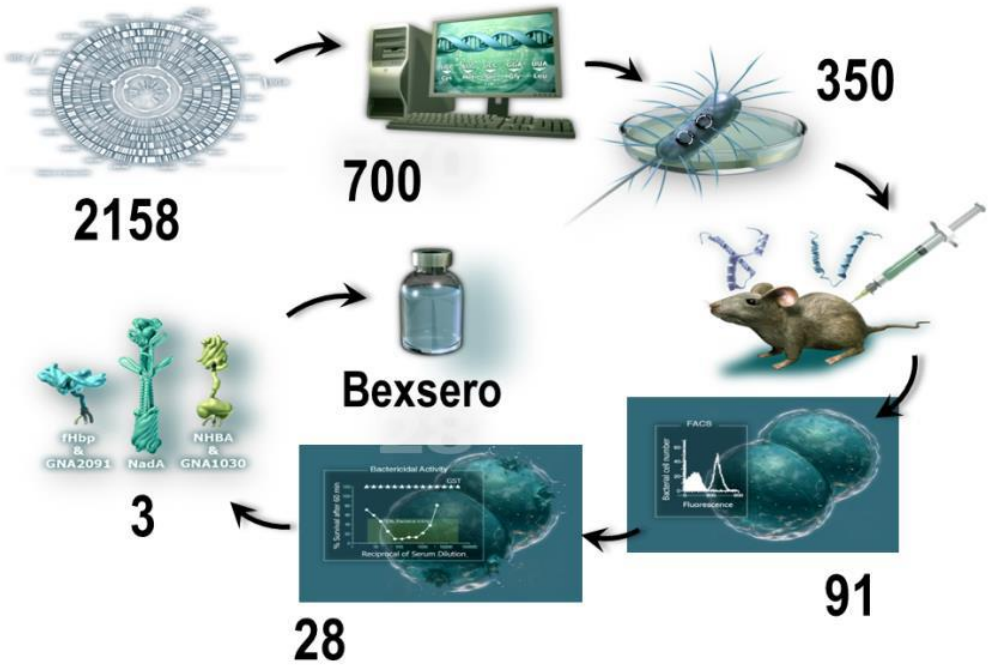

Fig. 4: Schematic representation of reverse vaccinology applied to Bexsero®

On 14 January 2013 the European Medicines Agency approved Bexsero®, the first recombinant vaccine against MenB.

The final vaccine is made of 4 components, which were selected so that between them they would provide a broad coverage of MenB strains. These are:

- *Factor H binding protein (fHbp)* fused with GNA2091 protein – A major function of fHbp is to protect the meningococcus from complement by binding factor H, a negative regulator of the complement cascade. Its inclusion in the vaccine means that complement can be activated leaving meningococcal bacteria vulnerable to bactericidal activity (Bai, Findlow, and Borrow 2011; Seib et al. 2009)

- *Neisseria meningitidis adhesin A (NadA)* – see next paragraph

- *Neisseria heparin binding antigen (NHBA)* fused with protein GNA1030 – NHBA can protect the meningococcus from complement by binding heparin to the cell surface. Heparin binding is an indicator of virulence in many bacteria. NHBA induces serum bactericidal activity in humans. Anti-NHBA antibodies may also act synergistically with antibodies to other meningococcal antigens (Bai, Findlow, and Borrow 2011; Su and Snape 2011; Serruto et al. 2010)

- Outer Membrane Vesicles (OMVs) NZ98/254 – PorA1.4 is the immunodominant portion of OMV NZ98/254, a tailor-made OMV successfully used as vaccine against a MenB epidemic in New Zealand in 2004. Although PorA is strain-specific, it has been shown to provide increased immunogenicity when combined with the other components of the vaccine (Su and Snape 2011; Bai, Findlow, and Borrow 2011; Vernikos and Medini 2014)

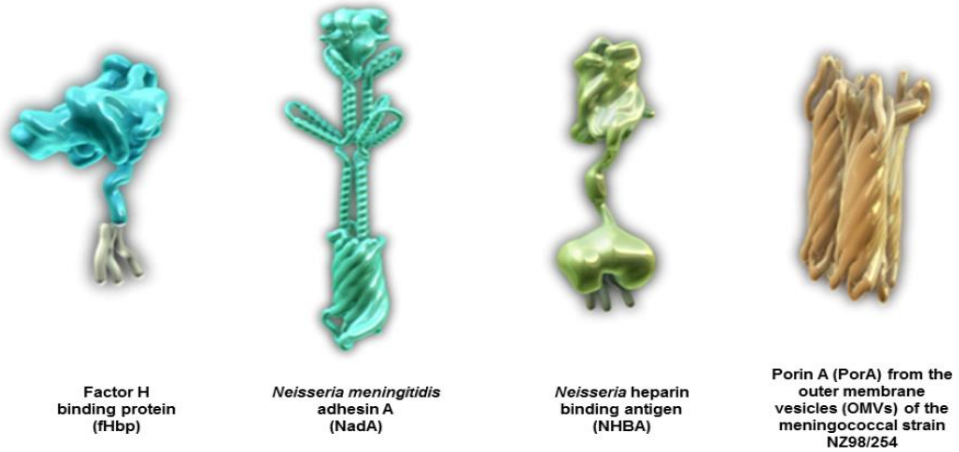

Fig. 5: Major component of Bexsero®: fHbp, NadA, NHBA and PorA

3.4 Neisseria meningitidis adhesin A (NadA)

3.4.1 Characteristics

Neisseria meningitidis adhesin A (NadA) is one of the antigenic components of Bexsero®, the first vaccine for the prevention of invasive meningococcal disease caused by serogroup B strains (Giuliani et al. 2006).

The *nadA* gene is present in ~30% of *N. meningitidis* major disease-associated strains and is associated mostly with strains belonging to 3 out of the 4 hypervirulent lineages (Bambini et al. 2014; Comanducci et al. 2002; Comanducci et al. 2004). NadA can be classified in two groups based on the sequence diversity: group I comprising protein variants 1, 2 and 3 (vaccine variant), that are frequently associated to pathogenic strains and highly cross-protective (Bambini et al. 2014; Bambini et al. 2009), and group II, including variants 4, 5 and 6, that are predominantly found in carrier isolates (Comanducci et al. 2004; Lucidarme et al. 2010).

Structurally, NadA belongs to the group of trimeric autotransporters and is composed of a C-terminal β-barrel that anchors the protein to the bacterial membrane, a long coiled-coil stalk domain with three protruding wing-like structures that create an unusual N-terminal globular head domain (Malito et al. 2014). NadA expression levels vary among isolates by more than 100-fold, and are induced by appropriate niche-specific signals during colonization and infection via the transcriptional regulator NadR, which binds the nadA promoter and represses transcription. DNA-binding activity of NadR is attenuated by 4-hydroxyphenylacetic acid (4-HPA), a natural molecule released in human saliva, thus leading to the de-repression of *nadA in vivo* (Fagnocchi et al. 2013; Metruccio et al. 2009).

Preclinical and clinical studies have shown its ability to induce a protective immune response in humans due to the production of neutralizing bactericidal antibodies (Bowe et al. 2004; Ciabattini et al. 2008; Litt et al. 2004).

3.4.2 Biological relevance in the pathophysiology of N. meningitidis

NadA has been found to adhere to many cell types. Several works (Capecchi et al. 2005; Montanari et al. 2012) have shown that NadA promotes adhesion to and invasion into Chang epithelial cells. Furthermore, its binding to human monocytes leads to the production of pro-inflammatory cytokines and chemotactic factors, as well as inhibition of apoptosis leading to macrophages differentiation (Franzoso et al. 2008). Recently, our group suggested an additional role at the host peripheral microvasculature and at the brain blood barrier (BBB) through the identification of a NadA putative receptor whose expression is restricted to endothelial cells (Scietti et al. 2016).

All considered, NadA is able to interact with all three cell types involved in the bacterium cycle of infection suggesting a crucial role during *Neisseria meningitidis* infections.

3.5 Sialic acid-binding immunoglobulin-type lectins

Sialic acid-binding immunoglobulin-type lectins (Siglecs) were discovered through converging studies on sialoadhesin (also known as Siglec 1 and CD169) and CD22 (also known as Siglec 2). Sialoadhesin was initially defined as a macrophage adhesion receptor recognizing sialic acids and was then shown to be a member of the immunoglobulin (Ig) superfamily, whereas CD22 was characterized as a B cell inhibitory receptor of the Ig superfamily that was later shown to recognize sialic acids (Crocker et al. 1994; Sgroi et al. 1993). The homology of these proteins with CD33 (also known as Siglec 3) and myelin-associated glycoprotein (MAG; also known as Siglec 4) led to the establishment of the Siglec family; to date, fifteen Siglecs have been identified in humans.

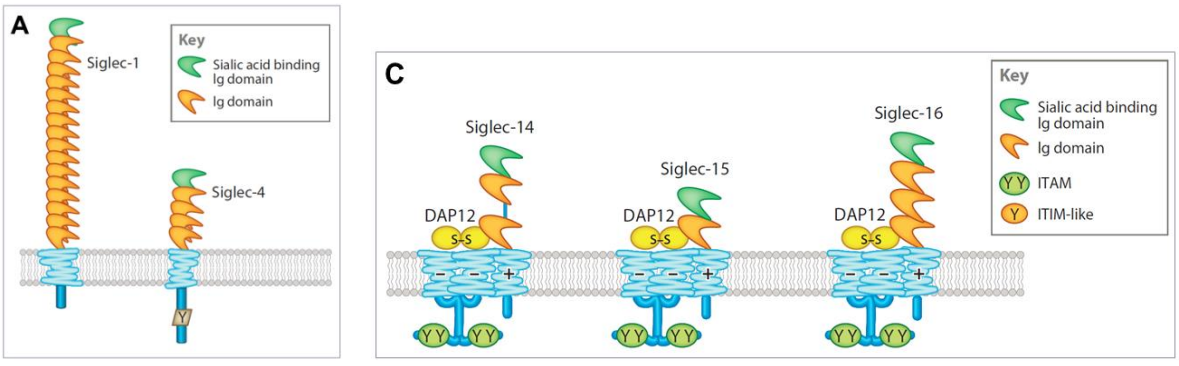

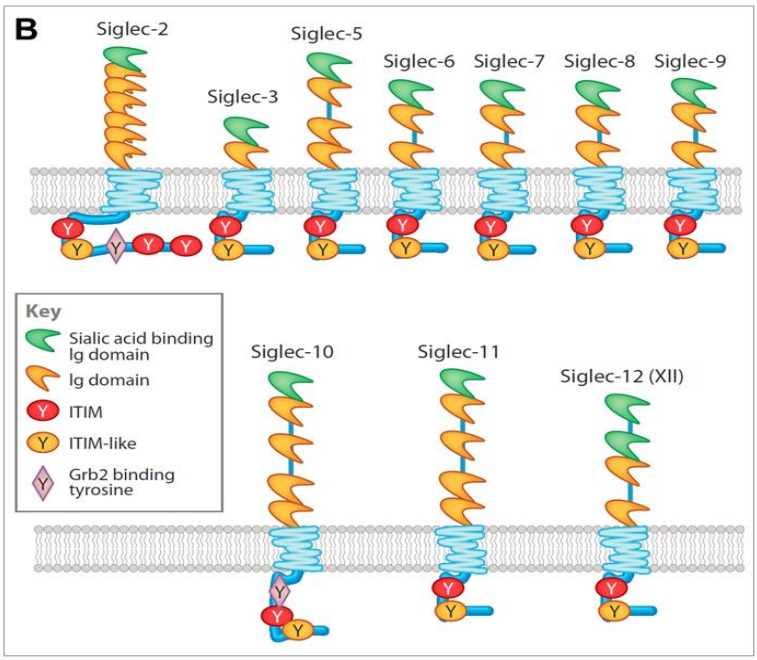

Fig. 6: Schematic representation of Sialic acid-binding immunoglobulin-type lectins (Siglecs):
(a) Siglecs that lack defined cytoplasmic tail signaling motifs or a charged transmembrane residue. The cytoplasmic tail of Siglec 4 has a tyrosine residue (Y) that does not fit into any known consensus for signaling
(b) Siglecs that contain ITIM motifs in their cytoplasmic tails. Siglec-12 is referred to as Siglec-XII in humans by convention because the in-frame human form lacks the crucial arginine for sialic acid recognition (but the arginine is present in other primates)
(c) Siglecs that contain a transmembrane lysine (+). Siglec-15 is shown associated with DAP12; it can also associate with DAP10. (Pillai et al. 2012)

Siglecs can be divided into two groups: those that are conserved across mammals — such as sialoadhesin, CD22, MAG and Siglec 15 — and a group of CD33-related Siglecs that are variable across mammals. The CD33-related Siglecs are thought to have expanded from a primordial cluster of SIGLEC genes that underwent an inverse duplication event more than 180 million years ago (Cao et al. 2009). Similar to many other members of the Ig superfamily, Siglecs are cell-surface Type I transmembrane receptors that are comprised of 2–17 extracellular Ig domains, including an amino-terminal V-type immunoglobulin domain that contains the sialic acid-binding site (Crocker, Paulson, and Varki 2007).

Siglecs may also be categorized into three groups based on features of the transmembrane and cytoplasmic tails of individual Siglecs that likely reflect the major mechanisms by which they mediate their biological functions:

- The first group is made up of Siglec 1 and Siglec 4, lectins that possess neutral transmembrane domains
- The second group of Siglecs is the largest and includes members that contain immunoreceptor tyrosine-based inhibitory motifs (ITIMs) or ITIM-like motif in their cytoplasmic tails
- The third category of Siglecs contains members with a positively charged residue in the transmembrane anchor region that acts as docking station for adaptors protein such as a disulfide-

linked homodimer of DAP12 (DNAX-associated protein of 12 kDa), which contains an aspartate transmembrane residue and a cytosolic immunoreceptor tyrosine-based activation motif (ITAM) motif

The mammalian glycome contains numerous sialylated glycans that can be potentially recognized as ligands by Siglecs. It is assumed that this recognition is important for modulating the functions of Siglecs as regulators of adhesion, cell signalling and endocytosis (Crocker and Varki 2001; Crocker 2002; Varki and Angata 2006). In general, Siglecs show low affinity (a Kd of 0.1–3 mM) for the sialic acid N-acetylneuraminic acid (Neu5Ac) alpha2–3 and alpha2–6 linkages to galactose (Neu5Acalpha2–3Gal and Neu5Acalpha2–6Gal) that are commonly found as terminal sequences on glycans of glycoproteins and glycolipids of most mammalian cells (Blixt et al. 2003). However, as revealed by a variety of methods, including glycan array analyses (Crocker, Paulson, and Varki 2007), each Siglec has a distinct preference for binding the diverse types of sialylated glycans (Tab. 2).

Siglec* (other names)	Expression pattern	Structure			Sialoside preference‡	Disease relevance§	Refs
		Number of Ig domains	Tyrosine motifs	DAP12 binding			
Human and mouse sialoadhesin (Siglec-1; CD169)	Macrophages (tissue subsets) and activated monocytes	17	None	No		Autoimmunity and infections including HIV-1, PRRSV, *C. jejuni* and GBS	3,34,35,44,45,137,138
Human and mouse CD22 (Siglec-2)	B cells	7	ITIM, ITIM-like and GRB2	No	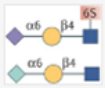	Lymphoma, leukaemia, SLE and rheumatoid arthritis	3,93
Human CD33 (Siglec-3)	Myeloid progenitors, macrophages, monocytes, microglia and granulocytes	2	ITIM and ITIM-like	No	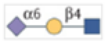	Acute myeloid leukaemia and Alzheimer's disease	3,74,75,76,79,80,82,137,138
Mouse CD33 (Siglec-3)	Macrophages and granulocytes	2	ITIM-like	Unknown	Not determined	Alzheimer's disease	74
Human and mouse MAG (Siglec-4)	Oligodendrocytes and Schwann cells	5	FYN kinase site	No		Neurodegeneration	137,138
Human Siglec-5	Neutrophils, monocytes and B cells	4	ITIM and ITIM-like	No	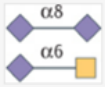	GBS infection	3,5,137,139
Human Siglec-6	Trophoblasts and B cells	3	ITIM and ITIM-like	No		Pre-eclampsia	3,138,140

Human Siglec-7	NK cells, monocytes and mast cells	3	ITIM and ITIM-like	No		Cancer and *C. jejuni* infection	3,42
Human Siglec-8	Eosinophils, mast cells and basophils	3	ITIM and ITIM-like	No		Eosinophilia and asthma	3
Mouse Siglec-F (paralogue of human Siglec-8)	Eosinophils, alveolar macrophages and activated microglia	4	ITIM and ITIM-like	No	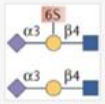	Eosinophilia	66,141
Human Siglec-9	Neutrophils, monocytes, DCs and NK cells	3	ITIM and ITIM-like	No	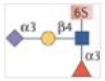	Chronic lung inflammation	3
Mouse Siglec-E (functional orthologue of human Siglec-9)	Neutrophils, monocytes, macrophages and DCs	3	ITIM and ITIM-like	No	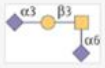	Acute lung injury and neuroinflammation	3,70,78
Human Siglec-10	B cells, monocytes and eosinophils	5	ITIM, ITIM-like and GRB2	No	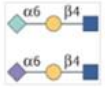	Lymphoma, leukaemia, eosinophilia and allergy	3,137,142
Mouse Siglec-G (orthologue of human Siglec-10)	B cells and myeloid DCs	5	ITIM, ITIM-like and GRB2	No	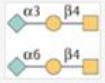	Tissue damage, sepsis, graft-versus-host disease and autoimmunity	33,40,41,86,97,143
Human Siglec-11	Macrophages and microglia	5	ITIM and ITIM-like	No		Neuroinflammation	77,78
Human Siglec-14	Neutrophils and monocytes	3	None	Yes	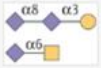	GBS infection and COPD	5,139
Human and mouse Siglec-15	Osteoclasts, macrophages and DCs	2	None‖	Yes		Osteopetrosis	131
Human Siglec-16	Macrophages and microglia	5	None	Yes		Unknown	8

C. jejuni, *Campylobacter jejuni*; COPD, chronic obstructive pulmonary disease, DC, dendritic cell; GBS, group B *Streptococcus*; GRB2, growth factor receptor-bound protein 2; Ig, immunoglobulin; ITIM, immunoreceptor tyrosine-based inhibitory motif; MAG, myelin-associated glycoprotein; NK, natural killer; PRRSV, porcine reproductive and respiratory syndrome virus; SLE, systemic lupus erythematosus.

*Two additional Siglec genes and proteins are found in chimpanzees that are either only expressed in some humans in a form that does not bind sialic acids (in the case of Siglec-12) or they have been deleted from the human genome (in the case of Siglec-13)[147, 148].

‡Specificities are summarized from the cited references or from glycan array data on the Functional Glycomics Gateway website. Sialoside structures are shown in diagrammatical form showing linkages (indicated by αX and βX, where X is number) between the following residues: *N*-acetylneuraminic acid (purple diamond), *N*-glycolyl-neuraminic acid (light blue diamond), galactose (yellow circle), *N*-acetylgalactosamine (yellow square), *N*-acetylglucosamine (dark blue square), fucose (red triangle). Sulphation is indicated by 'S'.

§Disease relevance is based on animal models or expression on cell types that are involved in disease processes. Additional references for disease relevance are cited in the main text.

‖Conserved tyrosine of unknown function.

Tab. 2: Summary of structural and functional properties of the Siglec family
(Macauley, Crocker, and Paulson 2014)

The local concentration of sialic acids on surfaces of immune cells is very high. As a consequence of this, Siglec binding sites are typically 'masked' by *cis* interactions with other glycan ligands expressed on the same cell (Freeman et al. 1995; Hanasaki, Varki, and Powell 1995; Razi and Varki 1998). Following exposure of cells to sialidase, which cleaves the *cis*-interacting Siglec ligands, or in some cases following cellular activation, Siglecs become unmasked, which allows them to make interactions with ligands in *trans* (Crocker, Paulson, and Varki 2007). Even when Siglecs are masked by *cis* interactions, *trans* interactions might occur during an encounter with another cell or a pathogen expressing higher affinity ligands that can out-compete the *cis* interactions.

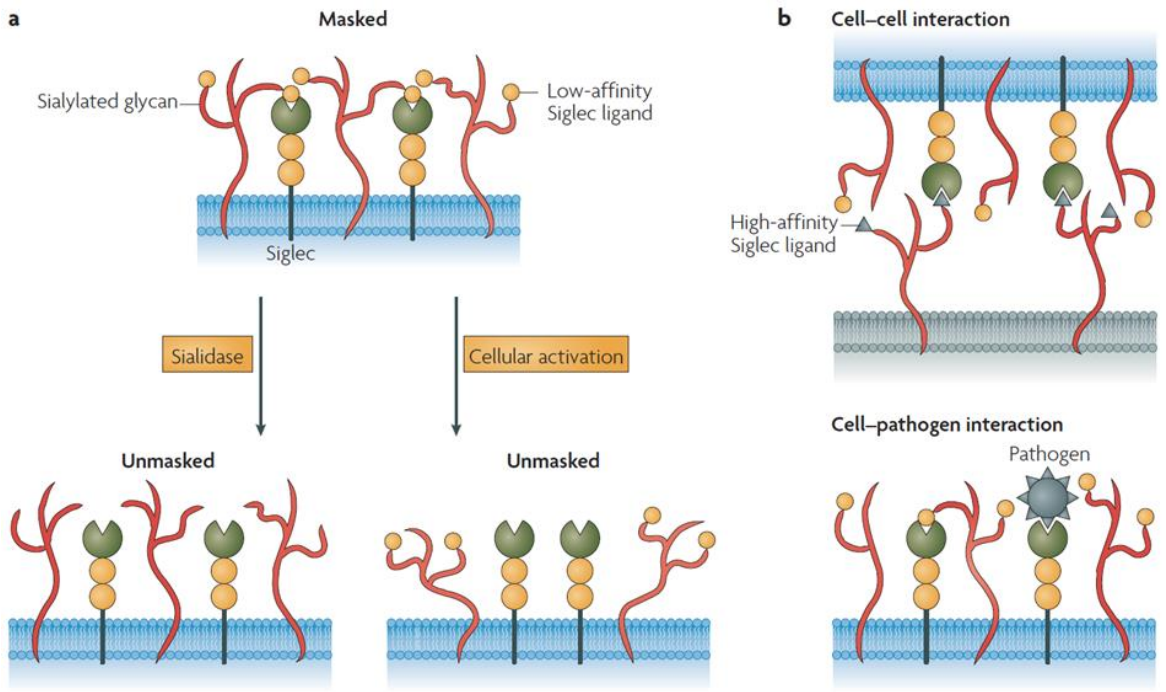

Fig. 7: Schematic representation of cis and trans interactions of Siglecs
(Crocker, Paulson, and Varki 2007)

Several human bacterial pathogens can display sialic acid-based ligands for Siglecs, including *Neisseria meningitidis*, *Haemophilus influenzae*, *Campylobacter jejuni*, *Pseudomonas aeruginosa* and group B *Streptococcus* (GBS) (Chang and Nizet 2014). So far, the best evidence that bacterial sialic acids can subvert immune responses via Siglec interactions is from studies on GBS. This bacterium expresses a sialylated capsule (where sialic acid is linked to N-acetyllactosamine; Siaα2,3Galβ1,4GlcNAc) that is recognized by Siglec-9 on human neutrophils and its equivalent Siglec-E in mice (Chang et al. 2014; Carlin et al. 2009). Ligand binding of Siglec-9 suppresses the neutrophil oxidative burst and extracellular trap

formation, and thus contributes to pathogen survival (Carlin et al. 2009). Certain GBS strains can also target Siglec-5 and Siglec-14 in a sialic acid-independent pathway via interactions with cell wall-anchored β-protein (Ali et al. 2014; Chang and Nizet 2014). Similar to Siglec-9 ligation, Siglec-5 ligation by β-protein suppresses neutrophil killing functions (Chang and Nizet 2014). By contrast, Siglec-14 ligation by β-protein triggers an activation pathway that counterbalances the inhibitory signalling of Siglec-5. Siglec-14 can also interact with *H. influenzae* in a sialic acid-dependent manner, which leads to increased production of IL-8 and tumour necrosis factor, and further supports a host-protective function of this receptor (Angata et al. 2013). Regarding to *Neisseria meningitidis* data, it has been demonstrated the binding to Siglec 5 thanks to NeuAcα2,3Gal, a terminal capping structure displayed on the lipopolysaccharide (LPS) of the bacteria (Jones, Virji, and Crocker 2003).

3.5.1 Siglec 5

Type-I transmembrane protein with 551 amino acid residues, consisting of: four Ig-like domains, a transmembrane domain and a cytoplasmic tail that contains a cytosolic ITIM motif as well as an ITIM-like motif. Due to the cytoplasmic regions, Siglec 5 interfere with cellular signalling, inhibiting immune cell activation. The tyrosine contained within the ITIM is phosphorylated and acts as a docking site for SH2 domain-containing proteins, like SHP phosphatases. This leads to de-phosphorylation of cellular proteins, down-regulating activating signalling pathways.

The gene is located in the chromosome 19, the protein is expressed by monocytic lineage cell (Macauley, Crocker, and Paulson 2014) and binds equally to alpha-2,3-linked and alpha-2,6-linked sialic acid (Blixt et al. 2003). In particular an Siglec-5 recognize the Neu5Acα2-3Gal moiety on the LPS of *N. meningitidis* , and in vitro studies employing transfected COS cells have shown Siglec-5 to be capable of phagocytosis of this gram-negative bacteria (Jones, Virji, and Crocker 2003). Siglec-5 has also been implicated in the clearance of apoptotic bodies by macrophages (Rapoport et al. 2005), but there is little evidence to indicate that apoptotic cells are more avidly decorated with Neu5Acα2-3Gal moieties (Meesmann et al. 2010; Malagolini et al. 2009).

3.5.2 Siglec 14

Type-I transmembrane protein with 396 amino acid residues, consisting of: three Ig-like domains, a transmembrane domain and cytoplasmic tail. The amino acid sequence of the signal peptide and the first 2 Ig-like domains of Siglec 14 are nearly identical with that of Siglec 5. The third Ig-like domain and beyond, however, is unique to Siglec 14 (Angata et al. 2006). Siglec 14 contains an arginine residue in its transmembrane region that allows the binding to ITAM-containing adaptors proteins, such as DAP12. When bound to its ligand, Siglec-14 leads to activation of cellular signalling pathways via the adaptors proteins.

The gene is located in the chromosome 19, adjacent to Siglec 5 and, as this receptor, the protein is expressed by monocytic lineage cell (Macauley, Crocker, and Paulson 2014) and binds equally to alpha-2,3-linked and alpha-2,6-linked sialic acid (Blixt et al. 2003).

Interestingly, functional Siglec 14 is missing from certain human individuals because of a fusion between the SIGLEC5 and SIGLEC14 genes leading to a new gene (SIGLEC5*; hereafter referred to as SIGLEC14/5), which is identical to SIGLEC5 in the coding sequence but is expressed under control of the SIGLEC14 promoter (Yamanaka et al. 2009).

3.5.3 Paired receptors

Several inhibitory receptors of the immune system are paired with activating counterparts that share highly related extracellular domains but differ in the transmembrane and cytoplasmic regions. As shown for the NK-cell receptor Ly49H, which binds the MHC-like protein m157 of mouse cytomegalovirus (Arase et al. 2002; Smith et al. 2002), some paired activating receptors may have evolved as a counter-strategy to bind host-derived pathogen ligands. This is the case of the inhibitory receptor Siglec 5 that is paired with the activating receptor, Siglec 14 (Ali et al. 2014; Angata et al. 2006). These proteins share more than 99% sequence identity in their first two immunoglobulin domains (1aa diversity in BLAST alignment) and then diverge in the rest of their coding sequences; therefore they are expected to deliver opposing signals in response to the same ligands (Ali et al. 2014; Angata et al. 2006).

3.6 Low affinity immunoglobulin gamma Fc region receptor II-a

Antibodies produced in response to a foreign antigen are characterized by polyclonality, not only in the diverse epitopes to which their variable domains bind but also in the various effector molecules to which their constant regions (Fc domains) engage. Thus, the antibody's Fc domain mediates diverse effector activities by engaging two distinct classes of Fc receptors (type I and type II FcRs) on the basis of the two dominant conformational states that the Fc domain may adopt (Pincetic et al. 2014).

Type I FcRs belong to the immunoglobulin receptor superfamily and are represented by the canonical Fcγ receptors. Three classes of human receptors have been described on human leukocytes: FcγR1 (CD64), FcγR2 (CD32) and FcγR3 (CD16) (van de Winkel and Capel 1993; Ravetch and Bolland 2001; Takai 2002).

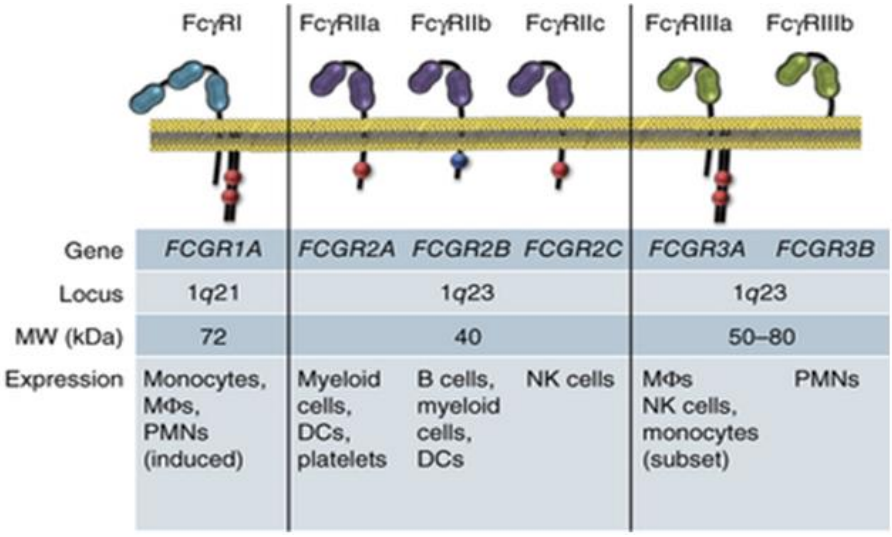

Fig. 8: Characteristics and expression profiles of the human receptors known to bind the Fc domain of IgG: MΦ, macrophage; PMN, polymorphonuclear leukocyte; NK, natural killer (Pincetic et al. 2014)

To FcγR2 class belong three Fc receptors: FcγR2A, FcγR2B and FcγR2C

a) The ***FcγR2A***, is a low affinity IgG receptor for monomeric IgG (KD ~10^{-6} M), but avidly binds immune complexes of IgG and has critical roles in phagocytosis of immune complexes, activation of inflammatory cells and destruction of antibody-coated pathogens (Hulett and Hogarth 1994; Hibbs et al. 1988; Nimmerjahn and Ravetch 2008). This receptor contains an immunoreceptor tyrosine-based activation (ITAM) motif in its intracellular domain that leads to oxidative burst, cytokine release and phagocytosis by macrophages (Takai 2002).

Two allelic variants (high responder [HR] and low responder [LR]) of Fc gamma RIIA that differ in their ability to ligate human IgG_2 exist. HR and LR forms differ by two amino acids, both located in the external domain. In the LR form, a glutamine is substituted by a tryptophan residue at aa position 63, located in the first Ig-like domain, and an arginine residue by a histidine residue at aa position 167 in the second Ig-like domain (Warmerdam et al. 1990).

b) Also the ***FcγR2B*** binds IgG with low affinity (KD ~10^{-6} M), interacting with immune complexes only at physiological concentration of antibody (Ravetch and Bolland 2001). This receptor is preferentially expressed in lymphocytes and characterized by immunoreceptor tyrosine-based inhibitory motifs (ITIMs) in its cytoplasmic domain.

c) The ***FcγR2C*** is the product of an unequal crossover between FCGR2A and FCGR2B genes, which share a high degree of homology (Warmerdam et al. 1993).

4 Investigating NadA role at oropharyngeal barrier

4.1 Article: Role of ARF6, Rab11 and External Hsp90 in the Trafficking and Recycling of Recombinant-Soluble Neisseria meningitidis Adhesin A (rNadA) in Human Epithelial Cells

Abstract

Neisseria meningitidis adhesin A (NadA) is a meningococcus surface protein thought to assist in the adhesion of the bacterium to host cells. We have previously shown that NadA also promotes bacterial internalization in a heterologous expression system. Here we have used the soluble recombinant NadA (rNadA) lacking the membrane anchor region to characterize its internalization route in Chang epithelial cells. Added to the culture medium, rNadA internalizes through a PI3K-dependent endocytosis process not mediated by the canonical clathrin or caveolin scaffolds, but instead follows an ARF6-regulated recycling pathway previously described for MHC-I. The intracellular pool of rNadA reaches a steady state level within one hour of incubation and colocalizes in endocytic vesicles with MHC-I and with the extracellularly labeled chaperone Hsp90. Treatment with membrane permeated and impermeable Hsp90 inhibitors 17-AAG and FITC-GA respectively, lead to intracellular accumulation of rNadA, strongly suggesting that the extracellular secreted pool of the chaperone is involved in rNadA intracellular trafficking. A significant number of intracellular vesicles containing rNadA recruit Rab11, a small GTPase associated to recycling endosomes, but do not contain transferrin receptor (TfR). Interestingly, cell treatment with Hsp90 inhibitors, including the membrane-impermeable FITC-GA, abolished Rab11-rNadA colocalization but do not interfere with Rab11-TfR colocalization. Collectively, these results are consistent with a model whereby rNadA internalizes into human epithelial cells hijacking the recycling endosome pathway and recycle back to the surface of the cell via an ARF6-dependent, Rab11 associated and Hsp90-regulated mechanism. The present study addresses for the first time a meningoccoccal adhesin mechanism of endocytosis and suggests a possible entry pathway engaged by *N. meningitidis* in primary infection of human epithelial cells.

Introduction

Neisseria meningitidis (meningococcus) is a Gram-negative diplococcus that causes severe invasive disease and represents one of the most devastating bacterial infections. Although fatal if not treated on time, meningococcus invasion appears to be more an undesirable event of a usually commensal bacterium, probably due to a combination of host susceptibility and strain specific propensity to invasiveness [1], [2]. The pathophysiology of the bacterium *N. meningitidis* is a process that requires several steps: penetration of the epithelial or mucosal barrier, reaching and surviving the bloodstream, crossing the blood-brain barrier, and eventually causing meningitis through extracellular proliferation [3]. Epithelia are the primary target of bacterial colonization, an event basically asymptomatic and common to both non-virulent and virulent strains. Disease is a rare event compared to the extent of meningococcal nasopharynx colonization. [2], [4], [5]. Experimental data support attachment of the bacterium to nonciliated cells of the respiratory epithelium [6] and transcellular route of passage through this barrier [6]–[9]. A recent report shows that bacterial capsule and type 4 pili are important for epithelial cell transcytosis [9] but host and pathogen players involved in this process are far from being defined.

Neisseria meningitidis adhesin A (NadA) was identified through genome wide analysis and afterward proved to be expressed on the bacterial surface [10]–[12]. NadA is a trimeric outer membrane protein whose gene is present in three out of four known hypervirulent lineages of serogroup B strains [13], [14]. NadA is classified as a trimeric autotransporter adhesion (TAA), a family of outer membrane adhesin, which are present only in Gram negative bacteria. TAAs differ from classical autotrasporter protein by the homotrimeric structure hanging on the bacterial surface and the Type Vc secretion system [10], [11], [15]–[17]. Like other TAA proteins, NadA has a common modular organization, composed of i) a conserved C-terminal membrane anchor through which the protein is translocated to the cell surface, ii) a long central alpha helical domain (stalk) with high propensity to form coiled-coil structures, iii) an N-terminal globular head that has been associated with binding to specific cellular receptors and iiii) a cleavable signal sequence [18], [19]. Generally, TAAs (previously classified as Oligomeric coiled-coil Adhesins (Oca) family [20]) mediate bacterial interaction with host cells or extracellular matrix (ECM) proteins or induce invasion into target cells [21]–[29]. The specificity of the biological function is thought to reside in the head, while the stalk is thought to ensure adequate exposure of the head from the outer membrane [19].

In previous reports, we have used a NadA heterologous expression system to demonstrate the invasive ability acquired by an *Escherichia coli* strain exposing surface NadA. Our data support the role of NadA in

the uptake of bacteria by Chang cells, a human epithelial cell line [10], [30]. A recombinant NadA (rNadA), expressed in *E. coli* and purified in a soluble form in absence of the anchor (translocator) domain, preserves its immunogenic properties and is included in a multicomponent vaccine against meningococcus B (Bexsero) [31], [32]. A peculiar feature of rNadA, perhaps unique among all members of the TAA family, is the ability to preserve a stable trimeric structure in solution [10], [13], [33]. This recombinant soluble homo-trimer still binds eukaryotic cells [10], [13], [33]–[35]. The gain-of-function phenotype acquired by heterologous bacteria expressing NadA and the conserved binding characteristics shown by the recombinant protein provide an opportunity to dissect the function of this adhesin in host-pathogen interaction(s).

When expressed on the surface of *E. coli*, NadA promotes bacterial internalization [10], by an undefined mechanism. Eukaryotic cells internalize a variety of extracellular substances as well as plasma membrane proteins via a remarkable diversity of endocytic pathways generally classified as clathrin-dependent or independent according to the involvement of clathrin [36]–[38]. Endocytic vesicles converge into early endosomes (EEs), the main sorting compartment from which most of the cargos are rapidly recycled back to the plasmamembrane (PM), while some are sorted into late endosomes and destined either to lysosomes or to the trans Golgi network (TGN) [39], [40]. While lysosome targeting is achieved by clathrin-coated endosomes, mechanisms of clathrin-independent endocytosis have been identified more recently and are emerging as complex, multi-pattern processes of internalization still poorly characterized [41], [42]. In particular, ADP ribosylation Factor 6 (ARF6) has been involved in internalization and sorting of cargos targeted to recycling endosome [43]. Initially described for the major histocompatibility complex (MHC) class I trafficking [44], the list of membrane proteins requiring this factor for internalization and recycling is growing [42], [43]. While ARFs coordinate vesicle formation [45], key regulators of endosome trafficking include the Rabs, a family of small GTPase proteins associated to all kind of vesicles [46]. The more than 60 Rabs found in eukaryotic cells communicate with each other through recruitment of effectors that regulate the correct destination of vesicles [39], [47].

In our attempt to identify eukaryotic cell proteins involved in the NadA-mediated interaction of bacteria, we found that such processes are sensitive to inhibition of Hsp90 activity, and the host chaperone itself was found to bind NadA *in vitro* [30]. Hsp90 is a ubiquitous molecular chaperone crucial for maintenance of cellular homeostasis [48]. The Hsp90 family of chaperones includes organelle specialized isoforms and two cytoplasm/nucleus localized factors, the inducible Hsp90α and the constitutive Hsp90β. More recently, several lines of evidence suggest that Hsp90α is also secreted by normal cells in response to stress or insults,

and by several tumor cell lines (reviewed in [49]). The major functions of this extracellular pool have been identified as protective response to several kinds of stress, assistance to antigen presentation and promoting tissue invasion by cancer cells [49]–[52]. Results from our previous study also indicated a protective role of Hsp90 toward NadA mediated invasion, although we did not differentiate the possible role of extracellular and intracellular pools of the chaperone [30].

In this report we have used the soluble recombinant $NadA_{\Delta 351\text{-}405}$ (rNadA) and demonstrated that it was able to internalize upon binding to the Chang human epithelial cell line. Evidence is provided on the stability of the rNadA trimer at 37°C and on the temperature dependence of NadA binding to Chang cells. In our analysis of the internalization pathway exploited by NadA, we found that the process triggered by NadA was clathrin independent. As reported for MHC class I internalization and recycling to cell surface, ARF6-dependence and recruitment of Rab 11 on rNadA vesicles suggested that the adhesin is sorted in a recycling endosomes pathway. The effect of two Hsp90 inhibitors on the internalization and recycling of the adhesin indicated that extracellular Hsp90 is involved in the trafficking of rNadA.

Material and methods

Cell culture and transfection

Chang epithelial cells (Wong-Kilbourne derivative, clone 1-5c-4, human conjunctiva, ATCC CCL-20.2) were grown in Dulbecco's Modified Eagle Medium (DMEM) supplemented with 15 mM glutamine, 100 U/ml penicillin, 100 µg/ml streptomycin, 10% FCS and maintained at 37°C in a controlled humidified atmosphere containing 5% CO_2. Transfection of Chang cells was performed using Hiperfect (Qiagen), jetPEI (Polyplus transfection) or lipofectamine (Invitrogen) according the manufacturer's instructions.

Antibodies, plasmid vectors and reagents

Anti-MHC-I (Biolegends); anti-EEA1 (Novus Biologicals); anti-ARF6 (Santa Cruz Biotechnology); anti-Rab5 (BD transduction Laboratories); anti clathrin (Sigma); anti-M6PR kindly provided by J. Gruenberg University of Geneva, Switzerland; anti-HSP90 (SPA-830, Stressgene); Alexa-488-conjugated Phalloidin, Cy3-conjugated transferrin, Alexa488- and 543-conjugated secondary antibodies (Invitrogen); Alexa488-

conjugated anti-MHC-I (Santa cruz Biotechnology). Antibodies against rNadA were previously described in [53]. Alexa-488-conjugated and Alexa-633 conjugated rNadA were obtained by labelling with Alexa Fluor Microscale Protein Labeling Kit (Molecular Probes-Invitrogen) following manufacturer instructions. cDNA expressing the wild type and ARF6-Q67L mutant were kindly provided by J. Donaldson (to M.S. and A.L.), National Institutes of Health, Bethesda, USA. 17-AAG (17-N-allylamino-17-demethoxygeldanamycin) and Wortmannin were from Sigma. FITC-GA was synthesized by labogen (Milan - Italy). The myc-AP180C plasmid containing the C-terminal portion of the AP180 gene fused in frame with N-terminal myc tag sequence was generated as described elsewhere [54]. Generation of plasmids coding for C-terminal EGFP fusion Rabs was performed as described previously [55].

Binding of rNadA to human Chang epithelial cells

Chang cells were non-enzymatically detached from the support by using cell dissociation solution (Sigma), harvested and resuspended in DMEM medium supplemented with 1% FBS. Then 3×10^5 cells were mixed with recombinant rNadA (200 µg/ml) for 30 minutes at four different temperatures (RT, 4°C, 30°C and 37°C). After two washes with 1% FBS in phosphate-buffered saline, cells were incubated with the mouse monoclonal anti-NadA antibody 9F11 (1.25 µg/ml to 160 µg/ml) or IgG mouse isotype control (Sigma) for 1 hr at 4°C. Samples were washed twice and then incubated for 30 minutes at 4°C with Allophycocyanin-conjugated goat $F(ab)_2$ antibody to mouse IgG (1:100, Jackson ImmunoResearch) and finally the cells were analyzed with the FACS-Scan flow cytometer Canto II. The mean fluorescence intensity for each sample was calculated. To analyze the time dependence of NadA binding to Chang, 3×10^5 cells were incubated with recombinant rNadA (200 µg/ml) at 37°C for different period of time (1 minute to 2 hours), washed and incubated with the mouse monoclonal anti-NadA antibody 9F11 (20 µg/ml) or IgG mouse isotype control for 1 hr at 4°C. FACS analysis was performed as described above.

Size Esclusion-HPLC–multiangle laser light-scattering (MALLS) analysis

Four identical aliquots (100 µl) of rNadA (1,7 mg/ml in 10 mM NaH_2P0_4 150 mM NaCl pH 7.2) were heated at 37°C for 30 min, 1, 2 and 4 hrs respectively. For each time point, sample was loaded on an analytical size exclusion TSK Super SW3000 (4.6×300-mm column of 4 µm and 300 Å) with a separation range on globular proteins from 10 to 500 kDa (Tosoh Bioscience, Tokyo, Japan). Samples were eluted

isocratically in 0.1 M NaH_2P0_4, 0,1 M $NaHSO_4$ buffer at pH 7.0. MALLS analyses were performed in real time using a multi-angle light-scattering detector Dawn TREOS (Wyatt Corp., Santa Barbara, CA, USA), with an incident laser of 658 nm; intensity of the scattered light was measured at 3 angles simultaneously. Data elaboration was performed using Astra V software (Wyatt). Zimm formalism was used to determine the weight-average molecular mass (MW) in daltons and polydispersity index (MW/Mn) for each oligomer present in solution.

Full length trimeric NadA purification on size exclusion chromatography

A 300 µl aliquot of rNadA (1,7 mg/ml Buffer 10 mM NaH_2P0_4 150 mM NaCl pH 7.2) was heated at 37°C for 4 hours. At end of this time period, sample was loaded on the gel filtration column. Size exclusion was performed using a Superdex 75 10–300 GL (GE-Healtcare) and elution was performed isocratically in 0.1 M NaH_2P0_4 pH 7.2, 0.15 M NaCl. Protein containing fractions were identified by OD at 280 nm and collected.

Immunofluorescence staining and confocal microscopy

Chang cells were cultured on coverslips to reach 70–80% of confluence, washed three times in medium without serum and then incubated with rNadA (200 µg/ml) in the same medium supplemented with 1% FCS. Incubation was performed at 37°C for the indicated times. Cells were then fixed in paraformaldehyde for 8–10 min at 37°C, permeabilized and incubated with primary antibodies for 1 hr at room temperature. Afterwards, cells were washed three times with PBS, incubated with fluorophore-conjugated secondary antibody for 30–45 min at room temperature, washed again three times in PBS and mounted on slides.

In vivo staining of MHC-I was performed as follows: cells were washed three times in medium without serum and incubated with a mouse monoclonal antibody against MHC-I (10–30 µg/ml) for 1 hr at 4°C. Afterwards, cells were washed 3 times and incubated with recombinant rNadA (200 µg/ml) for 1 hr at 37°C in a medium supplemented with 1% FCS, then fixed and permeabilized. rNadA was stained following the standard procedure while MHC-I was revealed using a fluorescence-conjugated secondary antibody directed against the mouse monoclonal primary antibody.

In vivo staining of HSP90 was performed as follows: cells were washed three times in medium without serum and incubated with a rabbit polyclonal HSP90 antibody (50 µg/ml) for 2–4 hrs at 4°C. Afterward, cells were washed 3 times and incubated with recombinant rNadA (200 µg/ml) for 1 h at 37°C in a medium supplemented with 1% FCS, then fixed and permeabilized. rNadA was stained following the standard procedure while HSP90 was detected using a Alexa543-conjugated secondary antibody directed against the rabbit polyclonal primary antibody.

Samples were analyzed by confocal microscopy (LSM 510, Zeiss) using a 60× oil-immersion objective, maintaining the pinhole of the objective at 1 airy unit. Images were scanned using an Argon 488 laser, a HeNe 543 laser and a HeNe 633 laser, under non-saturating conditions (pixel fluorescence below 255 arbitrary units). The colocalization analysis and the quantification of immunofluorescence (IF) intensity of rNadA in the cells was performed with LSM510-3.2 software (Zeiss). To assess the colocalization we removed the background immunofluorescence by adjusting the threshold levels and used the histo and colocalization functions of the above software. This software provides two colocalization coefficients that ranges from 0 (no colocalization) to 1 (complete colocalization). The colocalization coefficients indicate the amount of pixels of the channel A that colocalizes with pixels from channel B and viceversa. Finally, we expressed the colocalization extent as a percentage over the total immunofluorescence per channel. The immunofluorescence (IF) intensity was calculated as total immunofluorescence of rNadA in the cell divided by the area of the cell and expressed as arbitrary units (A.U.).

rNadA uptake in the presence of Hsp90 inhibitors

Internalization was performed by adding rNadA to the culture medium at a final concentration of 200 µg/ml and incubating at 37°C for the indicated period of time. Chang cells grown at about 50% confluence were pre-treated overnight with 0.5 µM 17-AAG and the then incubated with recombinant NadA (200 µg/ml) at 37°C for 1, 4 or 16 hrs in presence of the same concentration of 17-AAG. When 10 µM 17-AAG or FITC-GA were used, cells were grown to 70–80% confluence and pretreated for 1 hr with the inhibitors before adding rNadA (200 µg/ml) and subsequently incubated at 37°C for 1,4 or 16 hrs in the continued presence of the inhibitors. To temporarily permeabilize cells, growth medium was substituted with 0.01% saponin in PBS for 30 seconds at room temperature. Cells were then washed 3 times with PBS before adding fresh medium and incubate at 37°C for the indicated time. Afterwards, cells were fixed and labeled as detailed above.

AKT detection in Chang cell lysates

Chang cells were seeded on 24-well tissue culture plates (6–8×10^4 cells per well) and incubated at 37°C overnight. The following day, cells were treated with HSP90 inhibitors as described above. Total cell extracts were prepared in RIPA buffer (Sigma) supplemented with complete protease inhibitor (Roche). Equal amounts of proteins were prepared in NuPAGE SDS Buffer under reducing conditions and separated on NuPAGE polyacrylamide gels. Proteins were transferred to nitrocellulose membranes for Western blot analysis. Membranes were then blocked with PBS containing 0.1% Tween 20 (PBST)+10% dried skim milk at room temperature for 1 h. After extensive washings in PBST, proteins bound on nitrocellulose membranes were detected with specific anti-Akt rabbit antibody (Cell Signaling Technology) followed by HRP-conjugated goat anti-rabbit secondary antibody.

Time-lapse Microscopy

Chang cells at 70–80% of confluence on glass-bottom Petri dishes (MatTek Corporation-USA) were incubated overnight at 37°C. The day after, cells were incubated with Alexa488-conjugated anti-MHC-I antibody and 2.5 µg/ml Alexa633-conjugated rNadA, or 5 µg/ml of Cy3-conjugated transferrin and 2.5 µg/ml Alexa-488-conjugated rNadA, or pretreated overnight with 0.5 µM of 17AAG and then with Alexa-488-conjugated rNadA for 60 min at 37°C. Cells were washes three times and supplemented with the medium buffered with 20 mM Hepes pH 7.2. The Petri dish was then placed on a stage of LSM-510 confocal microscope (Zeiss, Germany) equipped with a thermoregulation device at 37°C. Images were acquired every 2 (for MHC-I and NadA; movie S1) or 4 seconds (for transferrin and rNadA, movie S2; rNadA in 17AAG treated or untreated cells, movie S3 and S4 respectively) at 25% laser power intensity.

Results

Purified rNadA binds Chang cells in a time and temperature dependent manner

In previous reports, rNadA binds Chang epithelial cells more than other human cell lines [10]. A temperature dependence has also been suggested, as binding to human monocytes/macrophages was detectable at 37°C but not at 0°C [35]. We sought to investigate the temperature dependence and kinetics of NadA binding to Chang epithelial cells. Non permeabilized Chang cells were incubated with rNadA and, after washing, the bound fraction was revealed by FACS analysis with anti-NadA antibody.

At first this analysis was performed after 30 minutes of incubation at different temperatures. The result is shown in figure 1A. The rNadA binding to Chang cells was temperature dependent, giving the highest value at 37°C while dropping to about 60% at 30°C (figure 1A). Lowering the incubation temperatures at 20°C caused a decrease of the binding ability at less than 20% of the value obtained at 37°C. However, even at 4°C the amount of cell-bound rNadA was measurably higher than the background (independent IgG used as control) Setting incubation temperature at 37°C, we then analyzed the kinetics of rNadA binding to Chang cells (figure 1B). The maximum level of surface bound rNadA was observed at 30 minutes of incubation and decreased at longer incubation times. The time-dependent decrease of surface localized rNadA was obtained with various monoclonal and polyclonal antibodies used for detection (data not shown).

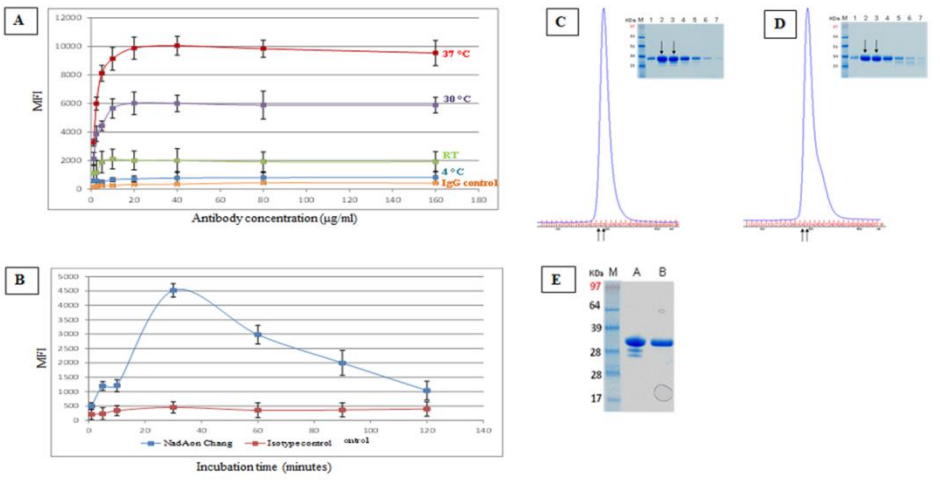

Figure 1: Purified rNadA binds Chang cells in a time- and temperature dependent manner. A and B. Chang cells were incubated with 200 µg/ml rNadA and then washed with PBS – 1% FBS. Binding was detected using anti-NadA 9F11 mouse mAb and Allophycocyanin-conjugated goat anti-mouse secondary antibody. Analysis was performed with Canto II instrument, and mean fluorescence intensity is reported (MFI). **A**: Binding of rNadA to cells for 30 minutes at the indicated temperatures, and using varying concentrations of the primary antibody **B**: Binding of rNadA was performed at 37°C for a period of time ranging from 1 minute to 2 hours as indicated. **C**: SE-HPLC profile of rNadA at room temperature. **D**: SE-HPLC profile of rNadA after heating period of 4 hrs at 37°C.**E**: SDS-Page of collected fractions. Black arrows in **D** indicate the fractions pooled.

To exclude a destabilization of the trimeric rNadA structure at 37°C over time, we incubated the recombinant adhesin for 30 min, 1, 2 and 4 hrs and analyzed the products by analytical size exclusion chromatography and MALLS (Multi Angle Laser Light Scattering). The results of such analysis, presented in figure S1 and table S1, showed that the native trimer is the predominant species (about 95%) although the rNadA preparation include C-terminus deleted forms previously characterized [33]. The 4 hour treatment at 37°C completely removed these truncated species and the full length homogenous trimeric population can be purified as shown in figure 1, panels C–E.

The size exclusion chromatography analysis of the sample before and after thermal treatment is shown in figure 1C and 1D, respectively. The SDS-PAGE of the eluted samples confirmed that all contaminants were removed from the fractions containing the majority of the trimeric rNadA following 4 hour incubation at 37°C (fractions 12 and 13 of figure 1C and 1D). The purified full length trimeric rNadA eluted in peak II (lane B of figure 1E) was used at least once in all our experiments and challenged with the crude rNadA preparations. Both samples gave identical results. Thus, trimers of rNadA form a stable structure in solution which is resistant to the temperature conditions used in our studies.

rNadA internalization into Chang epithelial cells

Having excluded that the time-dependent reduction of rNadA binding to Chang cells was caused by changes in the trimeric structure or stability of the protein, we investigated a possible internalization process by confocal immunofluorescence microscopy (figure 2).

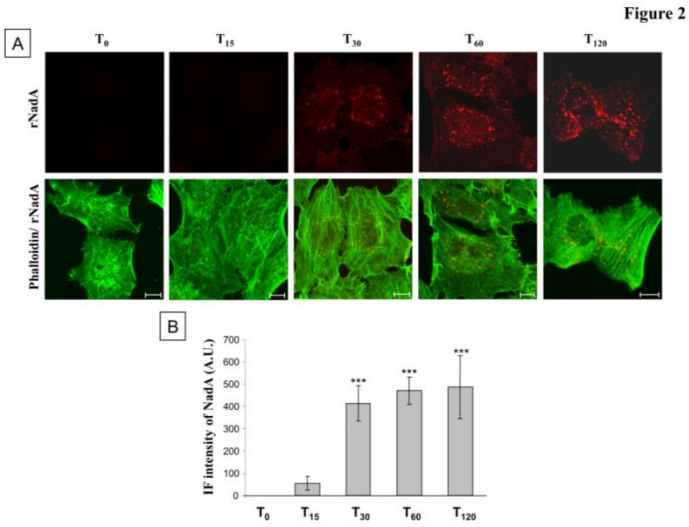

Figure 2: Time course of rNadA internalization. ***A:*** Chang cells were incubated with 200 µg/ml rNadA at 37°C for 0–120 min and then fixed, permeabilized and double stained for rNadA (upper panels; red) and Alexa488-conjugated phalloidin (green). Merged images of rNadA and phalloidin are shown in the lower panel. Scale bar is 10 µm. ***B:*** Quantification of IF intensity of rNadA in the experiment illustrated in panel A. Data are mean ± s.e.m representative of two independent experiments, each assessing 10–15 cells, and expressed as Arbitrary Units (A.U.). ***p<0.001, compared to T_0 treated cells (t-test).

Following 15 minutes of incubation with rNadA, cells showed minor amounts of detectable rNadA apparently distributed on the cell surface (figure 2). Upon 30 minutes of incubation, rNadA appeared mostly as dot-like structures. At a longer time of incubation the fluorescence of the dot-like structures slightly increased (figure 2A and B). Hypothesizing that the dot-like structures are indicative of rNadA internalization, this phenomenon could explain, at least partially, the observed loss of rNadA fluorescence observed by FACS analysis at prolonged incubation times. However, the confocal microscopy also indicated that the intracellular pool of rNadA reaches a steady state level at about 30–60 minutes incubation time, possibly because it recycles towards the cell exterior or because of intracellular degradation.

Phosphoinositide 3-kinase (PI3K) control of rNadA internalization

Src phosphorylation of several components of the clathrin dependent endocytosis, including cortactin, arrestin, dynamin and clathrin itself, is essential for internalization [56]. In addition, Src activity is also required for the alternative caveolar endocytosis [57]. Protein kinase C is involved in the endocytosis of several G protein coupled receptor through clathrin or caveolae pathways [58], [59]. The phosphoinositide 3-kinase (PI3K) is important in the early steps of endocytosis and and in the regulation of fusion and maturation dynamics of endocytic vesicles [60]. Here we used inhibitors of the different kinases to better understand the internalization pathway(s) exploited by rNadA.

Chang cells were incubated with or without kinase inhibitorsfor 1 hour with vehicle, 100 nM wortmannin (PI3K inhibitor more active on class I enzymes), 100 µM genistein (wide spectrum tyrosine kinase inhibitor known to prevent the caveolae mediated endocytosis [61]), 10 µM Bisindolylmaleimide I (BSMI, a general PKC inhibitor), and 10 µM SU6656 (Src family kinase inhibitor) and then for an additional hour with rNadA. The internalization of rNadA was unaffected by the action of the tyrosine kinase inhibitors (data not shown) whereas wortmannin treatment reduced the internalization of rNadA (figure 3A and B). The cellular localization of MHC-I was unaffected by exposure to rNadA, genistein, BSMI and SU6656 (not shown), whereas wortmannin shifted the localization of MHC-I towards the PM fraction (figure 3A and C).

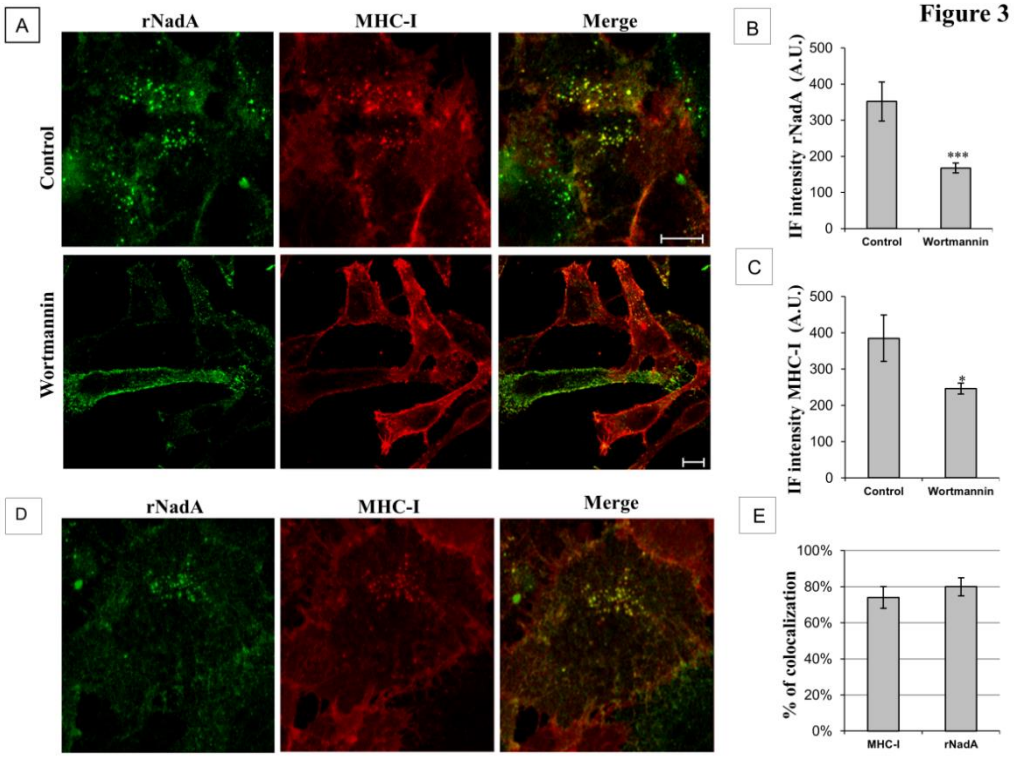

Figure 3: PI3K inhibition impairs rNadA internalization and colocalization of rNadA with MHC-I: ***A:*** Chang cells were treated with either vehicle (upper panel) or 100 nM Wortmannin (lower panel) for 1 h at 37°C, and then incubated with 200 µg/ml rNadA for an additional hour at 37°C in presence of the inhibitor or vehicle. Cells were then fixed, permeabilized and double stained for rNadA (green) and MHC-1 (red). Merged images are also shown. Scale bar 10 µm. ***B:*** Quantification of IF intensity of rNadA in the experiment illustrated in panel A. Data are mean ± s.e.m representative of two independent experiments, each assessing 20–25 cells, and expressed as Arbitrary Units (A.U.). ***p<0.001, compared to control cells (t-test). ***C:*** Quantification of IF intensity of MHC-I in the experiment illustrated in panel A. Data are mean ± s.e.m representative of two independent experiments, each assessing 20–25 cells, and expressed as Arbitrary Units (A.U.). *p<0.05, compared to control cells (t-test). ***D:*** Chang cells were treated with anti-MHC-I antibody for 1 h at 4°C and then incubated at 37°C for 1 h with 200 µg/ml rNadA. Cells were fixed and double stained for rNadA (green) and MHC-1 (red). Scale bar is 10 µm. ***E:*** Quantification of MHC-I and rNadA colocalization. MHC-I column indicate the percentage of MHC-I immunofluorescent pixels colocalizing with rNadA immunofluorescent pixels. Conversely, rNadA column indicate the percentage of rNadA immunofluorescent pixels colocalizing with MHC-I immunofluorescent pixels. Data are mean ± s.e.m representative of two independent experiments, each assessing 20–25 cells.

In these experiments, rNadA showed a certain extent of endosomal colocalization with MHC class I and we decided to further explore this observation. Antibody labelling of MHC-I following cell permeabilization would show the total pool of MHC-I (PM plus endosomally localized MHC-I). In order to visualize only the recently internalized MHC-I we decided to pre-label the PM-localized MHC-I. Chang cells were treated with an antibody against MHC-I for 1 hr at 4°C. This incubation allowed binding of the antibody to MHC-I at a temperature that prevents MHC-I internalization. The cells were then treated with rNadA for 60 minutes at 37°C, a temperature at which internalization is restored. As shown in figure 3D and E, rNadA appeared to colocalize with MHC-I in endosomes.

Confocal microscopy analysis of rNadA internalization pathway

In an attempt to elucidate the cellular entry mechanism of rNadA, we performed a confocal microscopy analysis in search of rNadA colocalization with different endocytic markers belonging to the clathrin-dependent and -independent pathways.

Chang cells were incubated with rNadA for 60 minutes at 37°C to allow internalization of the adhesin and then stained for rNadA and the endocytic markers, early endosome antigen 1 (EEA1), small GTPase Rab5, M6PR. As shown in figure 4A–C and F, rNadA showed a weak colocalization with early endosomal markers (EEA1, Rab5), as well as with the endo-lysosomal marker M6PR. We also analyzed the colocalization of internalized rNadA with clathrin itself and the transferrin receptor, a prototype cargo of the clathrin-dependent pathway. Remarkably, rNadA containing carriers did not associate with the scaffold protein clathrin, and the colocalization with transferrin receptor was negligible (figure 4D–F). As a control, we showed that transferrin receptor colocalized with clathrin in Chang cells (figure S2). Since these data suggested that the main rNadA internalization pathway does not rely on the clathrin- pathway, we sought to verify this aspect by the analysis of rNadA internalization in presence of an inhibitor of clathrin vesicles formation. The AP180 protein is a crucial adaptor involved in the early stage of chlatrin-dependent endocytosis [54].Expression of the C-terminus moiety of this adaptor, known as AP180C, inhibits transferrin and EGF receptors clathrin-dependent endocytosis by preventing coat formation and leading to clathrin redistribution [54], [62]. AP180C transfected Chang cells were incubated with rNadA for 60 minutes at 37°C before to be fixed and treated for confocal analysis. As control, we followed TfR internalization both in absence and presence of the truncated AP180. Results are shown in figure 4G and quantification of rNadA, TfR and AP180C colocalization reported in graph. As expected, TfR internalization was severely impaired by AP180C expression while the intracellular vesicular pattern of rNadA was not affected (figure 4G). Furthermore, the absence of rNadA colocalization with either TfR or AP180C confirmed that the two proteins follow different internalization pathways.

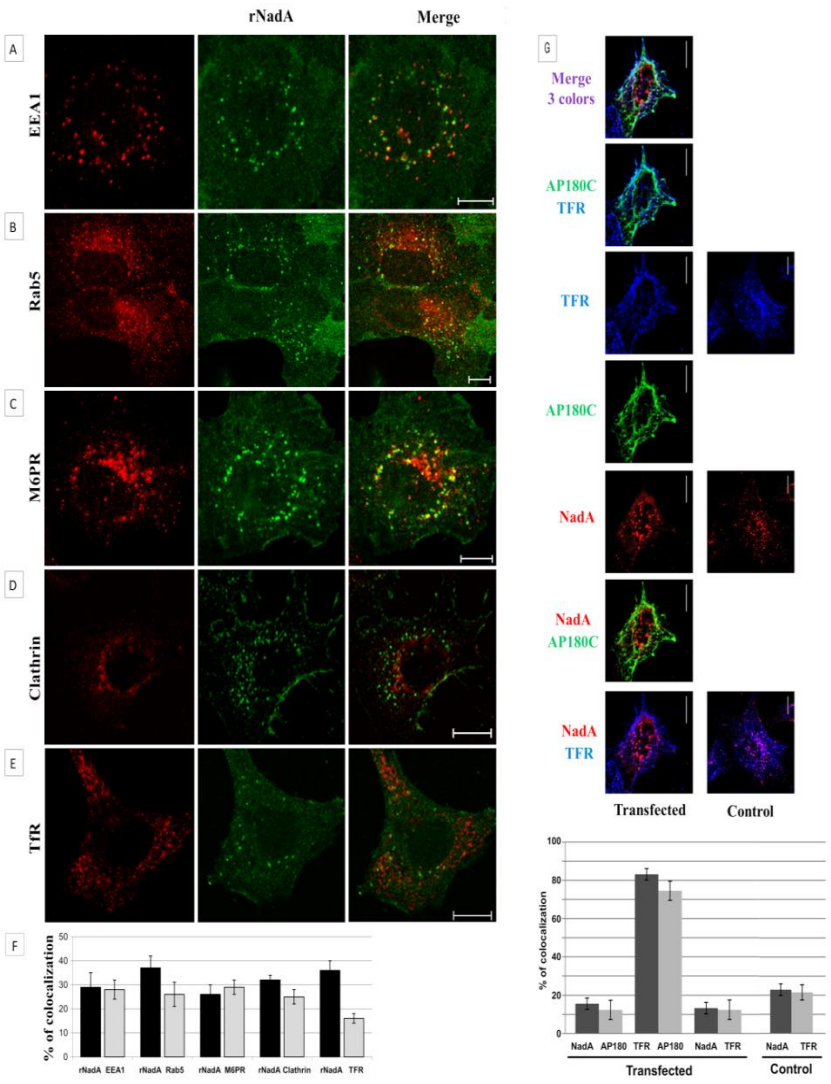

Figure 4: Colocalization of rNadA with endosome markers. ***A:*** Chang cells were incubated with 200 µg/ml rNadA for 1 h at 37°C, then fixed, permeabilized and double stained for rNadA (green) and EEA1 ***(A)***, Rab5 ***(B)***, M6PR ***(C)***, Clathrin ***(D)*** and TfR ***(E)*** (red). Merged images of the red and green signals are also shown. Images are representative of two independent experiments. Scale bar is 10 µm. ***F:*** Quantification of rNadA colocalization with endosome markers. The black columns indicate the percentage of rNadA immunofluorescent pixels colocalizing with the endosomal marker (EEA1, RAb5, M6PR, Clathrin, TfR as indicated) immunofluorescent pixels. Viceversa the grey columns indicate the percentage of the endosomal marker immunofluorescent pixels colocalizing with rNadA immunofluorescent pixels. Data are mean ± s.e.m representative of two independent experiments, each assessing 20–25 cells. ***G:*** Chang cells were transfected with an EGFR-AP180C expressing plasmid or with empty vector and incubated 24 hours at 37°C to recover. Cells were then incubated with rNadA, fixed and stained as indicated in point A. EGFR-AP190C is shown in green, rNadA in red and TfR in blu. Quantification was performed as indicated in point F.

To further explore the internalization pathway used by rNadA, we analyzed the presence of rNadA in the lysosomal compartment. rNadA showed a very minor colocalization with the lysosomal marker LAMP1 upon 60 minute of incubation as well as at longer incubation times up to 24 hours (not shown). This observation is consistent with a small presence of the adhesin in the early endosomal compartment and indicates that internalized rNadA is not directed towards the degradative lysosomal pathway.

Finally, we analyzed the involvement of the clathrin-independent ARF6-regulated pathway. To verify whether endosomal sorting of internalized rNadA involves the small GTPase ARF6 [60] we monitored the internalization/recycling of rNadA in Chang cells expressing wild-type, and GTP-locked ARF6 (ARF6-Q67L). Previous studies demonstrated that ARF6-Q67L transfection leads to the intracellular accumulation of MHC-I [60]. Indeed, when mutant cells overexpressing ARF6-Q67L were incubated with rNadA

overnight there was an accumulation of intracellular rNadA, while in cells overexpressing wild-type ARF6 the classical spotted distribution of rNadA was observed (figure 5).

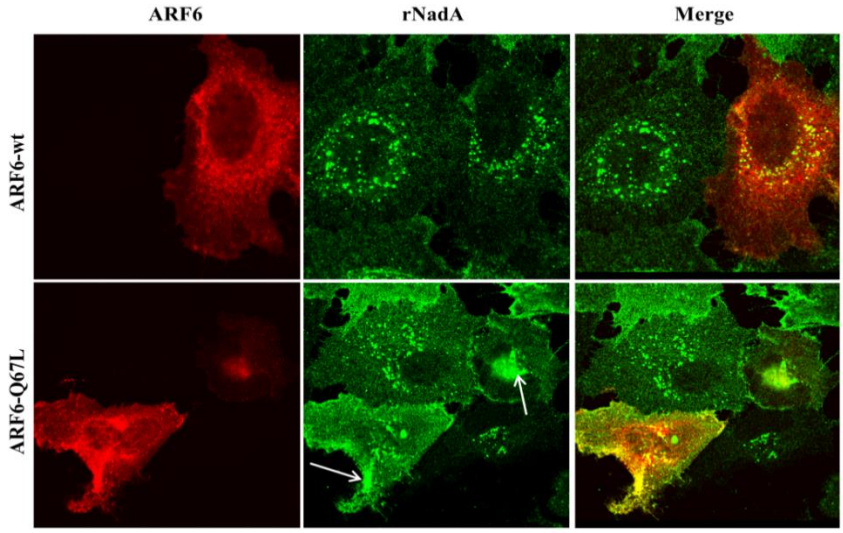

Figure 5: rNadA intracellular distribution is affected by ARF6. Chang cells were transfected in order to overexpress wild type ARF6 (ARF6-wt) or dominant-negative ARF6 (ARF6-Q67L) and then incubated overnight with 200 µg/ml rNadA at 37°C. Afterwards, cells were fixed, permeabilized and double stained for rNadA (green) and ARF6 (red). Merged images are also shown. Scale bar 10 µm. Images are representative of two independent experiments.

In conclusion, this indicates that the rNadA endosomal trafficking involves the clathrin independent ARF6-regulated pathway. The carriers generated along this pathway can fuse with the early endosome, or take a more direct route towards the PM [60], [63], [64]. Indeed, our data suggest that rNadA may use a more direct recycling pathway without involvement of the early endosomal compartment. This hypothesis would be consistent with the negligible colocalization with the lysosomal compartment [64].

rNadA, MHC-I and transferrin internalization dynamics in live cells

In order to validate that rNadA uses the MHC-I internalization/recycling route we investigated their co-internalization in live cells. Chang cells were incubated for 1 hour with fluorescent Alexa633-conjugated rNadA and fluorescent Alexa488-conjugated anti-MHC-I antibody. Cells were rapidly washed with PBS and imaged for 5 minutes by confocal microscope. The movies showed the presence of rapidly moving carriers, containing both rNadA and MHC-I (figure 6A and movie S1). A minor fraction of carriers contained either rNadA or MHC-I. This could be due to the previously described dual targeting of surface MHC class I [65].

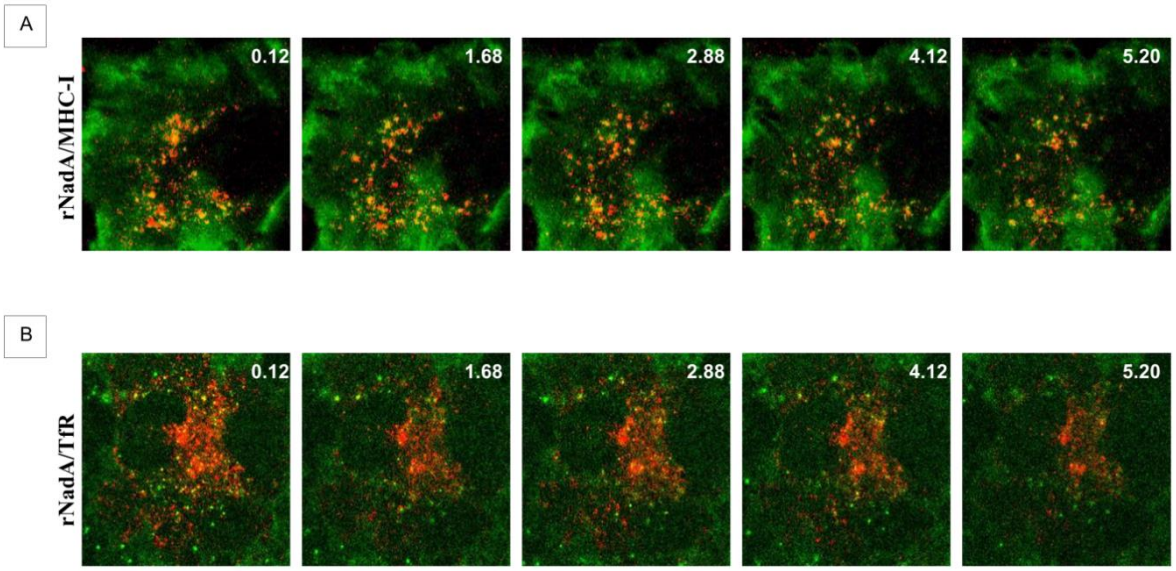

Figure 6: Time lapse rNadA internalization. ***A:*** Chang cells were incubated for 1 h with Alexa633-conjugated rNadA (shown in red) and Alexa488-conjugated anti-MHC-I antibody (green). Cells were then washed and live images were recorded every 2 seconds by confocal microscopy. Five frames from the Movie S1 are shown. Time (seconds) is indicated in the top right of each panel. ***B:*** Chang cells were incubated for 1 h with Alexa488-conjugated rNadA (green) and Cy3-conjugated transferrin (red). Cells were then washed and live images were recorded every 4 seconds by confocal microscope. Five frames from the Supplementary Movie S2 are shown. Time (seconds) is indicated in the top right of each panel.

To cross-check that the rNadA internalization route is clathrin-independent, we tested the overlap between endocytosed rNadA and transferrin, a cargo internalized via the clathrin-dependent pathway. Chang cells were incubated for 1 hour with fluorescent Alexa488-conjugated rNadA and fluorescent Cy3-conjugated transferrin. Cells were rapidly washed with PBS and imaged as above. The movies showed the presence of rapidly moving rNadA or transferrin containing carriers indicating that the intracellular trafficking of rNadA is essentially different from that of transferrin (figure 6B and movie S2). As expected, only a minor fraction of carriers showed the presence of both rNadA and transferrin, perhaps as a result of a sorting/recycling compartment where the clathrin-dependent and independent pathways converge. Taken together, these observations confirm that the intracellular trafficking route of rNadA is clathrin independent and mostly overlaps with that of MHC-I.

Functional involvement of intracellular and external Hsp90 in internalization and trafficking of rNadA

In our recent report [30], we identified Hsp90 as a cellular factor interfering with rNadA-mediated bacterial infection. Although Hsp90 is an intracellular chaperone, its presence in the extracellular space has also

been reported [50]. Here, we sought to verify the possible relationship between extracellular Hsp90 and rNadA internalization.

To this end, we selectively labeled the external Hsp90 in live cells by incubating them with an antibody against Hsp90 for 1 hr at 4°C. This approach allows the binding of the antibody to Hsp90 present on the external side of the PM, while the low temperature prevents internalization. Excess unbound anti-hsp90 antibodies were removed and the cells were treated with rNadA for 60 minutes at 37°C. Finally, the cells were fixed and rNadA was labeled with the appropriate primary and secondary antibodies. The anti-Hsp90 antibodies were revealed using fluorescence-conjugated secondary antibodies. As shown in figure 7A, externally labelled Hsp90 accumulated intracellularly in compartments containing rNadA, strongly suggesting that Hsp90 present on the external side of the PM is internalized and colocalizes with the rNadA (figure 7B).

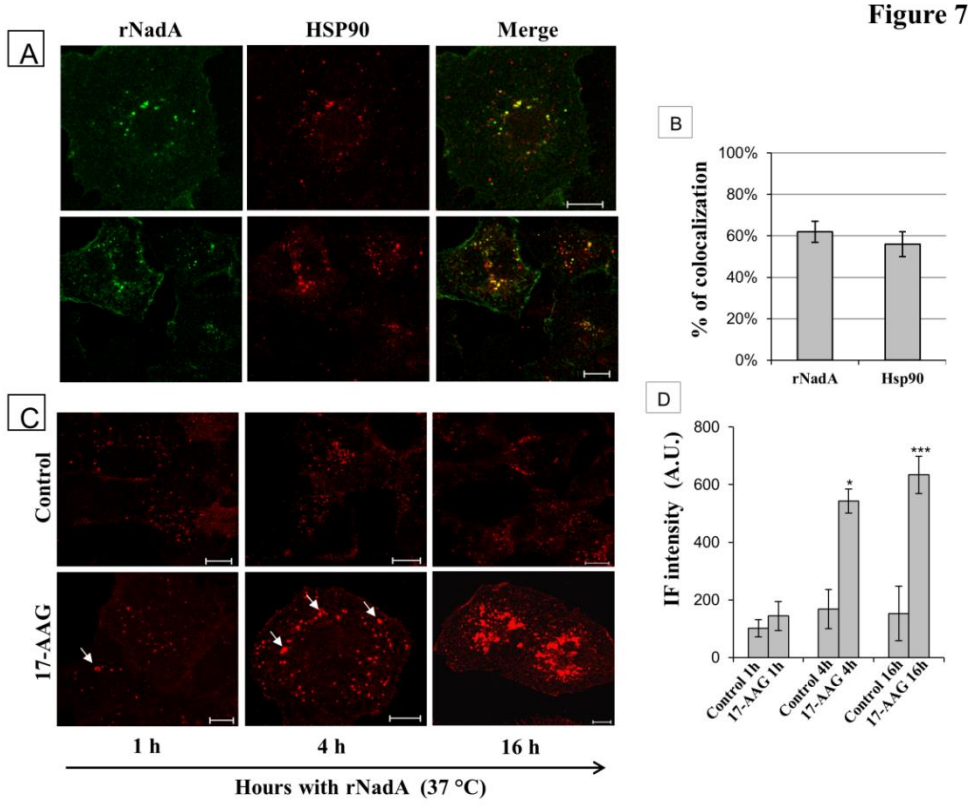

Figure 7: Colocalization of rNadA with HSP90. ***A:*** Chang cells, stained *in vivo* with a rabbit polyclonal anti-HSP90, were incubated with rNadA for 1 h at 37°C, then fixed, permeabilized and double stained for rNadA (green) and HSP90 (red). Panels are taken from two different experiments. Merged images are also shown. Scale bar 10 µm. ***B:*** Quantification of rNadA and Hsp90 colocalization. rNadA column indicate the percentage of rNadA immunofluorescent pixels colocalizing with HSP90 immunofluorescent pixels. Conversely, HSP90 columns indicate the percentage of HSP90 immunofluorescent pixels colocalizing with rNadA immunofluorescent pixels. Data are mean ± s.e.m representative of two independent experiments, each assessing 20–25 cells. ***C:*** Chang cells pre-treated overnight with either vehicle (upper panel) or 0.5 µM 17-AAG (lower panel), were incubated with 200 µg/ml rNadA for 1 h, 4 h and 16 hrs as indicated, then fixed, permeabilized and stained for rNadA (red). Intracellular accumulation of rNadA clusters are indicated by arrows. Scale bar 10 µm. ***D:*** Quantification of IF intensity of rNadA in the experiment illustrated in panel C. Data are mean ± s.e.m representative of two independent experiments, each assessing 20–25 cells, and expressed as Arbitrary Units (A.U.). ***$p<0.001$, compared to 1 h of 17-AAG treated cells (t-test). *$p<0.05$, compared to 1 h of 17-AAG treated cells (t-test).

The functional role of Hsp90 in rNadA internalization was further investigated using the specific Hsp90 inhibitor 17-AAG. Chang cells pre-treated overnight with 0.5 µM of 17-AAG were then incubated with rNadA for 1, 4 and 16 hours. After 1 hour of rNadA incubation in 17-AAG-treated cells, clusters of rNadA appeared as dot-like structures as compared to control inhibitor-untreated cells (figure 7C, left panels and andD).D). At longer times, clusters of rNadA-containing structures increased in size and number resulting in a remarkable accumulation of rNadA within the cells (figure 7C, central panels and andD).D). At 16 hours the intracellular rNadA amount was roughly double in 17-AAG treated cells compared to control cells (figure 7C, right panels and andD).D). Finally, we investigated the rNadA dynamics in 17-AAG treated cells. Chang cells were pre-treated overnight with 0.5 µM 17-AAG, incubated for 1 hour with fluorescent Alexa488-conjugated rNadA, rapidly washed with PBS and a movie recorded as above. In contrast to the rapidly moving rNadA containing carriers of the control cells, in 17-AAG treated cells, carriers containing rNadA appeared less mobile. In addition, their fusion to form larger structures or the emergence of small rNadA carriers from these aggregate appeared less frequent in 17-AAG than in controls (movie S3 and S4).

The functional role of external Hsp90 in rNadA internalization was further explored by means of a synthetic membrane-impermeable inhibitor, the FITC-GA, that specifically target the extracellular population of the chaperone. To verify that FITC-GA did not enter the cells we used the cellular AKT levels as a marker for the functionality of the intracellular chaperone [66]. Hsp90 inhibitors (e.g. 17-AAG) promote the proteasomal degradation of this intracellular kinase. Cells were incubated with medium containing 2.5 and 10 µM of either 17-AAG or FITC-GA for 1, 4, 24 and 48 hrs. At the end of each period, cell lysates were prepared and equal amount of proteins were analyzed by electrophoresis and Western blot to reveal the amount of intracellular AKT. As shown in figure 8A, the levels of AKT did not change until 4 hrs of treatment with the inhibitors (figure 8A, lanes 2–7). At 24 and 48 hrs the intracellular kinase was degraded in cells incubated in presence of 17-AAG at both concentrations (figure 8A, lanes 9–10, 13–14) while its amount was not modified in FITC-GA treated cells (figure 8A, lanes 11–12, 15–16). This result strongly suggested that the Hsp90 inhibitor FITC-GA do not exert any activity on the intracellular population of the chaperone.

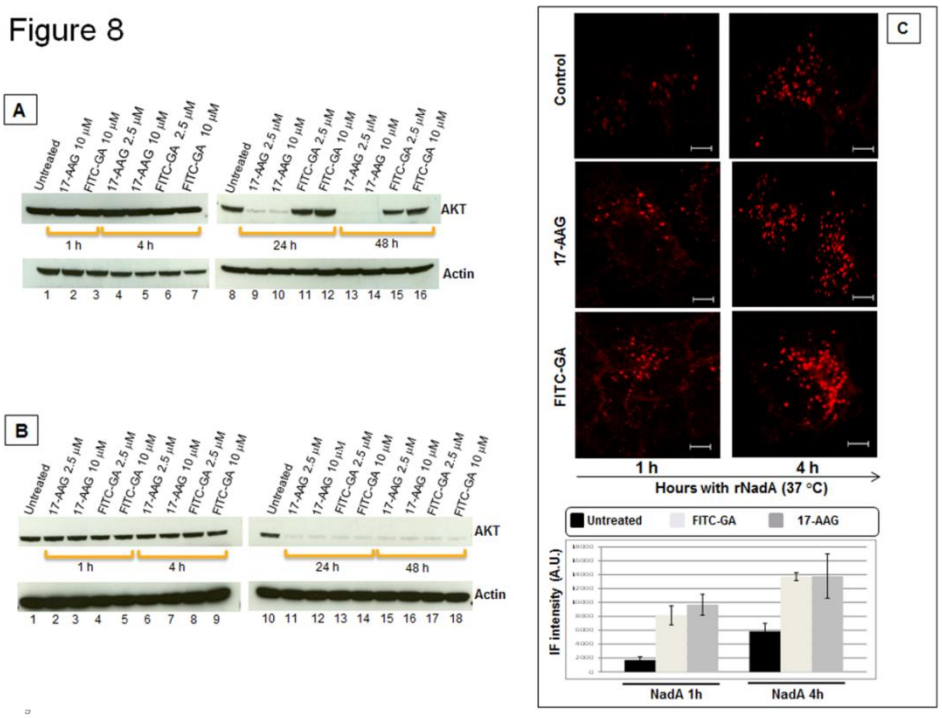

Figure 8: Inhibition of Hsp90 influences AKT degradation and intracellular accumulation of rNadA. ***A:*** Chang cells were incubated for 1, 4, 24 and 48 hours with either 17-AAG or FITC-GA at two different concentrations. At the end of each period cells were washed, trypsinized and RIPA-buffer total lysate prepared. Proteins from each extract were separated on NuSieve gel, blotted, and AKT or Actin (loading control) were detected using the respective primary antibodies. ***B:*** Chang cells were pre-treated with 0.01% saponin in PBS for 30 seconds at room temperature, washed three times with PBS and then handled as described in A. ***C:*** Chang cells were pre-treated for 1 hour with either vehicle (upper panels), 10 µM 17-AAG (middle panel) or 10 µM FITC-GA (lower panel), and then incubated with 200 µg/ml rNadA at 37°C for 1 (left panels) or 4 hours (right panels). Cells were then fixed, permeabilized and stained for rNadA. The drugs were present during the entire incubation period. IF intensity was calculated as mean ± s.e.m in two independent experiments, each assessing 10–15 cells and expressed as Arbitrary Units (A.U.). Scale bar 10 µm.

To verify that the membrane-impermeable inhibitor was an efficient Hsp90 inhibitor, we transiently permeabilized the cells. Chang cells were treated with saponin for 30 seconds in presence of FITC-GA and, once cell integrity was restored, incubated for 1, 4, 24 and 48 hrs. The amount of intracellular AKT was then detected as previously described. As shown in figure 8B, intracellular FITC-GA was revealed to be an efficient Hsp90 inhibitor leading to AKT degradation within 24 hours (figure 8B, lanes 11–18).

Chang cells were preincubated with either 10 µM 17-AAG or 10 µM FITC-GA at 37°C for 1 hr before addition of rNadA, and were further incubated for 1 and 4 hrs in presence of the inhibitors. Cells were then fixed, stained and subjected to confocal microscopy analysis (figure 8C). Compared to the control (upper panel of figure 8C), both inhibitors led to a similar accumulation of intracellular rNadA.

Taken together, the use of these inhibitors confirmed that the rNadA intracellular trafficking is somehow dependent upon functionally active Hsp90 and emphasized the role of the extracellular pool of this chaperone.

Colocalization of rNadA with Rab11 and effect of inhibitors

Our data strongly suggested that rNadA is reclycled back to the plasma membrane and possibly released back to the cell culture medium. Although several Rabs are known to regulate cellular membrane traffic [43], [67], Rab11 has been particularly associated with recycling endosomes and vesicular exocytosis at the plasma membrane [68]. We hypothesized that rNadA was colocalizing with Rab 11. Chang cells were incubated with rNadA for 1 hr and then stained for rNadA and Rab11. Confocal microscopy revealed that vesicles containing rNadA were also associated with Rab11 (figure 9A, upper panel) strongly suggesting that the adhesin moved into a recycling pathway.

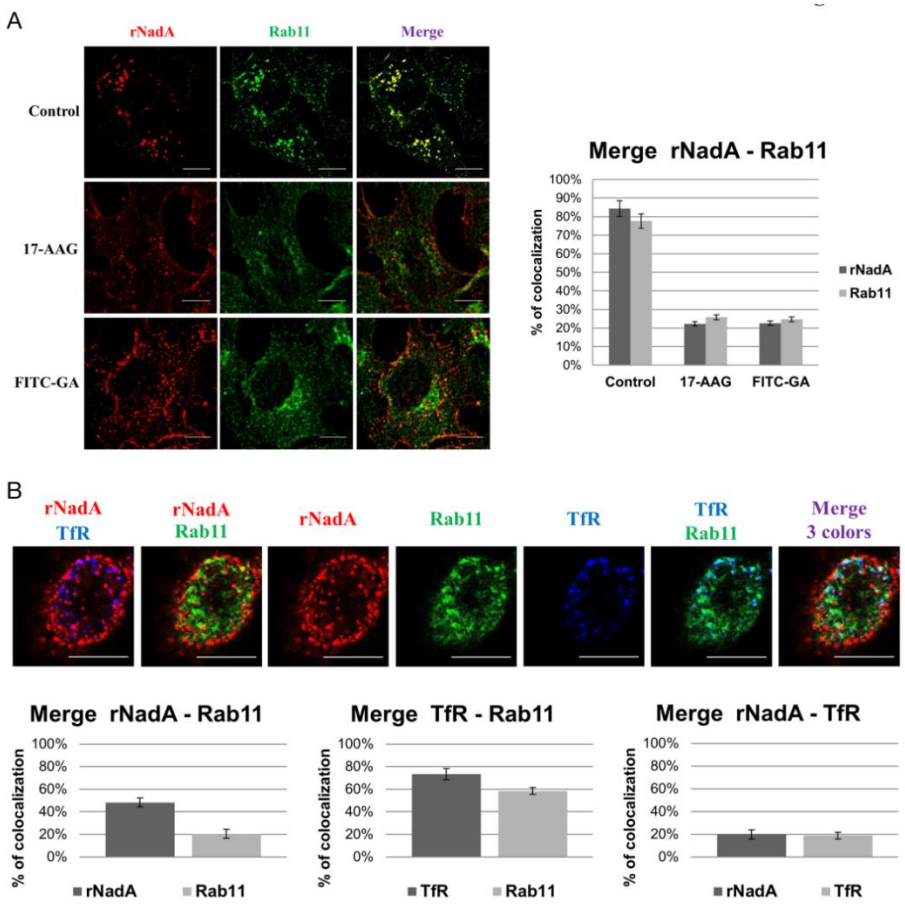

Figure 9: rNada internalization and colocalization with Rab11 and TfR. ***A: rNadA and Rab11 colocalization in presence of inhibitors***. The control untreated Chang cells are shown in the upper panel. Pre-treatment of cells was performed for 1 hour with 10 µM 17-AAG (middle panel) or 10 µM FITC-GA (bottom panel). Cells were then incubated with 200 µg/ml rNadA at 37°C for 1 hour. Afterward, cells were fixed, permeabilized and stained for NadA. The drugs were present during the entire incubation period. *Graph*: rNadA columns indicate the percentage of rNadA immunofluorescent pixels colocalizing with Rab11 immunofluorescent pixels in untreated, 17-AAG and FITC-GA cells (from left to right) respectively. Conversely, Rab11 columns indicate the percentage of Rab11 immunofluorescent pixels colocalizing with rNadA immunofluorescent pixels in untreated, 17-AAG and FITC-GA cells (from left to right) respectively. ***B: Rab11, rNadA and TfR colocalization.*** *A:* Chang cells were transfected with EGFP-Rab11 plasmid, incubated 24 hours at 37°C. and then incubated with 200 µg/ml of rNadA at 37°C for 2 hours. Afterward, cells were fixed, permeabilized and stained for NadA (Red) and TfR (blu). Rab11 is colored in green. *Graphs*: rNadA columns indicate the percentage of rNadA immunofluorescent pixels colocalizing with Rab11 fluorescent pixels (left) or with TfR immunofluorescent pixels (right). Rab11column indicate the percentage of fluorescent pixels colocalizing with rNadA immunofluorescent pixels (left) or TfR immunofluorescent pixels (right). TfR columns indicate the percentage of TfR immunofluorescent pixels colocalizing with Rab11 fluorescent pixels (middle) or with rNadA immunofluorescent pixels (left). Data are mean ± s.e.m representative of two independent experiments, each assessing 20–25 cells.

We also investigated the Rab11-rNadA colocalization in presence of the two Hsp90 inhibitors. Chang cells were pre-treated with 17-AAG, FITC-GA for 1 hr before adding rNadA and allow internalization for one more hr at 37°C in presence of the inhibitors. Confocal microscopy analysis revealed a different cellular distribution of Rab11 in the presence of either drug (figure 9A, middle and lower panels). In the absence of inhibitors, Rab11 was mostly localized in vesicular structures (figure 9A, upper panel). In presence of 17-AAG or FITC-GA the Rab11 cellular pattern was more distributed, with a tendency to perinuclear accumulation (figure 9, middle and lower panels). Interestingly, both 17-AAG (membrane permeable Hsp90 inhibitor) and FITC-GA (membrane-impermeable inhibitor) treatment resulted in the complete loss of Rab11-rNadA colocalization (figure 9, compare right panels) whereas intracellular accumulation of rNadA was observed. Treatment with the Hsp90 inhibitors did not interfere with the co-localization of TfR with Rab11 positive endosomes (figure S3).

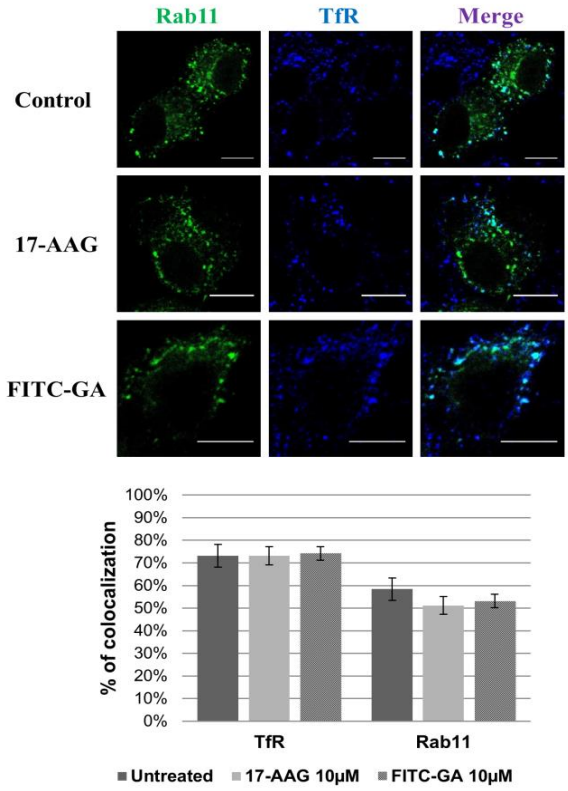

Figure S3: Co-localization of Transferrin receptor with Rab11 in presence of Hsp90 inhibitors. The control untreated Chang cells are shown in the upper panel. Pre-treatment of cells was performed for 1 hour with 10 µM 17-AAG (middle panel) or 10 µM FITC-GA (bottom panel). Chang cells were then fixed, permeabilized and double stained for Rab11 (green) and transferrin receptor (blu). Merged images are also shown. Graph report the percentage of colocalization obtained by 3 independent experiments.

Taken together, these observations indicated that Hsp90 activity was not essential for the formation of vesicles containing rNadA. Rather, it may affect the recruitment of effector molecules necessary for the formation of recycling endosomes.

Due to the high level of colocalization between internalized rNadA and Rab11, we reasoned that it was surprising not to have found rNadA-TfR colocalization in our previous experiment (figure 4E–F). Indeed, TfR recycling, has been reported to rely on Rab11 endosomes [43]. To decipher this apparent contradiction, we performed a simultaneous staining of TfR and Rab11 during rNadA internalization. Chang cells were transfected with an EGFP-Rab11 expressing plasmid and 24 hours later incubated with rNadA for 2 hours. Cells were then fixed and revealed for rNadA and TfR by using specific primary antibodies. Results from confocal microscopy analysis are shown in figure 9B in which, to better discriminate colocalization between pair of proteins, two colors at the time are also shown separately. Furthermore, percentages of colocalization are reported in the graphs of figure 9B.

Confocal microscopy revealed a significant colocalization of rNadA in Rab11 vesicles (figure 9B, upper panel and left graph) although the value was lower than previous experiment. This could be due to the different method used to reveal Rab11 in the experiments of figure 9A and 9B. Whereas physiological levels of Rab11 were detected in figure 9A by specific antibody, overexpression of a fluorescent tagged protein increase the amount of endogenous GTPase and may justify the lower percentage of association. Colocalization of TfR with Rab11 was significantly higher, consistent with data from the literature (figure 9A upper panel and middle graph), but rNadA and TfR did not show contemporary presence in Rab11 vesicles (figure 9B upper panel and right graph).

These data suggest that the rNadA and TfR enter distinct population of Rab11 endosomes. Although surprising, the existence of separate sub-population of Rab11 vesicles has already been observed in a different cell type [69].

Discussion

In this report we have shown that a purified bacterial adhesin binds human epithelial cells and triggers its own internalization. Once internalized, the intracellular trafficking of rNadA avoids lysosome targeting by entering an endosome recycling pathway and is likely transported back to the extracellular space. The extracellular pool of the molecular chaperone Hsp90, a cellular chaperone previously shown to bind rNadA *in vitro* [30], has been identified as a crucial factor for the intracellular trafficking of the meningococcal adhesin. The early steps of rNadA endocytosis remain poorly understood and, in particular, we still have not defined the cellular ligand on the membrane. Binding of rNadA to Chang cells is strongly temperature dependent and it dramatically drops below 30°C. Internalization of the adhesin is a slow event (about 30 min) compared to general mechanisms of endocytosis. In the last decade, the endocytic process has shown a surprising diversity of parallel mechanisms in a single cell [38], [70]. The rNadA entry process in human epithelial cells is clathrin-independent, insensitive to general tyrosine kinases or specific Src inhibitors, and thus excludes the involvement of a caveolin dependent entry pathway [38]. Treatment with the PI3K inhibitor wortmannin, in contrast, led to rNadA accumulation at the cell periphery, consistent with the role played by this kinase in the early steps of vesicle formation [71], [72]. Endocytic vesicles containing rNadA enter an ARF6-regulated trafficking pathway and over-expression of a constitutively activated form of this protein (Q67L) led to the rNadA accumulation in vacuolar structures. Activated ARF6 is described to have a dual role in cells: it promotes internalization at the level of the plasma membrane and is a targeting factor for recycling of cargo to the cell surface [43], [73]. Our data suggested that rNadA could avoid the lysosomes by steering into a recycling route. Thus far, a limited number of proteins have been described to use an ARF6-regulated pathway [43], [63], the list including β1-integrin and MHC-I that are continuously trafficking from endocytic vesicles back to the plasma membrane. Consistent with our results, expression of ARF6 Q67L mutant has been shown to induce vacuolar structures and blocks recycling to the cell surface of both β1-integrin and MHC-I [74]. The hypothesis that rNadA enters a recycling pathway was further reinforced by its significant colocalization with Rab11 coated vesicles. The small GTPase Rab11 is a recognized marker of recycling endosomes, and a crucial factor regulating the exocytic fusion event [43], [67], [68], [75]. Interestingly, stimulation-dependent recycling of β1-integrin follows an Arf-6 and Rab11 dependent pathway [76]. This integrin has been recently indicated as a putative ligand for NadA by using a heterologous system of invasion [77]. In our hands, the anti-β1 antibody failed to impair both binding and internalization of rNadA in Chang cells (GB and MM unpublished results) but, due to the different experimental system used, a role for this integrin in NadA-mediated binding and/or internalization

cannot be ruled out. Intriguingly, we found that Rab11 positive endosomes containing rNadA are distinct from Rab11 positive endosomes carrying TfR, although formation of both populations is PI3K dependent. Although we have not further characterized the identity of these vesicles, the existence of diversified Rab11 endosomes has been recently reported in the rat adrenal phaeochromocytoma cell line PC12 [69].

Our attempts to identify a rNadA cell surface ligand led us to extracellular Hsp90 [30], a finding that was independently supported by another laboratory [53]. In the present paper, we have shown that external Hsp90 internalizes and colocalizes with the rNadA containing endocytic vesicles in live cells, strongly suggesting that the initial interaction between rNadA and Hsp90 takes place in the extracellular milieu. The extracellular presence of Hsp90 has been controversial for a long time, but it is now accepted that secretion of this chaperone occurs in both tumor and normal cells. Moreover, the functions of extracellular Hsp90 do not rely on the classical chaperone ATPase activity [49], [51]. In our previous study we demonstrated a direct binding *in vitro* between rNadA and a complex of Hsp90 and ADP or 17-AAG. Meanwhile, in the presence of ATP, no such binding was observed [30]. Although the internalization of rNadA is not impaired by interfering with Hsp90, the ensuing intracellular trafficking is affected. Here we show that rNadA uptake in presence of the membrane-impermeable Hsp90 inhibitor FITC-GA led to intracellular accumulation of vesicles that contained the adhesin but were unable to engage Rab11. Interaction of rNadA with external Hsp90, thus, would be required to recruit a pattern of effector molecules for the targeting of the adhesin to the recycling endosomes. On the other hand, involvement of Hsp90 activity in intracellular trafficking has been poorly documented in literature. Its activity is required for activation of the Rho family of small G-protein that are known to regulate cytoskeleton rearrangement and endosomal trafficking [78], [79]. Very recently, Cortese et al. reported that recycling of ErbB2 is perturbed by cell treatment with the Hsp90 inhibitor geldanamycin, leading to targeting of the receptor to mixed endosomal compartments [80]. To our knowledge, however, there are no reports on the influence of external Hsp90 on intracellular trafficking. The data presented in this work led us to hypothesize that the binding of rNadA to extracellular Hsp90 may influence a selection of the signaling involved in internalization, but further studies are required to elucidate this aspect. The role of adhesins in meningococcal pathogenesis is thought to be confined to securing the bacteria to the host cell surface, whereas their contribution to bacterial trafficking is unaddressed [4]. We believe that the model exploited in this work, through the dissection of the pathways employed by an individual adhesin, has shed new light on the possible role that “minor” adhesion factors may have in the pathogenesis of bacterial invasion and, in the context of *N. meningitidis*, in transcellular passage through the epithelial barrier.

References

1. Emonts M, Hazelzet JA, de Groot R, Hermans PW (2003) Host genetic determinants of Neisseria meningitidis infections. Lancet Infect Dis 3: 565–577 [PubMed]

2. Stephens DS (2009) Biology and pathogenesis of the evolutionarily successful, obligate human bacterium Neisseria meningitidis. Vaccine 27 Suppl 2: B71–77 [PMC free article] [PubMed]

3. Hill DJ, Griffiths NJ, Borodina E, Virji M (2010) Cellular and molecular biology of Neisseria meningitidis colonization and invasive disease. Clin Sci (Lond) 118: 547–564 [PMC free article] [PubMed]

4. Virji M (2009) Pathogenic neisseriae: surface modulation, pathogenesis and infection control. Nat Rev Microbiol 7: 274–286 [PubMed]

5. Carbonnelle E, Hill DJ, Morand P, Griffiths NJ, Bourdoulous S, et al. . (2009) Meningococcal interactions with the host. Vaccine 27 Suppl 2: B78–89 [PubMed]

6. Stephens DS, Hoffman LH, McGee ZA (1983) Interaction of Neisseria meningitidis with human nasopharyngeal mucosa: attachment and entry into columnar epithelial cells. J Infect Dis 148: 369–376 [PubMed]

7. Birkness KA, Swisher BL, White EH, Long EG, Ewing EP Jr, et al. . (1995) A tissue culture bilayer model to study the passage of Neisseria meningitidis. Infect Immun 63: 402–409 [PMC free article] [PubMed]

8. Pujol C, Eugene E, de Saint Martin L, Nassif X (1997) Interaction of Neisseria meningitidis with a polarized monolayer of epithelial cells. Infect Immun 65: 4836–4842 [PMC free article] [PubMed]

9. Sutherland TC, Quattroni P, Exley RM, Tang CM (2010) Transcellular passage of Neisseria meningitidis across a polarized respiratory epithelium. Infect Immun 78: 3832–3847 [PMC free article] [PubMed]

10. Capecchi B, Adu-Bobie J, Di Marcello F, Ciucchi L, Masignani V, et al. . (2005) Neisseria meningitidis NadA is a new invasin which promotes bacterial adhesion to and penetration into human epithelial cells. Mol Microbiol 55: 687–698 [PubMed]

11. Scarselli M, Serruto D, Montanari P, Capecchi B, Adu-Bobie J, et al. . (2006) Neisseria meningitidis NhhA is a multifunctional trimeric autotransporter adhesin. Mol Microbiol 61: 631–644 [PubMed]

12. Pizza M, Scarlato V, Masignani V, Giuliani MM, Arico B, et al. . (2000) Identification of vaccine candidates against serogroup B meningococcus by whole-genome sequencing. Science 287: 1816–1820 [PubMed]

13. Comanducci M, Bambini S, Brunelli B, Adu-Bobie J, Arico B, et al. . (2002) NadA, a novel vaccine candidate of Neisseria meningitidis. J Exp Med 195: 1445–1454 [PMC free article] [PubMed]

14. Comanducci M, Bambini S, Caugant DA, Mora M, Brunelli B, et al. . (2004) NadA diversity and carriage in Neisseria meningitidis. Infect Immun 72: 4217–4223 [PMC free article] [PubMed]

15. Cotter SE, Surana NK, St Geme JW 3rd (2005) Trimeric autotransporters: a distinct subfamily of autotransporter proteins. Trends Microbiol 13: 199–205 [PubMed]

16. Linke D, Riess T, Autenrieth IB, Lupas A, Kempf VA (2006) Trimeric autotransporter adhesins: variable structure, common function. Trends Microbiol 14: 264–270 [PubMed]

17. Surana NK, Cutter D, Barenkamp SJ, St Geme JW 3rd (2004) The Haemophilus influenzae Hia autotransporter contains an unusually short trimeric translocator domain. J Biol Chem 279: 14679–14685 [PubMed]

18. Lyskowski A, Leo JC, Goldman A (2011) Structure and biology of trimeric autotransporter adhesins. Adv Exp Med Biol 715: 143–158 [PubMed]

19. Dautin N, Bernstein HD (2007) Protein secretion in gram-negative bacteria via the autotransporter pathway. Annu Rev Microbiol 61: 89–112 [PubMed]

20. Roggenkamp A, Ackermann N, Jacobi CA, Truelzsch K, Hoffmann H, et al. . (2003) Molecular analysis of transport and oligomerization of the Yersinia enterocolitica adhesin YadA. J Bacteriol 185: 3735–3744 [PMC free article] [PubMed]

21. Yang Y, Isberg RR (1993) Cellular internalization in the absence of invasin expression is promoted by the Yersinia pseudotuberculosis yadA product. Infect Immun 61: 3907–3913 [PMC free article] [PubMed]

22. McMichael JC, Fiske MJ, Fredenburg RA, Chakravarti DN, VanDerMeid KR, et al. . (1998) Isolation and characterization of two proteins from Moraxella catarrhalis that bear a common epitope. Infect Immun 66: 4374–4381 [PMC free article] [PubMed]

23. Laarmann S, Cutter D, Juehne T, Barenkamp SJ, St Geme JW (2002) The Haemophilus influenzae Hia autotransporter harbours two adhesive pockets that reside in the passenger domain and recognize the same host cell receptor. Mol Microbiol 46: 731–743 [PubMed]

24. Zhang P, Chomel BB, Schau MK, Goo JS, Droz S, et al. . (2004) A family of variably expressed outer-membrane proteins (Vomp) mediates adhesion and autoaggregation in Bartonella quintana. Proc Natl Acad Sci U S A 101: 13630–13635 [PMC free article] [PubMed]

25. O'Rourke F, Schmidgen T, Kaiser PO, Linke D, Kempf VA (2011) Adhesins of Bartonella spp. Adv Exp Med Biol 715: 51–70 [PubMed]

26. Serruto D, Spadafina T, Scarselli M, Bambini S, Comanducci M, et al. . (2009) HadA is an atypical new multifunctional trimeric coiled-coil adhesin of Haemophilus influenzae biogroup aegyptius, which promotes entry into host cells. Cell Microbiol 11: 1044–1063 [PubMed]

27. El Tahir Y, Skurnik M (2001) YadA, the multifaceted Yersinia adhesin. Int J Med Microbiol 291: 209–218 [PubMed]

28. Hill DJ, Virji M (2003) A novel cell-binding mechanism of Moraxella catarrhalis ubiquitous surface protein UspA: specific targeting of the N-domain of carcinoembryonic antigen-related cell adhesion molecules by UspA1. Mol Microbiol 48: 117–129 [PubMed]

29. Riess T, Andersson SG, Lupas A, Schaller M, Schafer A, et al. . (2004) Bartonella adhesin a mediates a proangiogenic host cell response. J Exp Med 200: 1267–1278 [PMC free article] [PubMed]

30. Montanari P, Bozza G, Capecchi B, Caproni E, Barrile R, et al. . (2012) Human heat shock protein (Hsp) 90 interferes with Neisseria meningitidis adhesin A (NadA)-mediated adhesion and invasion. Cell Microbiol 14: 368–385 [PubMed]

31. Bowe F, Lavelle EC, McNeela EA, Hale C, Clare S, et al. . (2004) Mucosal vaccination against serogroup B meningococci: induction of bactericidal antibodies and cellular immunity following intranasal

immunization with NadA of Neisseria meningitidis and mutants of Escherichia coli heat-labile enterotoxin. Infect Immun 72: 4052–4060 [PMC free article] [PubMed]

32. Litt DJ, Savino S, Beddek A, Comanducci M, Sandiford C, et al. . (2004) Putative vaccine antigens from Neisseria meningitidis recognized by serum antibodies of young children convalescing after meningococcal disease. J Infect Dis 190: 1488–1497 [PubMed]

33. Magagnoli C, Bardotti A, De Conciliis G, Galasso R, Tomei M, et al. . (2009) Structural organization of NadADelta(351-405), a recombinant MenB vaccine component, by its physico-chemical characterization at drug substance level. Vaccine 27: 2156–2170 [PubMed]

34. Mazzon C, Baldani-Guerra B, Cecchini P, Kasic T, Viola A, et al. . (2007) IFN-gamma and R-848 dependent activation of human monocyte-derived dendritic cells by Neisseria meningitidis adhesin A. J Immunol 179: 3904–3916 [PubMed]

35. Franzoso S, Mazzon C, Sztukowska M, Cecchini P, Kasic T, et al. . (2008) Human monocytes/macrophages are a target of Neisseria meningitidis Adhesin A (NadA). J Leukoc Biol 83: 1100–1110 [PubMed]

36. McMahon HT, Boucrot E (2011) Molecular mechanism and physiological functions of clathrin-mediated endocytosis. Nat Rev Mol Cell Biol 12: 517–533 [PubMed]

37. Mayor S, Pagano RE (2007) Pathways of clathrin-independent endocytosis. Nat Rev Mol Cell Biol 8: 603–612 [PubMed]

38. Doherty GJ, McMahon HT (2009) Mechanisms of endocytosis. Annu Rev Biochem 78: 857–902 [PubMed]

39. Huotari J, Helenius A (2011) Endosome maturation. EMBO J 30: 3481–3500 [PMC free article] [PubMed]

40. Saftig P, Klumperman J (2009) Lysosome biogenesis and lysosomal membrane proteins: trafficking meets function. Nat Rev Mol Cell Biol 10: 623–635 [PubMed]

41. Sandvig K, Pust S, Skotland T, van Deurs B (2011) Clathrin-independent endocytosis: mechanisms and function. Curr Opin Cell Biol 23: 413–420 [PubMed]

42. Donaldson JG, Porat-Shliom N, Cohen LA (2009) Clathrin-independent endocytosis: a unique platform for cell signaling and PM remodeling. Cell Signal 21: 1–6 [PMC free article] [PubMed]

43. Grant BD, Donaldson JG (2009) Pathways and mechanisms of endocytic recycling. Nat Rev Mol Cell Biol 10: 597–608 [PMC free article] [PubMed]

44. Radhakrishna H, Donaldson JG (1997) ADP-ribosylation factor 6 regulates a novel plasma membrane recycling pathway. J Cell Biol 139: 49–61 [PMC free article] [PubMed]

45. D'Souza-Schorey C, Chavrier P (2006) ARF proteins: roles in membrane traffic and beyond. Nat Rev Mol Cell Biol 7: 347–358 [PubMed]

46. Jean S, Kiger AA (2012) Coordination between RAB GTPase and phosphoinositide regulation and functions. Nat Rev Mol Cell Biol 13: 463–470 [PubMed]

47. Hutagalung AH, Novick PJ (2011) Role of Rab GTPases in membrane traffic and cell physiology. Physiol Rev 91: 119–149 [PMC free article] [PubMed]

48. Li J, Soroka J, Buchner J (2012) The Hsp90 chaperone machinery: Conformational dynamics and regulation by co-chaperones. Biochim Biophys Acta 1823: 624–635 [PubMed]

49. Li W, Sahu D, Tsen F (2012) Secreted heat shock protein-90 (Hsp90) in wound healing and cancer. Biochim Biophys Acta 1823: 730–741 [PMC free article] [PubMed]

50. Tsutsumi S, Neckers L (2007) Extracellular heat shock protein 90: a role for a molecular chaperone in cell motility and cancer metastasis. Cancer Sci 98: 1536–1539 [PubMed]

51. Schmitt E, Gehrmann M, Brunet M, Multhoff G, Garrido C (2007) Intracellular and extracellular functions of heat shock proteins: repercussions in cancer therapy. J Leukoc Biol 81: 15–27 [PubMed]

52. Binder RJ, Vatner R, Srivastava P (2004) The heat-shock protein receptors: some answers and more questions. Tissue Antigens 64: 442–451 [PubMed]

53. Cecchini P, Tavano R, Polverino de Laureto P, Franzoso S, Mazzon C, et al. . (2011) The soluble recombinant Neisseria meningitidis adhesin NadA(Delta351-405) stimulates human monocytes by binding to extracellular Hsp90. PLoS One 6: e25089. [PMC free article] [PubMed]

54. Ford MG, Pearse BM, Higgins MK, Vallis Y, Owen DJ, et al. . (2001) Simultaneous binding of PtdIns(4,5)P2 and clathrin by AP180 in the nucleation of clathrin lattices on membranes. Science 291: 1051–1055 [PubMed]

55. Rojas R, van Vlijmen T, Mardones GA, Prabhu Y, Rojas AL, et al. . (2008) Regulation of retromer recruitment to endosomes by sequential action of Rab5 and Rab7. J Cell Biol 183: 513–526 [PMC free article] [PubMed]

56. Delom F, Fessart D (2011) Role of Phosphorylation in the Control of Clathrin-Mediated Internalization of GPCR. Int J Cell Biol 2011: 246954. [PMC free article] [PubMed]

57. Shajahan AN, Tiruppathi C, Smrcka AV, Malik AB, Minshall RD (2004) Gbetagamma activation of Src induces caveolae-mediated endocytosis in endothelial cells. J Biol Chem 279: 48055–48062 [PubMed]

58. Cha SK, Wu T, Huang CL (2008) Protein kinase C inhibits caveolae-mediated endocytosis of TRPV5. Am J Physiol Renal Physiol 294: F1212–1221 [PubMed]

59. Alvi F, Idkowiak-Baldys J, Baldys A, Raymond JR, Hannun YA (2007) Regulation of membrane trafficking and endocytosis by protein kinase C: emerging role of the pericentrion, a novel protein kinase C-dependent subset of recycling endosomes. Cell Mol Life Sci 64: 263–270 [PubMed]

60. Naslavsky N, Weigert R, Donaldson JG (2003) Convergence of non-clathrin- and clathrin-derived endosomes involves Arf6 inactivation and changes in phosphoinositides. Mol Biol Cell 14: 417–431 [PMC free article] [PubMed]

61. Sharma DK, Brown JC, Choudhury A, Peterson TE, Holicky E, et al. . (2004) Selective stimulation of caveolar endocytosis by glycosphingolipids and cholesterol. Mol Biol Cell 15: 3114–3122 [PMC free article] [PubMed]

62. Zhao X, Greener T, Al-Hasani H, Cushman SW, Eisenberg E, et al. . (2001) Expression of auxilin or AP180 inhibits endocytosis by mislocalizing clathrin: evidence for formation of nascent pits containing AP1 or AP2 but not clathrin. J Cell Sci 114: 353–365 [PubMed]

63. Eyster CA, Higginson JD, Huebner R, Porat-Shliom N, Weigert R, et al. . (2009) Discovery of new cargo proteins that enter cells through clathrin-independent endocytosis. Traffic 10: 590–599 [PMC free article] [PubMed]

64. Eyster CA, Cole NB, Petersen S, Viswanathan K, Fruh K, et al. . (2011) MARCH ubiquitin ligases alter the itinerary of clathrin-independent cargo from recycling to degradation. Mol Biol Cell 22: 3218–3230 [PMC free article] [PubMed]

65. Zagorac GB, Mahmutefendic H, Tomas MI, Kucic N, Le Bouteiller P, et al. . (2012) Early endosomal rerouting of major histocompatibility class I conformers. J Cell Physiol 227: 2953–2964 [PubMed]

66. Powers MV, Workman P (2006) Targeting of multiple signalling pathways by heat shock protein 90 molecular chaperone inhibitors. Endocr Relat Cancer 13 Suppl 1: S125–135 [PubMed]

67. Stenmark H (2009) Rab GTPases as coordinators of vesicle traffic. Nat Rev Mol Cell Biol 10: 513–525 [PubMed]

68. Takahashi S, Kubo K, Waguri S, Yabashi A, Shin HW, et al. . (2012) Rab11 regulates exocytosis of recycling vesicles at the plasma membrane. J Cell Sci 125: 4049–4057 [PubMed]

69. Kobayashi H, Fukuda M (2013) Arf6, Rab11 and transferrin receptor define distinct populations of recycling endosomes. Commun Integr Biol 6: e25036. [PMC free article] [PubMed]

70. Kumari S, Mg S, Mayor S (2010) Endocytosis unplugged: multiple ways to enter the cell. Cell Res 20: 256–275 [PubMed]

71. Amyere M, Payrastre B, Krause U, Van Der Smissen P, Veithen A, et al. . (2000) Constitutive macropinocytosis in oncogene-transformed fibroblasts depends on sequential permanent activation of phosphoinositide 3-kinase and phospholipase C. Mol Biol Cell 11: 3453–3467 [PMC free article] [PubMed]

72. Araki N, Egami Y, Watanabe Y, Hatae T (2007) Phosphoinositide metabolism during membrane ruffling and macropinosome formation in EGF-stimulated A431 cells. Exp Cell Res 313: 1496–1507 [PubMed]

73. Schweitzer JK, Sedgwick AE, D'Souza-Schorey C (2011) ARF6-mediated endocytic recycling impacts cell movement, cell division and lipid homeostasis. Semin Cell Dev Biol 22: 39–47 [PMC free article] [PubMed]

74. Brown FD, Rozelle AL, Yin HL, Balla T, Donaldson JG (2001) Phosphatidylinositol 4,5-bisphosphate and Arf6-regulated membrane traffic. J Cell Biol 154: 1007–1017 [PMC free article] [PubMed]

75. Ullrich O, Reinsch S, Urbe S, Zerial M, Parton RG (1996) Rab11 regulates recycling through the pericentriolar recycling endosome. J Cell Biol 135: 913–924 [PMC free article] [PubMed]

76. Powelka AM, Sun J, Li J, Gao M, Shaw LM, et al. . (2004) Stimulation-dependent recycling of integrin beta1 regulated by ARF6 and Rab11. Traffic 5: 20–36 [PubMed]

77. Nagele V, Heesemann J, Schielke S, Jimenez-Soto LF, Kurzai O, et al. . (2011) Neisseria meningitidis adhesin NadA targets beta1 integrins: functional similarity to Yersinia invasin. J Biol Chem 286: 20536–20546 [PMC free article] [PubMed]

78. Amiri A, Noei F, Feroz T, Lee JM (2007) Geldanamycin anisimycins activate Rho and stimulate Rho- and ROCK-dependent actin stress fiber formation. Mol Cancer Res 5: 933–942 [PubMed]

79. Yang W, Jansen JM, Lin Q, Canova S, Cerione RA, et al. . (2004) Interaction of activated Cdc42-associated tyrosine kinase ACK2 with HSP90. Biochem J 382: 199–204 [PMC free article] [PubMed]

80. Cortese K, Howes MT, Lundmark R, Tagliatti E, Bagnato P, et al. . (2013) The HSP90 inhibitor geldanamycin perturbs endosomal structure and drives recycling ErbB2 and transferrin to modified MVBs/lysosomal compartments. Mol Biol Cell 24: 129–144 [PMC free article] [PubMed]

4.2 Material and methods

4.2.1 Hydrogen and deuterium exchange (HDX)

4.2.1.1 Sample preparation for HDX-MS analysis

The hydrogen-deuterium exchange (HDX) experiments of NadA, with and without the recombinant Hsp90, were performed in the same experimental session. The antigen/interactor complex was formed by adding 250 pmol NadA3 vaccine antigen ($NadA_{\Delta 351\text{-}405}$) to Hsp90, using a molar ratio of 1:1 and incubated for 30 minnutes at room for the equilibration step. The labelling was initiated by adding the proper deuterated buffer at pH of 7 (300 mM KCl; 10 mM $MgCl_2$; 0.81 Na_2HPO_4; 0.19 mM KH_2PO_4; 13.7 mM NaCl, plus the addition of 50mM ADP and 1mM DTT final), reaching a deuterium excess of 93.3%. The labelling reaction was performed at room temperature. Over the time course of the experiment (ranging from 30 seconds to 1 hour), 30 mL of the sample was removed and quenched with the same volume of an ice-cold 200 mM sodium phosphate buffer added with 4 M guanidinium chloride, to dissociate the antigen/interactor complex and to lower the pH to 2.4. In parallel, a control experiment without Hsp90 was prepared using the same conditions previously described (PBS was used instead of the interactor preparation). All quenched samples were immediately flash frozen in liquid nitrogen, stored at -80°C and treated for analysis within the following 24 hours.

4.2.1.2 Local HDX-MS analysis

Labelled samples were thawed rapidly to 0°C and injected into a nanoacquity ultra-performance liquid chromatography (UPLC) system (Waters, Milford, MA, USA) with HDX technology. The injector, switching valve, columns, solvents and all associated tubings were kept at 0°C to limit back exchange. For local HDX-MS, protein samples were online digested for 2.5 minutes at 20°C with a flow rate of 200 µL/min using a Poroszyme Immobilized Pepsin Cartridge (2.1 x 20 mm; Applied Biosystems, Foster City, CA, USA) equilibrated with 100% buffer A (0.1% formic acid in water). The generated peptides were immediately trapped, concentrated, and desalted using a VanGuard ethylene bridged hybrid (BEH) pre-column (1.7 µm, 2.1 x 5mm; Waters). The 2.5 min digestion and desalting step allows deuteron atoms located at fast exchanging sites (e.g., side chains, exposed loops, and N/C termini) to be replaced with hydrogens. Peptides were then separated on an Acquity UPLC BEH C18 reverse-phase column (1.7 µm, 1.0 x 100 mm;

Waters) with a linear gradient from 15 to 45% solvent B [acetonitrile:water (9:1), 0.1% formic acid] over 6.8 min at 40 µL/min.

4.2.1.3 Mass spectra acquisition and interpretation

Mass spectra were acquired in resolution mode (m/z 100–2000) on a Waters SynaptG2 mass spectrometer equipped with a standard electrospray ionization source. Mass accuracy was ensured by continuously infusing a green fluorescent protein solution (600fmol/µL in 50% acetonitrile, 0.1% formic acid) through the reference probe of the electrospray ionization source. The identity of each peptide was confirmed by mass spectrometry elevated energy analyses. All fragmentations were performed using argon as collision gas. Data were processed using ProteinLynx Global Server 2.5 (Waters), and each fragmentation spectrum was manually inspected to confirm the assignment. Only peptic peptides present in at least 3 repeated digestions of the unlabelled proteins were considered for the analysis. Deuterium uptake of each peptide is calculated as the difference between extracted centroid mass of each undeuterated peptic peptide and respective deuterium-labeling time point peptide using DynamX software (Weis, Engen, and Kass 2006).

4.3 Results

4.3.1 Identification of the NadA/Hsp90 interacting region

To locate accurately the NadA region involved in the binding with Hsp90, mapping by hydrogen–deuterium exchange (HDX)-MS was performed. The HDX approach is based on the differential rate of deuterium incorporation by an antigen when it is free or bound to the partner protein/receptor following incubation in appropriate deuterated solvents. The rate at which backbone amide hydrogens exchange in solution is directly dependent on the dynamics and structure of the protein. When a protein complex forms, the interface between the binding partners can occlude solvent accessibility, reducing the exchange rate (Hager-Braun and Tomer 2005). Mapping by HDX-MS was performed in 2 parallel steps as described above. Deuterium incorporation was performed on NadA alone (reference experiment) and on the complex with Hsp90. Both samples were digested by pepsin, and deuterium incorporation was monitored for 73 peptides covering 98% of NadA sequence (data not shown) and compared. HDX-MS analysis of NadA revealed that H-D exchange was reduced in the presence of Hsp90 for the three consecutive peptides (Ala^{24}-Ala^{37}; Val^{36}-Asp^{59} and Ile^{60}-Leu^{93}). In addition the NadA peptides Phe^{51}-Asp^{59} and Thr^{72}-Leu^{84} were not affected by deuterium protection when bound to Hsp90 (Fig. 9). As result the binding region involved the NadA segments Ala^{24}-Gly^{50}; Ile^{60}-Ala^{71} and Gly^{85}-Leu^{93} forming a conformational region of interaction located in the head domain of the protein, as mapped on the NadA3 homology model (Fig. 9).

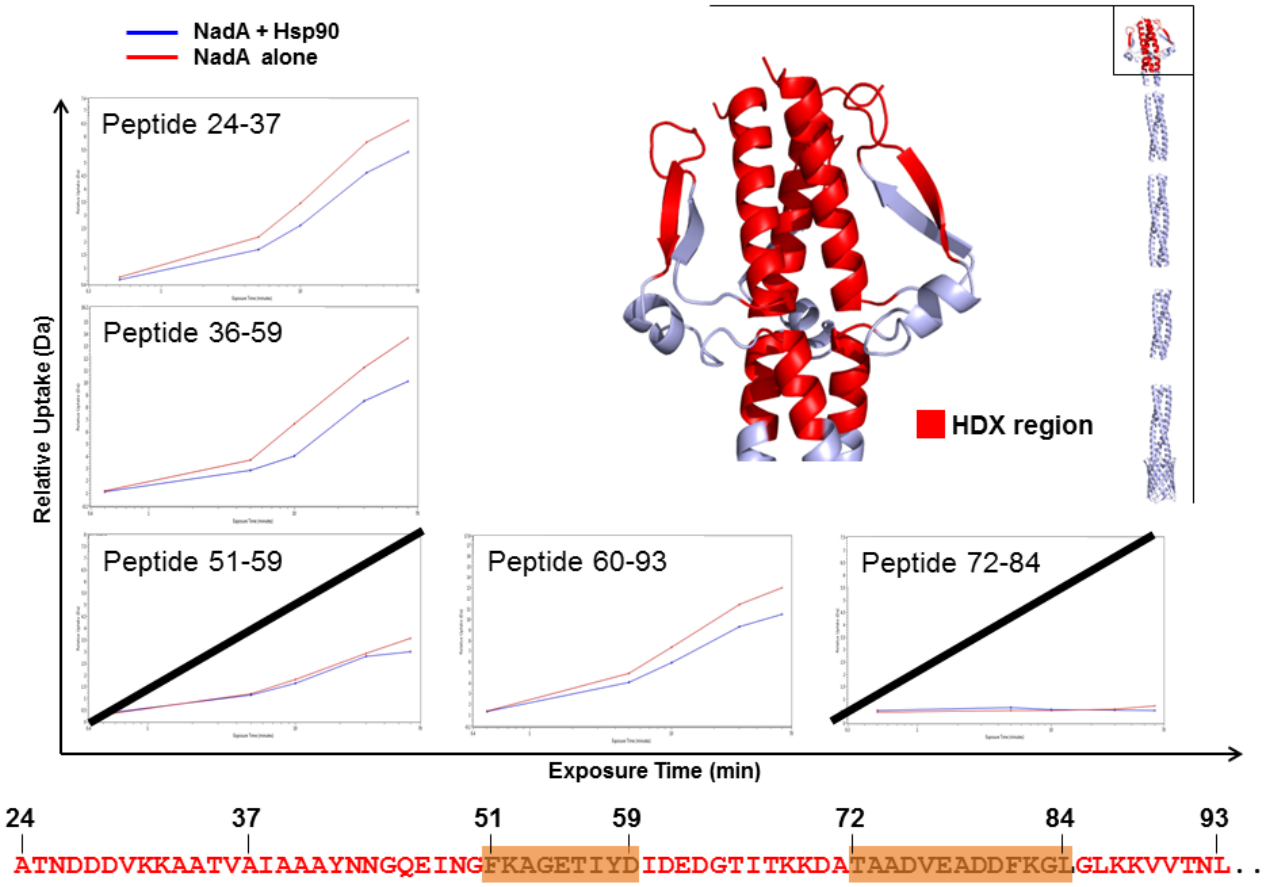

Fig. 9: Time course of deuterium incorporation for the peptides covering the NadA head domain. Deuterium uptake of each peptide is calculated as the difference between extracted centroid mass of each undeuterated peptic peptide and respective deuterium-labeling time point peptide using DynamX software. The blue curves are derived from complex NadA–Hsp90, whereas the red curves are derived from NadA alone. The 3 peptides showing a significant difference in deuterium uptake between the free and bound NadA forms are Ala^{24}-Ala^{37}; Val^{36}-Asp^{59} and Ile^{60}-Leu^{93} while the 2 peptides not affected by deuterium protection are highlighted with a black bar (peptide Phe^{51}-Asp^{59} and Thr^{72}-Leu^{84}). The figure also reports the amminoacid sequence and the *in silico* model of NadA variant 3 head domain built from the X-ray structure of NadA variant 5. Dashes show regions with low sequence homology or unknown secondary structure (Malito et al. 2014). The NadA/Hsp90 interacting region (peptide la^{24}-Gly^{50}; Ile^{60}-Ala^{71} and Gly^{85}-Leu^{93}) is colored in red.

5 Investigating NadA role in the bloodstream

5.1 Material and methods

5.1.1 NadA and NadA constructs cloning, expression, purification and characterization

The *nadA* gene fragments from *N. meningitidis* strain 2996 were cloned by PCR, using the polymerase incomplete primer extension (PIPE) method, as described previously (Malito et al. 2014). The cloned fragments, lacking of the first 23 residues of NadA which encode a signal peptide, were inserted into a pET-21 vector (Novagen), enabling cytoplasmic expression of the NadA proteins with a C-terminal 6xHis tag, and expressed in *Escherichia coli* BL21D3 ($T1^R$) as described by Scietti et all (Scietti et al. 2016).

5.1.2 Protein microarray construction, processing and data analysis

The Genomics Institute of the Novartis Research Foundation protein microarrays (GNF PATH) were generated by spotting about 7000 recombinant soluble proteins (almost 6500 human and 500 mouse proteins) (0.5mg/mL in a final glycerol concentration of 40%) from the GNF library, which were produced as described by Gonzalez et al. (Gonzalez et al. 2010)). Each protein was spotted in duplicates per array onto ultra-thin nitrocellulose coated glass slides (PATH slides; Grace Bio Labs) using the ink-jet spotter Marathon (Arrayjet) resulting in spots of ~150 µm in diameter. Printing was performed in a cabinet with controlled humidity and temperature (55-60% and 12°C respectively). A Chrompure human IgG (Jackson IR 009-000-003) was printed at 0.4 fmol per spot several times on each single block and served as a printing control and to define the blocks.

Since all proteins of the library have a 6-His tag and approximatively 1/3 have an additional mouse Fc-tag, the printing efficiency of the proteins and the microarray quality was evaluated by probing the microarrays with a mouse anti-His antibody (Sigma H1029) followed by a detection using AlexaFluor®647-conjugated anti-mouse IgG secondary antibody (Jackson Immunoresearch).

Nonspecific binding was minimized by preincubating arrays with a blocking solution (BlockIt, ArrayIt) for 1 hour. rNadA was diluted in Nap-PBS at final concentration of 1µM and overlaid on the arrays at RT for 1 h. After washing with 0.1% Tween 20 in PBS buffer (TPBS), arrays were incubated with rabbit polyclonal serum against NadA (diluted 1:2000) at RT for 1 h. Slides were washed again as before and interactions were detected by incubating with an AlexaFluor®647-conjugated anti-rabbit IgG secondary antibody (Jackson Immunoresearch). Fluorescence images were obtained using Power scanner (Tecan Trading AG, Switzerland) and the 16-bit images were generated with PowerScanner software v1.2 at 10 µm/pixel resolution and spot fluorescence intensities were determined using ImaGene 7.0 software (Biodiscovery Inc.). Microarray data analysis was performed using in-house developed software. For each protein, the mean fluorescence intensity (MFI) of replicated spots was determined, after subtraction of the background value surrounding each spot.

Proteins with a high coefficient variation (CV) between the two replicates were discarded. All obtained MFI score (excluding the ones found in the control microarray where the AlexaFluor®647-conjugated anti-rabbit IgG alone were probed to determine its non-specific binding to the printed proteins) were classified in four categories:

- High reactivity: MFI>30000
- Medium reactivity 15000>MFI>30000
- Low reactivity 5000>MFI>15000
- No reactivity MFI<5000

5.1.3 RNA extraction, cDNA synthesis and sequencing

Total RNA was used as a template for cDNA synthesis in RT-PCR. Total RNA was extracted from THP-1 monocytic cells with the Purelink RNA mini kit (Ambion 12183018A) according to manufacturer's protocol. Briefly, cells were lysed in Lysis buffer with addition of β-mercaptoethanol and homogenized passing the lysate 5–10 times through an 18–21-gauge needle attached to an RNase-free syringe. 70% ethanol was

added to the sample and the mixture transferred to a Spin Cartridge. Total RNA was recovered after two washes of the column followed by elution with RNase–Free Water.

In order to remove contaminating DNA from RNA preparation a DNase treatment was performed using the RQ1 RNase-Free DNase kit (Promega Cat.# M6101). The integrity and quantity of total RNA was checked spectrophotometrically and by gel electrophoresis.

The SuperScript™ III Reverse Transcriptase (Invitrogen) was then used for first-strand cDNA synthesis. Following manufacturer's instructions a 20 µl reaction volume was realized by adding 1 µl random primers (50 ng/µl) (Invitrogen), 10 pg to 5 µg total RNA, 1 µl dNTP Mix (10 mM) and sterile RNase–Free Water to 13 µl. The sample was heated at 65°C for 5 min, incubated on ice for at least 1 min and then 4 µl 5X First-Strand Buffer (250 mM Tris-HCl [pH 8.3], 375 mM KCl, 15 mM $MgCl_2$), 1 µl DTT (0.1M), 1 µl RNaseOUT™ Recombinant RNase Inhibitor (40 units/µl) and 1 µl of SuperScript™ III RT (200 units/µl) were added. The mixture was incubated at 25°C for 5 min followed by a second incubation at 50°C for 50 min. The reaction was then inactivated by heating at 70°C for 15 min and the resulting cDNA was used as a template for amplification in Reverse Transcription polymerase chain reaction (RT-PCR).

5.1.4 Plasmid construction

The full-length coding region of Siglec 5, Siglec 14 and Siglec 9 (GenBank accession N° NP_003821.1; NP_001092082.1; NP_055256.1 respectively) were obtained from GeneCopoeia as pEZ-M14 FLAG-tag vectors while the full-length coding region of human and mouse FcγRIIA (GenBank accession N° NP_001129691.1 and N° XP_006496722.1 respectively) were obtained from GeneArt as pCDNA3.1 Strep-tag vector.

In order to express the full-length proteins with a fluorescent tag the full-length coding regions were subcloned into the mammalian expression vector pEYFP_N1 and pECFP_N1 with the use of PCR. The ligation products were transformed into *E. coli DH5α* (Invitrogen). DNA cloning and *E. coli* transformations were performed according to the standard protocols (Sambrook et al., 1989). All the constructs were confirmed by sequencing prior use.

5.1.5 Expression and Purification of the Recombinant Soluble proteins

The cDNA encoding the Siglecs predicted extracellular domain (Siglec 5 residues 1-437; Siglec 14 residues 1-352; Siglec 9 residues 1-330) were subcloned into a pFUSE-IgG1-Fc2e3 vector (Invivogen, San Diego, CA, USA) containing sequences encoding the mouse IL-2 signal peptide and a modified Fc region of human IgG1; while the human and mouse FcγRIIA (residues 34-217 and 38-216 respectively) into a pSecTag2 B vector (Invitrogen) containing sequences encoding the murine Ig k-chain V-J2-C signal peptide and a myc/6xHis tag.

All described constructs were expressed into Expi293F cells according to the manufacturer's instructions (Life Technologies). Briefly, 30 µg of DNA were transfected into 30 mL culture containing 75 x 10^6 Expi293F cells using ExpiFectamine 293 Reagent. Cells were incubated at 37°C, 125 rpm, 8% CO_2 and after 24 h, ExpiFectamine 293 Transfection Enhancer 1 and 2 were added. Cells were further incubated at 37°C for 144 h. Aliquots of cultures were harvested every 24 h and analysed for protein expression by Western Blot. Seventy-two and 144 h after transfection, cell cultures were centrifuged at 800 rpm for 8 min and the protein-containing supernatants were harvested, pooled, clarified by centrifugation, filtered through a 0.22 µm filter, and stored at 4°C until purification.

Fc tagged recombinant Siglec were purified by protein A affinity chromatography using hiTrap rProtein G Columns (GE Healthcare) while FcγRIIA with a Ni.Nta superflow (Qiagen). Fractions of interest were pooled and were concentrated by using 10 kDa cutoff spin concentrator (Millipore Amicon Ultra); sodium dodecyl sulphate-poly-acrylamide gel electrophoresis (SDS-PAGE) was performed to check purity and samples aliquotated and stored at -20°C for further analysis.

5.1.6 BioLayer Interferometry (BLI)-based OCTET analysis

Octet QKe (ForteBio, Pall Science) was used for binding studies. Streptavidin (SA) biosensors (ForteBio) were used to immobilize biotinylated proteins in a 600 seconds loading. The equilibration time was 300 seconds to achieve a sufficient baseline signal. Immediately before analysis, tips were prewet in kinetic buffer HBS-P, composed by 10 mM HEPES, 150 mM NaCl, 0,02% P-20 Surfactant, pH 7.4 (GE Healthcare

Life technology). To calculate affinity of Human rSiglec-5/Fc Chimera (R&D System - 1072-SL-050) and Human rSiglec-14/Fc Chimera (R&D System - 4905-SL-050) on immobilized biotinylated $NadA_{24-342}$ (25 µg/mL in kinetic buffer), serial dilutions (from 500 nM to 7,81 nM) were tested. Kinetic was then monitored. A ligand-loaded biosensor was used in association with kinetic buffer as baseline. During the entire kinetic assay the sample plate was kept at 30°C shaking 1000 rpm. Reference subtracted BLI response curves were used for the affinity constant determination. Inter-step correction and Y-alignment were used to minimize tip-dependent variability. KD was calculated at response at 1190-1195 seconds, using the Data Analysis Software v7.1 (Forte Bio).

For the binding characterization after 180 sec baseline in kinetic buffer, SA biosensor tips were directly immersed in ligand solution for 600 sec loading (biotinylated $NadA_{24-342}$, $NadA_{24-170}$ and $NadA_{91-342}$ at 25µg/mL diluted kinetic buffer) and a second 300 sec baseline in kinetic buffer was performed and kinetic was monitored. During the entire kinetic assay the sample plate was kept at 30°C shaking 1000rpm.

5.1.7 Hydrogen and deuterium exchange (HDX)

5.1.7.1 Sample preparation for HDX-MS analysis

The hydrogen-deuterium exchange (HDX) experiments, with and without recombinant Siglec 5, were performed in the same experimental session. The antigen/receptor complex was formed by adding 200 pmol NadA3 vaccine antigen ($NadA_{\Delta 351-405}$) to Siglec 5, using a molar ratio of 1:1 and incubated for 30 minutes at room temperature for the equilibration step. The labelling was initiated by adding the proper deuterated buffer (PBS at pH of 7.4), reaching a deuterium excess of 84%. The labelling reaction was performed at room temperature. Over the time course of the experiment (ranging from 30 seconds to 30 minutes), 30 mL of the sample was removed and quenched with the same volume of an ice-cold 200 mM sodium phosphate buffer added with 4 M guanidinium chloride, to dissociate the antigen/receptor complex and to lower the pH to 2.4. In parallel, a control experiment without Siglec 5 was prepared using the same conditions previously described (PBS was used instead of the receptor preparation). All quenched samples were immediately flash frozen in liquid nitrogen, stored at -80°C and treated for analysis within the following 24 hours.

5.1.7.2 Local HDX-MS analysis

Labelled samples were thawed rapidly to 0°C and injected into a nanoacquity ultra-performance liquid chromatography (UPLC) system (Waters, Milford, MA, USA) with HDX technology. The injector, switching valve, columns, solvents and all associated tubings were kept at 0°C to limit back exchange. For local HDX-MS, protein samples were online digested for 1 hour at 60°C with a flow rate of 200 µL/min using a Poroszyme Immobilized Pepsin Cartridge (2.1 x 20 mm; Applied Biosystems, Foster City, CA, USA) equilibrated with 100% buffer A (0.1% formic acid in water). The generated peptides were immediately trapped, concentrated, and desalted using a VanGuard ethylene bridged hybrid (BEH) pre-column (1.7 µm, 2.1 x 5mm;Waters). The 1 hour digestion and desalting step allows deuteron atoms located at fast exchanging sites (e.g., side chains, exposed loops, and N/C termini) to be replaced with hydrogens. Peptides were then separated on an AcquityUPLC BEH C18 reverse-phase column (1.7 µm, 1.0 x 100 mm; Waters) with a linear gradient from 15 to 45% solvent B [acetonitrile:water (9:1), 0.1% formic acid] over 6.8 min at 40 µL/min.

5.1.7.3 Mass spectra acquisition and interpretation

Mass spectra were acquired in resolution mode (m/z 100–2000) on a Waters SynaptG2 mass spectrometer equipped with a standard electrospray ionization source. Mass accuracy was ensured by continuously infusing a green fluorescent protein solution (600fmol/µL in 50% acetonitrile, 0.1% formic acid) through the reference probe of the electrospray ionization source. The identity of each peptide was confirmed by mass spectrometry elevated energy analyses. All fragmentations were performed using argon as collision gas. Data were processed using ProteinLynx Global Server 2.5 (Waters), and each fragmentation spectrum was manually inspected to confirm the assignment. Only peptic peptides present in at least 3 repeated digestions of the unlabelled proteins were considered for the analysis. Deuterium uptake of each peptide is calculated as the difference between extracted centroid mass of each undeuterated peptic peptide and respective deuterium-labelling time point peptide using DynamX software (Weis, Engen, and Kass 2006).

5.1.8 Cell culture

5.1.8.1 Human THP-1 monocytic leukemia cells

The human THP-1 monocytic leukemia cells (ATCC® TIB-202™) were cultured at 37°C under 5% CO_2 at a density of 2–9 × 10^5/mL. The cell culture medium was RPMI-1640 (Gibco) supplemented with 0.05 mM 2-mercaptoethanol, 1 mM Sodium pyruvate, 10% heat-inactivated fetal bovine serum (iFBS), 100 U/mL penicillin, 100 mg/mL streptomycin. Differentiation was achieved by suspending cells in complete growth medium with addition of 100 ng/mL phorbol 12-myristate 13-acetate (PMA) (Sigma). PMA was prepared as a stock solution (5 mg/mL) in DMSO (Sigma); stocks were diluted with medium to obtain the final concentrations. Differentiated, adherent THP-1 cells, derived from 72-h treatment, were submitted to recovery conditions for further 24-h in PMA-free complete medium before proceeding with experiments.

5.1.8.2 Peripheral blood monocyte cells

Peripheral blood mononuclear cells (PBMC) were isolated from buffy coats using Ficoll Paque (GE healthcare) density gradient. Buffy coats from healthy donors were obtained from the Blood Transfusion Section, Empoli Hospital. Informed consent was obtained before all blood donations. The study protocol was approved by the GSK Research Center ethical committee and conforms to the ethical guidelines of the 1975 Declaration of Helsinki.

5.1.8.3 Chinese hamster ovary CHO-K1 cells

Chinese hamster ovary CHO-K1 cells (ATCC® CCL-61™) were grown in F-12K Medium supplemented with 100 U/mL penicillin, 100 mg/mL streptomycin, 10% iFBS and maintained at 37°C in a controlled humidified atmosphere containing 5% CO_2. Transfection was performed using Lipofectamine® LTX Reagent with PLUS™ Reagent (Life technologies) according the manufacturer's instructions.

5.1.9 Fluorescence-activated cell sorting (FACS) experiments

In order to assess the expression of selected proteins on cell's surface, approximately $3X10^5$ cells were mixed with blocking solution (phosphate-buffered saline (PBS) + 1% iFBS) for 30 min at 4°C. Cells were then incubated with specific polyclonal primary antibody (diluted in PBS + 1% iFBS) for 1 h at 4°C, and with Allophycocyanin (APC)-conjugated secondary F(ab)2 antibody (diluted in PBS + 1% iFBS; Thermo scientific) for 30 min at 4°C. Cells were analysed with a FACS-Scan flow cytometre (Beckton-Dickinson). The mean fluorescence intensity (MFI) for each population was calculated using FlowJo software (version 9.8; Tree Star, Inc, Ashland, OR).

Binding assay was performed as previously described (Comanducci et al. 2002). Briefly, normal or transfected cells were non-enzymatically detached using cell dissociation solution (CDS, Sigma), harvested and suspended in RPMI-1640 (Gibco) medium supplemented with 1% iFBS. Approximately $3X10^5$ cells were mixed with 200 µg/mL rNadA or blocking solution (PBS + 1% iFBS) alone for time and temperature indicated in the graph. Cells were then incubated with mouse polyclonal serum against NadA (diluted 1:1000) for 1 h at 4°C, and with Allophycocyanin (APC)-conjugated goat F(ab)2 antibody to mouse Ig (diluted 1:100; Thermo scientific) for 30 min at 4°C.

To enzymatically modify cell surface proteins, $3x10^5$ cells were pre-incubated with three concentrations of pronase (1000, 500, 250 mg/mL) (Sigma) or phospholipase A_2 (800, 200, 50 mg/mL) (Sigma) in FBS-free medium for 30 min at 37°C in 5% CO_2, and subsequently incubated with 200 µg/mL rNadA or blocking solution alone for 30 min.

For inhibition of the binding experiments cells were incubated with 50 µg/mL of selected antibody prior to rNadA incubation.

Antibodies used in the study: Anti-Siglec 5 (N-term) antibody produced in rabbit (SAB1303597 Sigma); Anti-Siglec 5 (C-term) antibody produced in rabbit (SAB1304846 Sigma); Anti-Siglec 14 (N-term) antibody produced in rabbit (SAB1303894 Sigma); Human Fc gamma RIIA/CD32a Antibody (AF1875 R&D System); IgG from human serum (I2511 Sigma); Mouse IgG1 pure (349040 BD Biosciences); Anti-Flag tag antibody produced in mouse (Sigma F3165).

5.1.10 Bacterial strains, growth conditions

5.1.10.1 Escherichia coli BL21(DE3)T1R

Escherichia coli BL21(DE3)T1^{R} (New England BioLabs) was the strain used to express full-length NadA (variant 3) following transformation with pET21b-NadA, as previously described (Capecchi et al. 2005), or the empty vector as control. *E. coli* was cultured at 37°C in Luria–Bertani (LB) broth supplemented with 100 µg/mL ampicillin. Surface protein expression for full-length NadA was achieved without addition of IPTG exploiting the expression due to the leakage in the induction system.

5.1.11 Confocal immunofluorescence microscopy

3 x10^{5} THP-1 cells were incubated with 200µg/mL rNadA in blocking buffer (PBS + 5% iFBS) for 30 min at 37°C before staining with primary and secondary antibodies in PBS + 1%iFBS for 60 minutes at room temperature.

Antibodies used in the study: Anti-Siglec 5 (N-term) antibody produced in rabbit (SAB1303597 Sigma); Anti-Siglec 14 (N-term) antibody produced in rabbit (SAB1303894 Sigma); Human Fc gamma RIIA/CD32a Antibody (AF1875 R&D System); Alexa Fluor–conjugated secondary antibodies (1/300). Image acquisition and analysis were performed with a Zeiss LMS 710 confocal microscope and images were captured using ZEN software (Carl Zeiss, Oberkochen, Germany). Three-dimensional (3D) reconstructions and quantification histograms were obtained using ImageJ software (NIH). Each experiment was repeated at least 3 times in triplicate.

5.1.12 Statistical Analyses

All experiments were performed at least three times in triplicate. All data were graphed using Microsoft Excel 2010 software and show mean and standard deviation.

5.2 Results

5.2.1 rNadA binds human monocytes via a proteinaceous receptor

rNadA cell labelling of peripheral blood mononuclear cells (PBMCs) from human blood was performed and anti-NadA staining was subsequently used to search for specific NadA targets. Results showed that a single subpopulation, corresponding to monocytes, efficiently binds the adhesin (Fig. 10A). The interaction was also confirmed using the human monocytic cell line THP-1 (Fig. 10B). Furthermore, to explore the biochemical nature of the interaction, we treated both PBMC and THP-1 with pronase or phospholipase A2, to modify the protein or lipid content of the cell membrane respectively (Okuma et al. 2001). Subsequently, the binding of rNadA was determined by FACS analysis. Only the pronase treatment was able to reduce the capability of rNadA to bind to monocytes (Fig. 10C-D) suggesting that a protein receptor is likely to mediate the interaction.

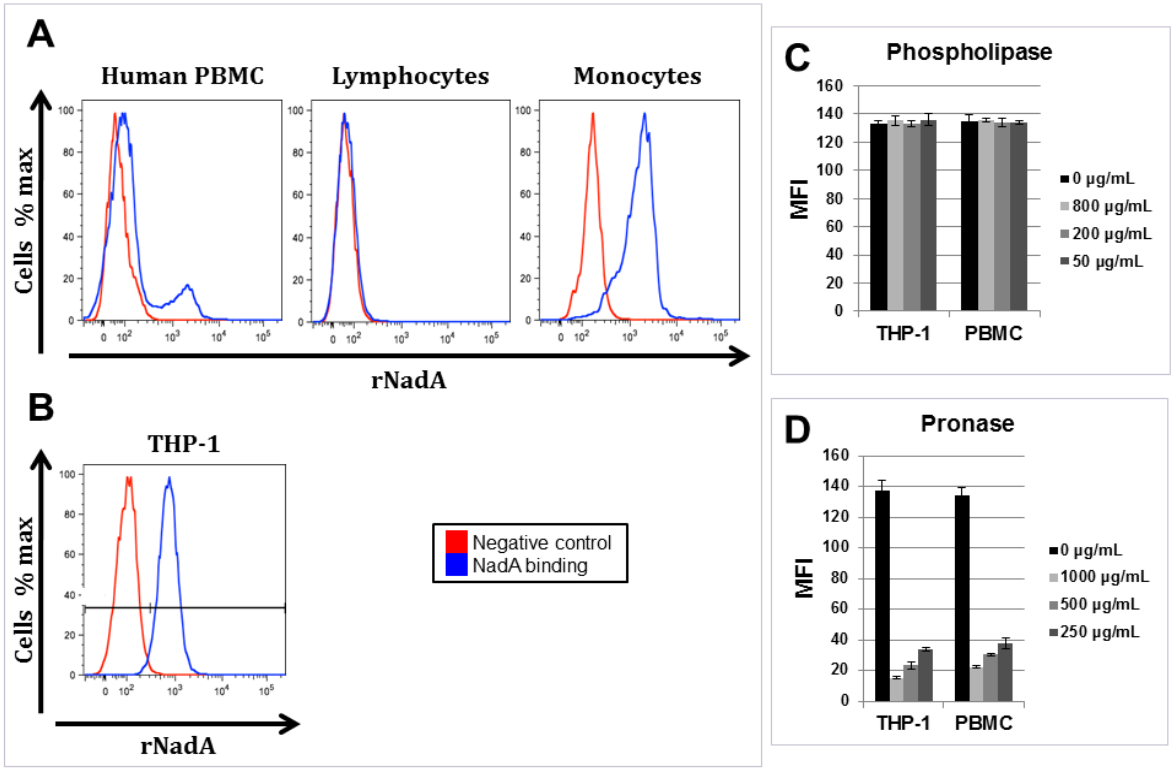

Fig. 10: Characterization of the binding of rNadA to human monocytes: (a) Fresh human PBMC or **(b)** human immortalized THP-1 monocytic cells were incubated with rNadA (200 µg/mL) for 30 minutes at 37°C prior to FACS analysis using an anti-NadA antibodies**. (c)/(d)** THP-1 and human PBMC were treated with medium alone (black bars), pronase (1000, 500 and 250 mg/mL) or phospholipase A2 (800, 200 and 50 mg/mL) and subsequently incubated with rNadA (200 µg/mL). In both cases, the binding was analysed by FACS using an anti-NadA antibody. The values are reported as net mean fluorescence intensity (MFI)

5.2.2 Protein microarray revealed novel human monocytes interactors for NadA

In order to identify proteins that mediate the NadA interaction with monocytes, a large scale protein microarray screening was performed spotting almost 6500 human recombinant proteins from the GNF library. rNadA was used at 1 µM and interactions were detected using specific anti-NadA antibody.

Among all the identified hits (Fig. 11), we obtained high score interactions with three proteins expressed on the monocyte/macrophages surface; two replicates of the Sialic acid-binding immunoglobulin-type lectins receptor 14 (Siglec 14) with a MFI score of 65477 and 65471 respectively, the Sialic acid-binding immunoglobulin-type lectins receptor 5 (Siglec 5) with a MFI score of 58551 and the Low affinity immunoglobulin gamma Fc region receptor II-a (FCγR2A) with a MFI score of 46609. Interestingly the B isoform of FCγR2 did not give a positive signal for the interaction with rNadA (MFI score of 4019), as well as the Sialic acid-binding immunoglobulin-type lectins receptor 9 (Siglec 9) (MFI score of 47) that we decided to use as Siglec negative control in our experiments.

In addition to these proteins, further putative hits were identified; in particular we confirmed the interaction with the Oxidized low density lipoprotein (lectin-like) receptor 1 (Lox-1) already described by Scietti *et al.* (Scietti et al. 2016).

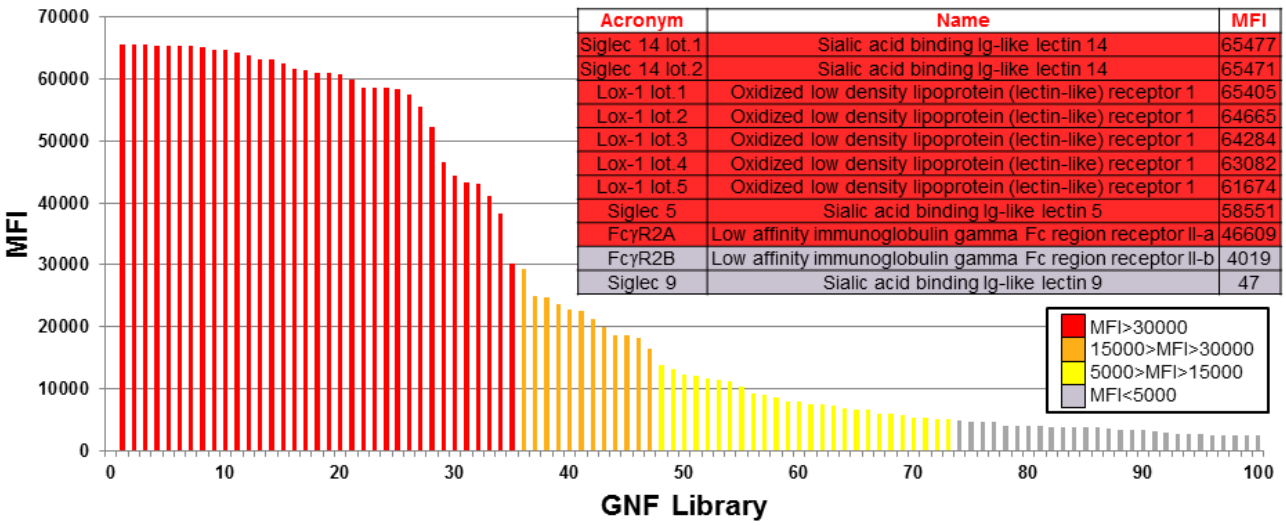

Acronym	Name	MFI
Siglec 14 lot.1	Sialic acid binding Ig-like lectin 14	65477
Siglec 14 lot.2	Sialic acid binding Ig-like lectin 14	65471
Lox-1 lot.1	Oxidized low density lipoprotein (lectin-like) receptor 1	65405
Lox-1 lot.2	Oxidized low density lipoprotein (lectin-like) receptor 1	64665
Lox-1 lot.3	Oxidized low density lipoprotein (lectin-like) receptor 1	64284
Lox-1 lot.4	Oxidized low density lipoprotein (lectin-like) receptor 1	63082
Lox-1 lot.5	Oxidized low density lipoprotein (lectin-like) receptor 1	61674
Siglec 5	Sialic acid binding Ig-like lectin 5	58551
FcγR2A	Low affinity immunoglobulin gamma Fc region receptor II-a	46609
FcγR2B	Low affinity immunoglobulin gamma Fc region receptor II-b	4019
Siglec 9	Sialic acid binding Ig-like lectin 9	47

Fig. 11: Screening for NadA interactors. Plotting of MFIs of spotted human and mouse proteins tested against NadA at 1 µM. Red bars represent high reactivity proteins (MFI>30000), orange bars represent medium reactivity proteins (15000>MFI>30000), yellow bars represent low reactivity proteins (5000>MFI>15000) and grey bars no reactivity proteins (MFI<5000). Inset table shows protein acronym, name and the respective MFI values of the relevant interactions.

5.2.3 Restore of the NadA binding in CHO-K1 non-permissive cells

In order to validate the interactions between NadA and the monocytic receptors Siglec 5 & 14 and FcγR2A, binding assays on eukaryotic cell line were performed. FACS analysis confirmed that CHO-K1 cells are not permissive to NadA binding (Fig. 12A left panel) and do not constitutively express these receptors (Fig. 12A right panels). CHO-K1 cells were transiently transfected with vectors expressing the putative receptors as single species (Siglec 5; Siglec14 and FcγR2A) or the control ones (Human Siglec 9 and Mouse FcγR2A). The surface exposure of the receptors was checked by FACS and confocal analysis using specific antibodies (data not shown). Transiently transfected cells were then incubated with rNadA and analysed by FACS. The anti-NadA staining showed that only cells expressing the putative receptors were able to bind rNadA (Fig. 12B blue curve) while no rNadA binding was observed on cells transfected with control receptors. Pre-incubation of transfected cells with polyclonal anti-receptors antibodies prior to rNadA incubations, inhibit the binding (Fig. 12B pink curve). All together, these results indicate a specific interaction between the receptors and the meningococcal adhesin validating, in a cellular context, the finding of the protein array.

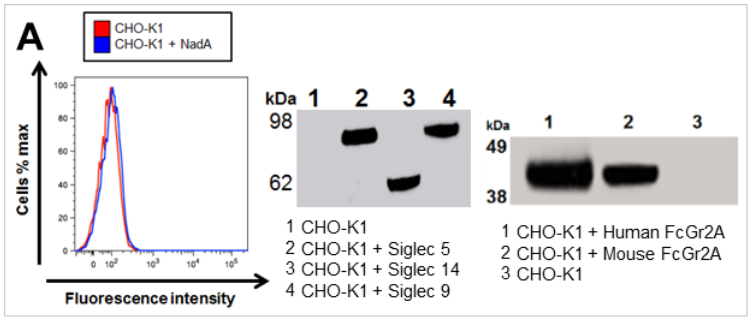

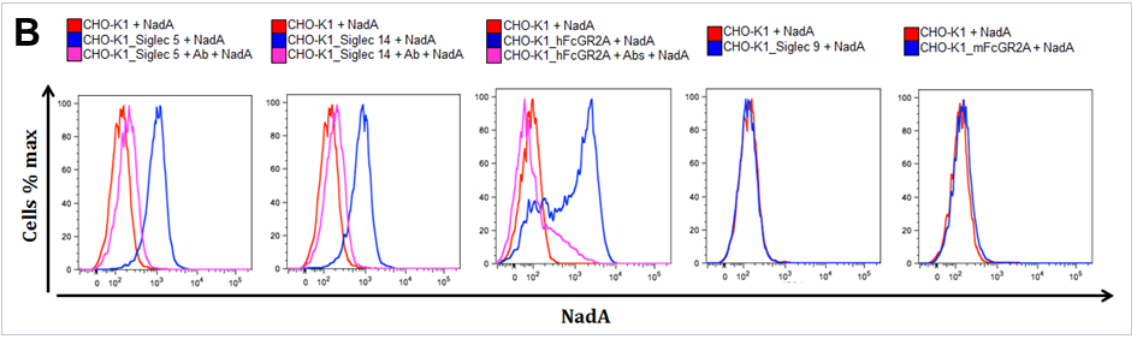

Fig. 12: rNadA binds CHO-K1 cells expressing the putative receptors. (a) CHO-K1 cells were incubated with rNadA (200 µg/mL) for 30 minutes at 37°C prior to FACS analysis using anti-NadA Abs. Cells lysates form transfected and non-transfected CHO-K1 were analyzed by Western blotting . **(b)** FACS plots representative of rNadA binding on transfected and non-transfected CHO-K1. Red curves represent the negative control (CHO-K1 cells incubated with rNadA), blue curves represent the rNadA binding on transfected cells and the pink curves the inhibition of the binding on transfected cells.

5.2.4 Characterization of rNadA receptors on THP-1 monocytic cells

In order to assess the presence of the identified rNadA receptors on THP-1 monocytes, FACS analysis with specific anti-receptor antibodies was performed. As shown in figure 13A, THP-1 monocytes express Siglec 5, Siglec 14 and FcγR2A on the surface. In particular, RNA extraction followed by cDNA synthesis and sequencing, highlighted that the FcγR2A allelic variant on THP-1 presents a glutamine at aa position 63 (inside the first Ig-like domain) and an histidine residue at aa position 167 (inside the second Ig-like domain), therefore the same variant of the recombinant protein spotted on the GNF protein microarrays (Fig. 13B).

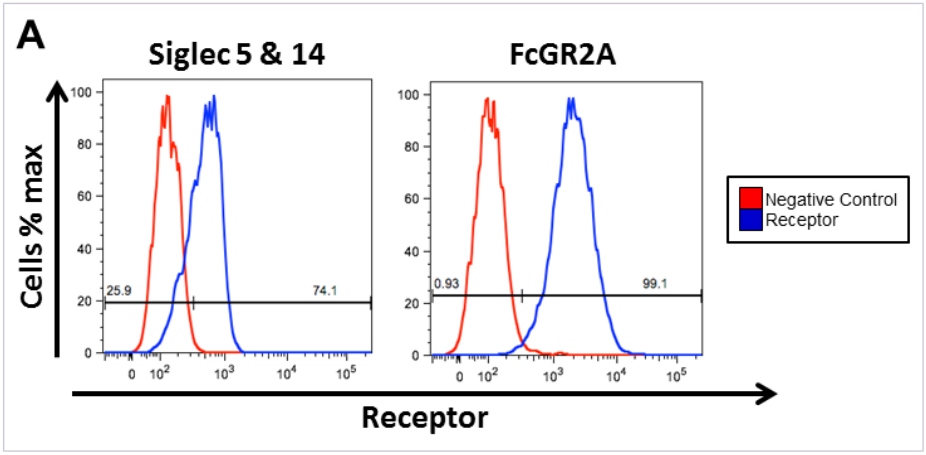

Fig. 13: Characterization of rNadA receptors on THP-1 monocytic cells: (a) Surface antibodies staining against the putative receptors was performed on human immortalized THP-1 monocytic cells. Sample were then analysed by FACS analysis. **(b)** Clustal Omega allignements of FcγR2A cDNA from THP-1 cells to asses the allelic variants expressed

5.2.5 Characterization of the binding specificity between rNadA and Siglec 5&14

To assess the binding kinetics between NadA and Siglec 5 and Siglec 14 receptors, BLI technology was used. rNadA was first immobilized onto the BLI biosensor, and each receptor used individually as analyte. Results of these experiments are shown in Fig. 14A-B. The calculated KDs were 6.20E-08 M for Siglec 5 and 2.60E-07 M for Siglec 14 indicating a very strong interaction between NadA and its cellular targets on monocytic cells. Furthermore, these analyses assessed that the binding was effective also in solution with the recombinant soluble proteins.

To identify the NadA region involved in the binding, we first screened the ability of two different NadA constructs to interact with the receptors still using BLI technique. In addition to the soluble NadA full length, we expressed and purified: a) the NadA "Head domain" comprising aa 24-170 and b) the NadA "Stalk domain" spanning aa 91-342 (Fig. 14C). Both constructs were demonstrated to produce trimeric species in solution (data not shown).

Results from these experiments, shown in Fig. 14D, indicate that the interaction between NadA and Siglec receptors occurs via the Head domain.

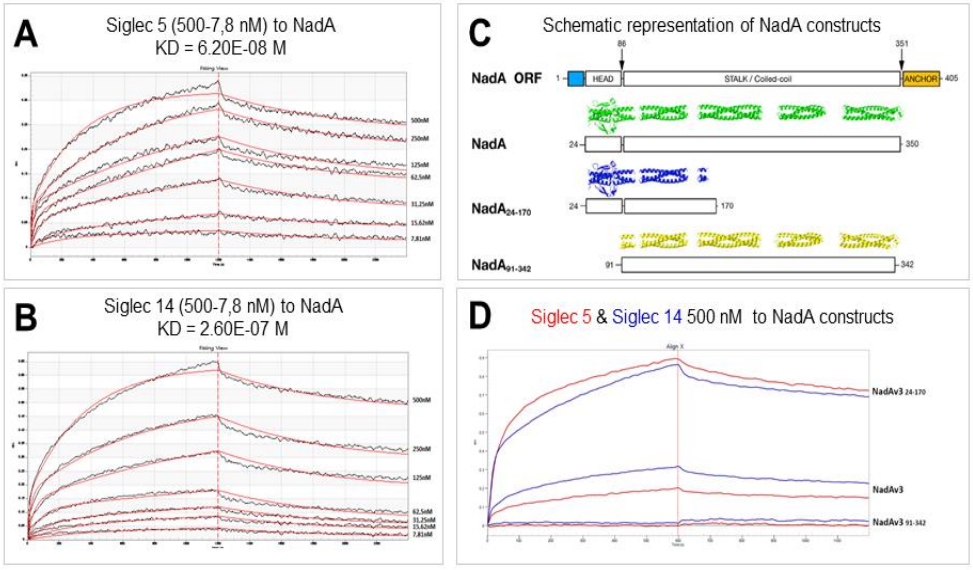

Figure 14: Biophysical characterization of the NadA/Siglec 5 & 14 interaction.

(a) Blank subtracted sensograms of Siglec 5 (500 - 7.8 nM) tested on biotinylated NadA immobilized on SA biosensors. Association and dissociation curves were fitted in a 2:1 model

(b) Blank subtracted sensograms of Siglec 14 (500 - 7.8 nM) tested on biotinylated NadA immobilized on SA biosensors. Association and dissociation curves were fitted in a 2:1 model

(c) Schematic representation of NadA constructs used to determine NadA binding site on Siglec 5 & 14. NadA gene, rNadA (green), $NadA_{24–170}$ (blue) and $NadA_{91–342}$ (yellow) structure are shown. Signal peptide (light blue) and membrane anchor (orange) are shown in the cartoon

(d) Blank subtracted sensograms of 500 nM Siglec 5 (red) and Siglec 14 (blue) on biotinylated rNadA, $NadA_{24–170}$ and $NadA_{91–342}$.

To accurately locate the NadA region involved in the binding with Siglec 5, mapping by hydrogen–deuterium exchange (HDX)-MS was performed. Epitope mapping by the HDX approach is based on the differential rate of deuterium incorporation by an antigen when it is free or bound to the partner protein/receptor following incubation in appropriate deuterated solvents. The rate at which backbone amide hydrogens exchange in solution is directly dependent on the dynamics and structure of the protein. When a protein complex forms, such as antigen–receptor complex, the interface between the binding partners can occlude solvent accessibility, reducing the exchange rate (Hager-Braun and Tomer 2005). Mapping by HDX-MS was performed in 2 parallel steps as described above; deuterium incorporation was performed on NadA alone (reference experiment) and on the complex with Siglec 5 receptor. Both samples were digested by pepsin, and deuterium incorporation was monitored for 95 peptides covering 96.3% of NadA sequence (Malito et al. 2014) and compared.

In Fig. 15A, the HDX-MS results have been simplified reporting only the extent of deuterium uptake for 5 sequential peptide fragments covering the head domain of NadA. HDX-MS revealed that H-D exchange was reduced in the presence of Siglec 5 for two nonconsecutive NadA peptides, allowing mapping of the interaction region involving segments Val^{36}-Gly^{50} and Ile^{60}-Ala^{71}.

In summary, HDX-MS analysis revealed the location of the binding region of Siglec 5 on the head domain of NadA, in agreement with BLI-based OCTET measurements. In addition, this finding strongly suggests a conformational nature of the region of interaction as highlighted by the 3D view on NadA3 homology model (Fig. 15B).

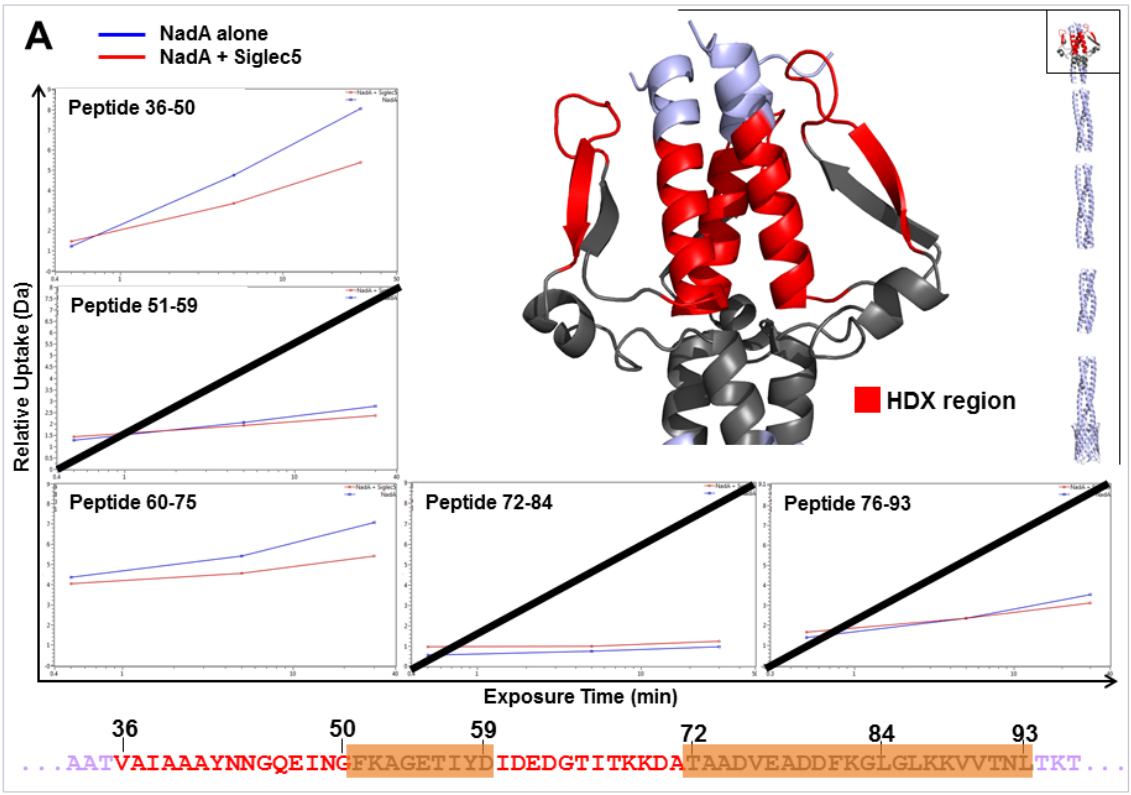

Fig. 15A: Time course of deuterium incorporation for the peptides covering the NadA head domain. Deuterium uptake of each peptide is calculated as the difference between extracted centroid mass of each undeuterated peptic peptide and respective deuterium-labeling time point peptide using DynamX software. The red curves are derived from complex NadA–Siglec 5, whereas the blue curves are derived from NadA alone. There are 2 peptides showing a significant difference in deuterium uptake between the free and bound NadA forms (peptide Val^{36}-Gly^{50} and Ile^{60}-Asp^{75}) while the 3 peptides not affected by deuterium protection are highlighted with a black bar (peptide Phe^{51}-Asp^{59}, Thr^{72}-Leu^{84} and Val^{76}-Leu^{93}). The figure also reports the amminoacid sequence and the *in silico* model of NadA variant 3 built from the X-ray structure of NadA variant 5. Dashes show regions with low sequence homology or unknown secondary structure (Malito et al. 2014). The NadA/Siglec 5 interacting region (peptide Val^{36}-Gly^{50} and Ile^{60}-Ala^{71}) is colored in red.

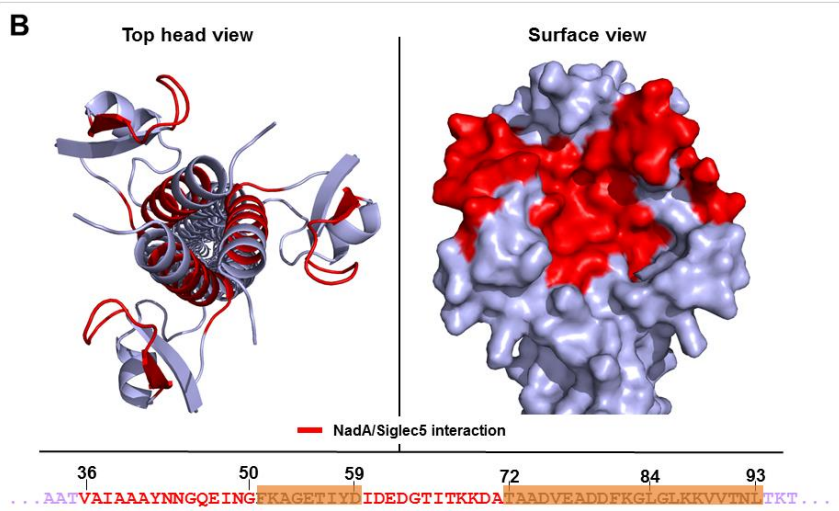

Fig. 15B: NadA/Siglec 5 interaction region highlighted on the *in silico* model of NadA variant 3 head domain. NadA/Siglec 5 interaction region is reported in red on the top and surface views of the *in silico* model of NadA variant 3 head built from the X-ray structure of NadA variant 5. Dashes show regions with low sequence homology or unknown secondary structure (Malito et al. 2014).

Comparison studies (Fig. 15C) highlighted the overlapping nature of the NadA/Siglec 5 binding region with the NadA epitopes recognized by the bactericidal murine monoclonal antibody 33E8 (Malito et al. 2014) and the NadA interaction region with Hsp90 (see 4.3.1 paragraph).

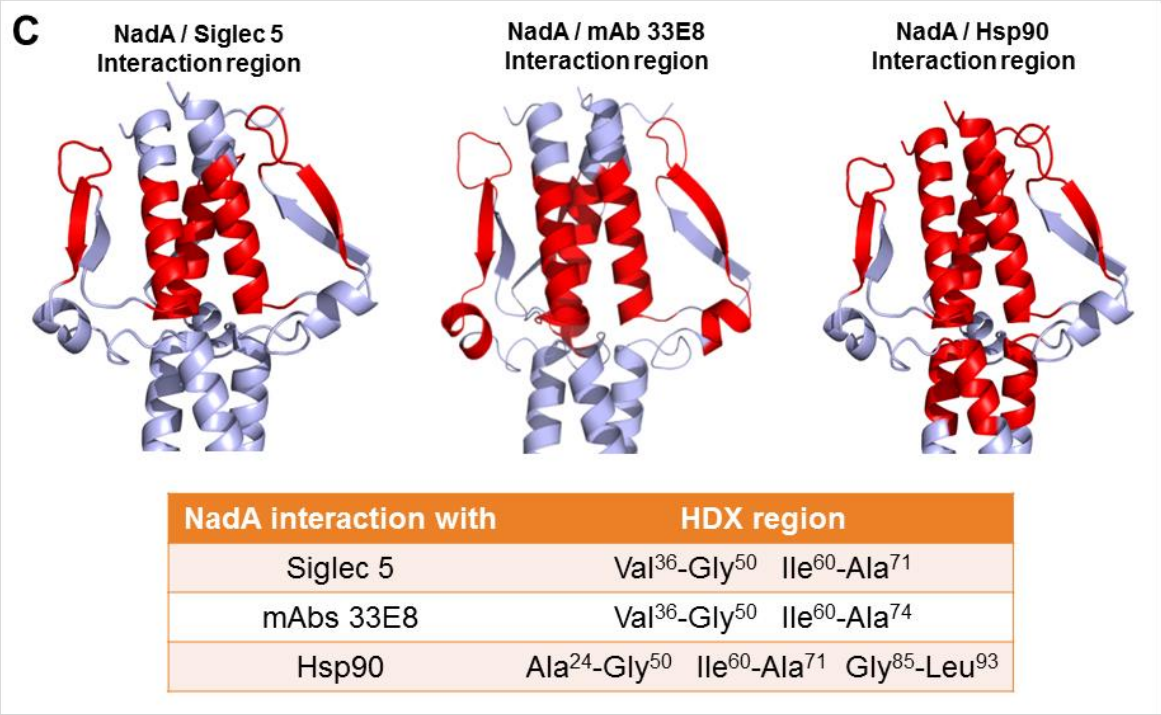

NadA interaction with	HDX region
Siglec 5	Val^{36}-Gly^{50} Ile^{60}-Ala^{71}
mAbs 33E8	Val^{36}-Gly^{50} Ile^{60}-Ala^{74}
Hsp90	Ala^{24}-Gly^{50} Ile^{60}-Ala^{71} Gly^{85}-Leu^{93}

Fig. 15C: Comparision between the NadA binding region with Siglec 5, mAb 33E8 and Hsp90. The NadA region involved in the binding are decribed in the table and highlighted in red on the *in silico* model of NadA variant 3 head built from the X-ray structure of NadA variant 5. Dashes show regions with low sequence homology or unknown secondary structure (Malito et al. 2014).

To further validate the interaction between NadA and the monocytes receptors in a cellular context, a co-localizations analysis on THP-1 cells was conducted. Cells were incubated with rNadA or PBS alone prior to anti Siglec 5 & 14 and anti FcγR2A antibody staining. Confocal analysis of the control samples revealed a co-localization between Siglec 5 & 14 and FcγR2A signals, suggesting the proximity of these receptors inside the cells, likely within the same lipid raft (Fig. 16A). Regarding samples incubated with rNadA a strong co-localization signal was achieved with both receptors, confirming the interaction within a "natural" cellular context (Fig. 16B).

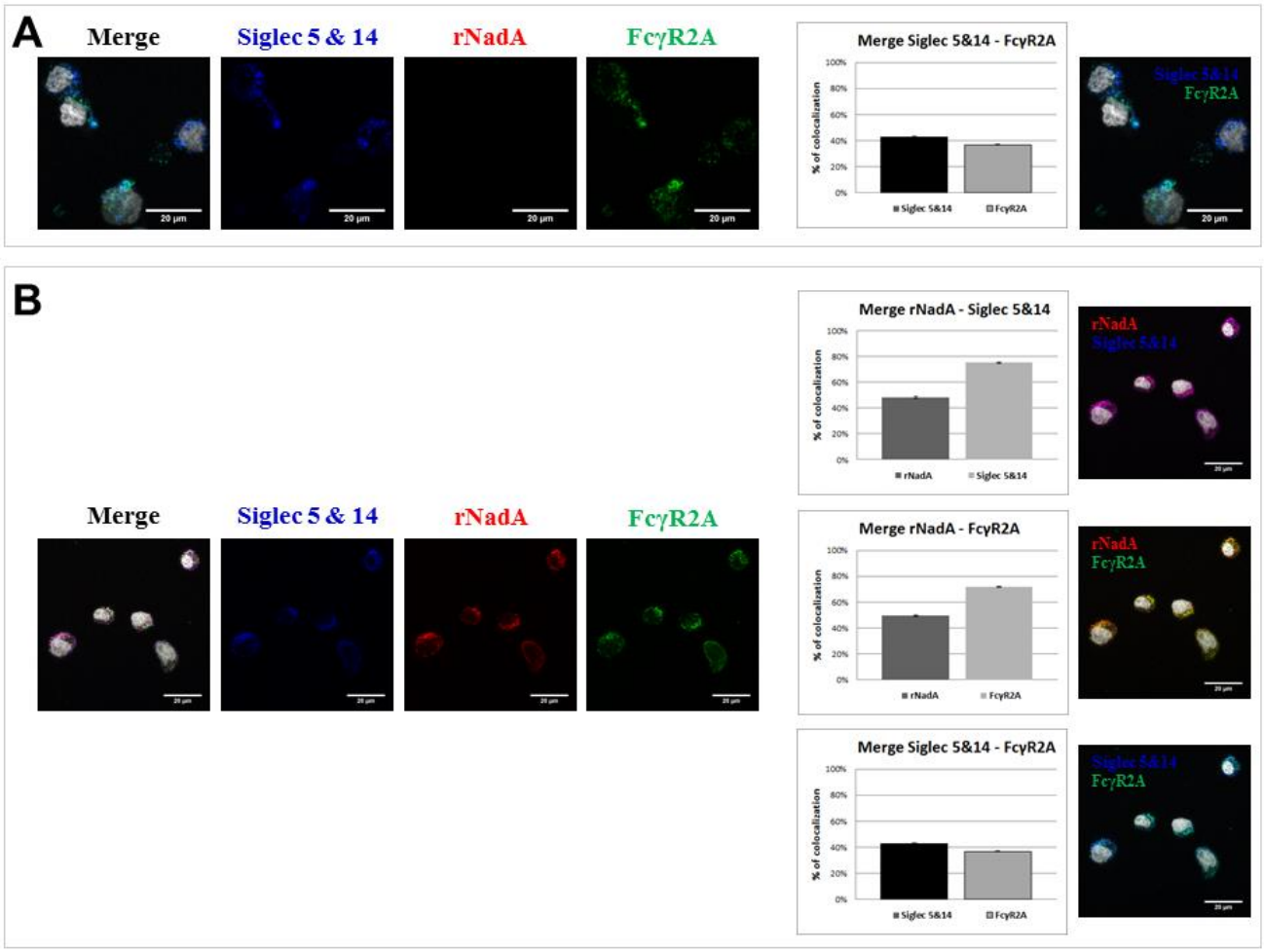

Figure 16A&B: Co-localization analysis of rNadA binding to THP-1. THP-1 cells were incubated with PBS alone (Fig. A) or 200 µg/mL rNadA (Fig. B) for 30 minutes at 37°C, then fixed and stained for rNadA (red), Siglec 5 & 14 (blue), FcγR2A (green) and nuclei (grey). Merged images of all signals are shown as well as the merge for all the couples. Images are representative of three independent experiments. Scale bar is 20 µm. The dark/light grey graphs report the quantification of rNadA co-localization with the receptors signals. The dark grey columns indicate the percentage of rNadA immunofluorescent pixels co-localizing with the receptors (Siglec 5 &14 or FcγR2A as indicated) immunofluorescent pixels. *Vice versa* the light grey columns indicate the percentage of receptors immunofluorescent pixels co-localizing with rNadA immunofluorescent pixels. The black/grey graph reports the quantification for the Siglecs/FcγR2A co-localization signals. Data are mean ± s.e.m representative of three independent experiments, each assessing 25–30 cells.

A more accurate characterization of the binding to THP-1 was achieved incubating monocytic cells with a high concentration of human or mouse IgG, alone or together with anti-Siglec antibodies, prior to rNadA incubation. NadA binding was then measured by FACS analysis. Results indicate that incubation with human IgG alone drastically reduce the NadA binding to cells while, when anti-Siglec antibodies are added in the incubation mixture too, the binding is almost abolished (Fig. 17A right panel). The control

experiment, using mouse IgG, highlighted no effect of these immunoglobulins on the rNadA binding while, as expected, a partial inhibition is obtained with the addition of anti-Siglec antibodies (Fig. 17A left panel).

We have previously shown that the NadA binding to epithelial cells is temperature dependent and is almost undetectable at temperature below 15°C (see paragraph 4.1 (Bozza et al. 2014)). We performed a temperature dependence analysis also of the NadA binding to THP-1. To separate the binding to either receptor, FcγR2A was blocked by pre-incubating cells with human IgG (or mouse IgG as control) allowing the observation of the binding to Siglec 5 & 14; on the contrary, pre-incubation with anti Siglec antibodies allowed to observe only the NadA binding to FcγR2A. The binding was then performed at 4°, 25° and 37°C and revealed by FACS as previously described. The results, shown in Fig. 17B, suggest that the binding between NadA and Siglec 5 & 14 is influenced by temperature while no dependence is observed for the binding to FcγR2A.

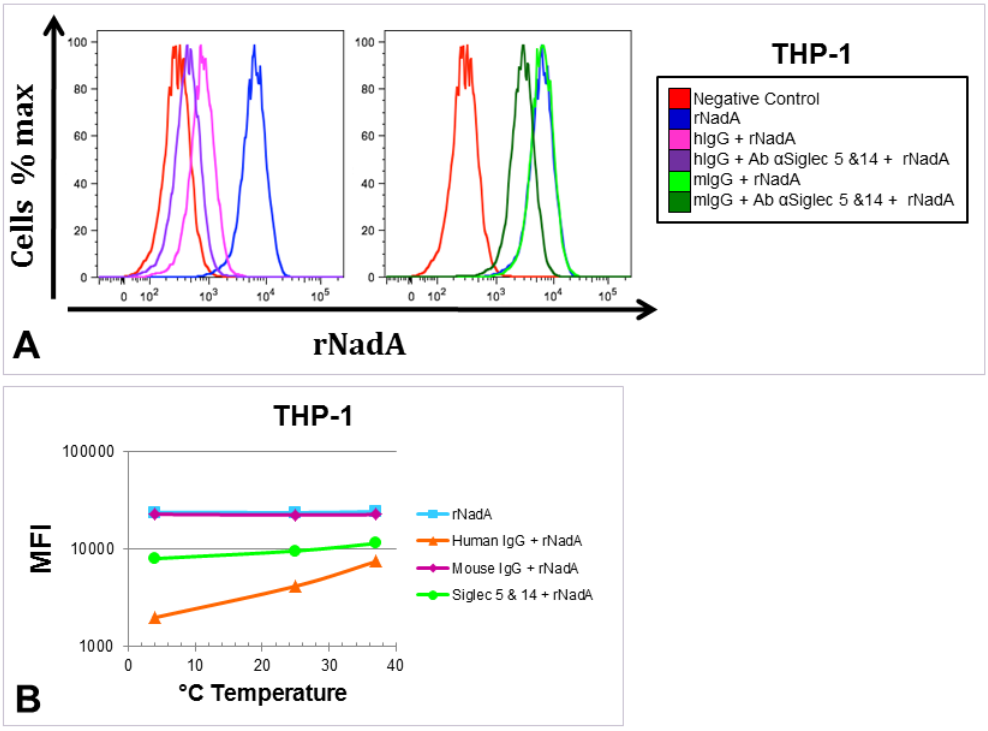

Fig. 17: Characterization of the binding to THP-1. (a) Human immortalized THP-1 monocytic cells were incubated with PBS alone or in combination with: human IgG (pink curve), human IgG and anti Siglec 5&14 antibodies (violet curve), mouse IgG (light green curve) or mouse IgG and anti Siglec 5&14 antibodies (dark green curve) prior to 30 minutes incubation with rNadA (200 µg/mL) at 37°C. Samples were analysed by FACS analysis. **(b)** Human immortalized THP-1 monocytic cells were incubated with PBS alone or in combination with: human IgG (orange curve), mouse IgG (pink curve) or anti Siglec 5&14 antibodies (light green curve) prior to 30 minutes incubation with rNadA (200 µg/mL) at different temperatures (4°C, 25°C and 37°C). Samples were analysed by FACS analysis and the values reported as net mean fluorescence intensity (MFI).

6 Investigating NadA role at blood brain barrier

6.1 Article: Exploring host-pathogen interactions through large-scale protein microarray analysis

Abstract

During bacterial pathogenesis extensive contacts between the human and the bacterial extracellular proteomes take place. The identification of novel host-pathogen interactions by standard methods using a case-by-case approach is laborious and time consuming. To overcome this limitation, we took advantage of large libraries of human and bacterial recombinant proteins. We applied a large-scale protein microarray-based screening on two important human pathogens using two different approaches: (I) 75 human extracellular proteins were tested on 159 spotted *Staphylococcus aureus* recombinant proteins and (II) *Neisseria meningitidis* adhesin (NadA), an important vaccine component against serogroup B meningococcus, was screened against ≈2300 spotted human recombinant proteins. The approach presented here allowed the identification of the interaction between the *S. aureus* immune evasion protein FLIPr (formyl-peptide receptor like-1 inhibitory protein) and the human complement component C1q, key players of the offense-defense fighting; and of the interaction between meningococcal NadA and human LOX-1 (low-density oxidized lipoprotein receptor), an endothelial receptor. The novel interactions between bacterial and human extracellular proteins here presented might provide a better understanding of the molecular events underlying *S. aureus* and *N. meningitidis* pathogenesis.

Introduction

Protein-protein interactions (PPIs) play a fundamental role in initiating and sustaining bacterial infections in the human body. PPIs are key to penetration of host barriers, from colonization of mucosal epithelia to invasion of host cells and tissues, as well as to evasion of host innate and adaptive immune responses[1]. Despite the biological relevance of PPIs at the host-pathogen interface, their systematic characterization is still challenging.

Microarrays represent a powerful tool for large-scale screenings, and this technology has been successfully applied to the identification of novel PPIs in different organisms. However, only a few examples exist where interactions between extracellular proteins from human and pathogen libraries were tested. The highest throughput was achieved by Wright and collaborators in studies reporting the systematic screen for interactions involved in the recognition of the host erythrocyte by the blood stage of the malaria parasite, where 40 human erythrocyte receptors were screened against 35 *Plasmodium falciparum* extracellular proteins and led to the identification of two novel erythrocyte receptors for *P. falciparum* parasites[2,3,4]. Similar studies were carried out to identify bacterial/human interactions, but involved a very limited number of human proteins[5,6].

A large collection of human recombinant proteins exists at the Genomic Institute of the Novartis Research Foundation (GNF)[7]. In its current version, the GNF library consists of ≈2300 distinct proteins that have been prioritized from approximately 3500 human genes *in silico* predicted to code for secreted or single-pass transmembrane proteins. Such a large collection of recombinant human extracellular proteins represents a rich source of targets for bacterial effectors. In the present work, we describe a large-scale screening of such a library against relevant bacterial proteins of two important pathogens, *i.e. Staphylococcus aureus* and Serogroup B *Neisseria meningitidis* (meningococcus B, *N. meningitidis* group B) to identify new interactions.

S. aureus is a gram-positive bacterium and opportunistic pathogen living as a commensal in human skin and nasal cavities in 20% of the human population[8]. Several human proteins are targeted by *S. aureus* extracellular proteins[9]. In recent years it also became evident that staphylococcal evasion molecules may have multiple targets[10]. This suggests a complex network of interactions between *S. aureus* and the human extracellular proteome, providing the rationale for further investigations at the host-pathogen interface.

N. meningitidis group B is a Gram-negative encapsulated bacterium and commensal of human nasopharynx, which can become an aggressive pathogen leading to fulminant sepsis and meningitis. Recently, a four component protein-based vaccine (Bexsero®) was licensed by Novartis vaccines (now a GSK company). The Bexsero formulation contains the Neisserial adhesin A (NadA) which constitutes a key determinant of the vaccine-induced immunity[11]. NadA is a trimeric coiled-coil outer membrane protein constituted by an N-terminal “head” domain, a coiled-coil “stalk” and a transmembrane domain that anchors the protein to the bacterial membrane[12]. The gene is present in three out of four known hyper virulent lineages of *N. meningitidis* group B strains and several studies already demonstrated its importance during bacterial

pathogenesis[13,14,15]. In addition, the crystal structure of a soluble ectodomain fragment of NadA variant 5 was recently solved[16]. Nevertheless, a global picture of the NadA interactions with the human extracellular proteome is still missing and might help in the understanding of *N. meningitidis* group B pathogenesis.

To our knowledge, we report here the largest microarray screening carried out so far between human and bacterial extracellular proteins using two different approaches. The *S. aureus* extracellular proteome was screened against a selection of human complement factors and extracellular matrix proteins, and led to the identification of the human complement factor C1q as a new target for the well-known staphylococcal immune evasion protein FLIPr. In a second experimental set-up, the complete library consisting of 2354 human extracellular proteins was screened to identify novel human receptors for NadA, and the oxidized low-density lipoprotein receptor LOX-1 was identified as the first putative endothelial receptor for this important neisserial adhesin.

Methods

Selection, Cloning and Purification of SA Surface Proteins

The staphylococcal proteins printed on the arrays belong to the *S. aureus* strain NCTC 8325 and were selected *in silico* using a combined bioinformatics approach. They were first selected for the presence of extracellular signals, *e.g.* signal peptides, lipoprotein motifs, transmembrane regions and cell wall anchoring sequences–the so-called "surfome" and "secretome"[17]–and then for the presence of "protectome" signatures, *i.e.* specific functional/structural features occurring in bacterial vaccine protective antigens[18].

Genomic DNA coding for the mature portion of the *S. aureus* proteins were cloned into the pET21b expression vector (Novagen) after PCR amplification using *Escherichia coli* BL21(DE3) (Novagen) as competent strain. Recombinant proteins (108 as single constructs and 10 as multiple constructs for a total of 159), obtained as C-terminal His or Glutathione *S*-transferase (GST) tag fusions, were expressed in High Throughput Medium Complex (HTMC) (3% yeast extract, 40 mM KH_2PO_4, 90 mM K_2HPO_4, 2 mM $MgSO_4$, 1.5% glycerol, pH7.4) auto-inducing medium for 30 h at 27 °C and cell were then harvested at 6500 × g for 1 h. Bacterial lysis was obtained using B-PER buffer (Thermo Scientific) and the lysate was clarified by centrifugation at 30.000 × g for 30 min. The soluble fraction was loaded onto a His Multitrap HP 96-well plate system (GE Healthcare), washed with phosphate buffer (50 mM sodium phosphate,

300 mM NaCl, 20 mM imidazole pH 8.0) and the protein was finally eluted with the same buffer containing 250 mM imidazole as previously described[30]. GST tagged proteins were purified using a GST Multitrap HP 96-well plate system (GE Healthcare), washed with phosphate buffer (50 mM Tris, 300 mM NaCl pH 8.0). The proteins were eluted with the same buffer containing 10 mM reduced glutathione. Proteins purified in a tagless form were obtained as described by Klock *et al*. (27). Briefly, the PCR product of the portion of the gene coding for the mature protein was cloned using the Polymerase Incomplete Primer Extension (PIPE) method into plasmid pSpeedET, which encodes an expression and purification tag followed by a tobacco etch virus protease site (MGSDKIHHHHHHENLYFQG) at the N terminus of the protein. *E. coli* strain HK100 was transformed with the plasmid coding for the protein and was grown in Luria-Bertani (LB) arabinose-containing broth until OD_{600} = 0,4–0,6. Protein expression was achieved using IPTG (Isopropyl-β-D-thiogalactopyranosid) 1 mM for 3 h at 25 °C. Cells were harvested at 6500 × g for 1 h and lysed in B-PER buffer (Thermo Scientific). Lysate was clarified by centrifugation at 30.000 × g for 30 min and the protein contained in the soluble fraction was purified using an automated AKTA x-PRESS system on a nickel affinity column, followed by a desalting step using 3 × 5 ml HiTrap Desalting columns equilibrated in 50 mM HEPES pH 8.0, 1 mm tris(2-carboxyethyl)phosphine (TCEP). Purified protein was digested overnight at 4 °C with 1 mg of tobacco etch virus (TEV) protease/10 mg of eluted protein and was passed over a nickel affinity column collecting the flow-through. Purified proteins were stored at −20 °C and analysed by SDS-PAGE and Matrix-Assisted Laser Desorption Ionization-Time Of Flight (MALDI-TOF) to assess their integrity, identity, and purity level (range of purity 60–90%).

Staphylococcal Surface Protein Microarray construction, imaging and data analysis

The Staphylococcal protein microarray was generated by spotting purified recombinant proteins (0.5 mg/ml in a final glycerol concentration of 40%) in 16 replicates on nitrocellulose coated slides (FAST slides; Whatman) using the ink-jet spotter Marathon (Arrayjet) resulting in spots of ~110 µm in diameter. Printing was performed in a cabinet with controlled humidity and temperature (55–60% and 12 °C respectively). A standard curve made of eight concentrations (twofold dilution from 0.5 to 0.004 mg/ml) of an amino terminal FLAG-tagged protein (P7582 Sigma) was used to assess comparison of replicate experiments (Supplementary Fig. S6A). Mean fluorescence intensities (MFI) of FLAG-tagged protein spots obtained after detection with Cy5-conjugated anti-FLAG were fitted best by sigmoid curves, showing a signal dynamic range of about 2 logs of fluorescence intensity values and a lower detection limit corresponding to

ca. 0.03 ng (Supplementary Fig. S6B). The MFI value (63000) of the two highest points of the control dots was arbitrary set as 100%. For each of the spotted protein, the obtained MFI was normalized and expressed as a percentage of the reference spots using the following formula: (MFI of the protein × 100)/63000. Fluorescent BSA Cy3/Cy5 conjugated at 0,5 mg/ml and a standard curve of mouse IgGs were used to obtain eight replicates of a fluorescence standard curve to assess array coordinates. Meningococcal factor H binding protein (fHbp) was printed as a positive control for interaction with human factor H.

Each *S. aureus* protein was printed in 16 replicates all over the slide in a random fashion to minimize detection of false-positives that might occur by possible contamination between adjacent spots. Preliminary slide validation experiments, in which the slides were probed with mouse anti-GST and anti-6xHis monoclonal antibodies followed by detection with a Cy5-conjugated anti-mouse IgG secondary antibody, were performed to confirm the efficiency and reproducibility of the protein deposition on the chips.

Nonspecific binding was minimized by preincubating arrays with a blocking solution containing NAP blocker (G-Bioscences) diluted 1:3 in PBS (Nap-PBS) for 1 hour. Human tagged proteins were diluted in Nap-PBS at final concentration of 10 µg/ml and overlaid on the arrays (1 µg protein per slide) at RT for 1 h. After washing with 0.1% Tween 20 in PBS buffer (TPBS), arrays were incubated with mouse anti-FLAG (1:200– Sigma Aldrich) at RT for 1 h. Slides were washed again as before and interactions were detected by incubating with a Cy5 labeled anti-mouse antibody (Jackson Immunoresearch). Fluorescence images were obtained using Power scanner (Tecan Trading AG, Switzerland) and the 16-bit images were generated with PowerScanner software v1.2 at 10 µm/pixel resolution and spot fluorescence intensities were determined using ImaGene 7.0 software (Biodiscovery Inc.). Microarray data analysis was performed using in-house developed software. For each protein, the mean fluorescence intensity (MFI) of replicated spots was determined, after subtraction of the background value surrounding each spot.

MFI values greater than 3000 (equal to the mean signal of the controls spots after detection with anti-Flag and anti-mouse alone, plus ten times standard deviation values) were considered as a positive interaction. Three arbitrary MFI thresholds were also assigned for low (3000 to 15000 MFI), medium (15000 to 30000 MFI) and high (30000 to saturation) reactivity between two interacting proteins.

Negative control experiments were represented by slides incubated with anti-FLAG and anti-mouse antibodies only; the measured signals for each spot of the negative control slide was subtracted from those

obtained for the same spot in the slides probed with human proteins. The average of the 16 spots replicates constitutes the mean fluorescent intensity (MFI) value taken in consideration for the validation experiments.

FLIPr expression and purification

To obtain an amount of protein in a mg range, FLIPr (25–133) was expressed in BL21 E. *coli* (DE3) cells in HTMC autoinducing media (3% yeast extract, 40 mM KH_2PO_4, 90 mM K_2HPO_4, 2 mM $MgSO_4$, 1.5% glycerol, pH7.4). Bacteria were grown for 30 h at 27 °C and cell were then harvested at 10000 × g for 1 h. Bacterial pellets were suspended in lysis buffer (50 mM NaH_2PO_4 pH 8,2, 300 mM NaCl supplemented with Roche EDTA-free protease inhibitors) lysate was clarified by centrifugation at 30.000 × g for 30 min. The histidine-tagged protein was purified using a nickel column (His Trap FF, 5 ml–GE Healthcare) following the manufacturer's instructions. An additional step on Superdex 75 26/60 (GE Healthcare) was performed to remove possible aggregates. Sample purity was checked by 4–12% SDS-PAGE and SE-UPLC.

Construction of a flipR mutant

Primers for mutant and complementing plasmid construction are listed in Table 1. For the construction of an unmarked in-frame deletion mutant in *flipR* (NWMN_1067), a 1004 bp long fragment upstream of *flipR* and comprising the first six nucleotides of the gene as well as a 1029 bp fragment downstream of *flipR* and comprising the last six nucleotides of the gene was amplified from *S. aureus* strain Newman by PCR using KAPA HiFi DNA polymerase (Kapa Biosystems is based in Wilmington, Massachusetts, USA) and primers NWMN_1067_−998_KpnI_F2 and NWMN_1067_+6_R or primers NWMN_1067_+397_F and NWMN_1067_+1425_SacI_R2, respectively. The two flanking regions were then fused by PCR using primers NWMN_1067_−998_KpnI_F2 and NWMN_1067_+1425_SacI_R2 by combining equimolar ratios of the flanking regions and cycling without primers for five cycles followed by another 30 cycles after addition of the primers. The resulting product was digested by *Kpn*I and *Sac*I, cloned into pIMAY[31] passaged through RN4220 and transformed into the *S. aureus* USA300 strain LAC. Recombination and excision of the plasmid were performed as described previously[31]. In brief, the transformed strains were grown in TSB in the presence of 10 µg ml^{-1} chloramphenicol at 28 °C and 250 rpm overnight and integration of the plasmid into the genome triggered by incubating overnight at 37 °C and 250 rpm. The

culture was then streaked out onto TSA + chloramphenicol and incubated overnight at 37 °C. To promote excision of the plasmid cultures were then grown at 28 °C for 8 h and serial dilutions were plated onto TSA supplemented with 1 µg ml^{-1} anhydrotetracycline to select for loss of the plasmid. Ten large single colonies were screened by colony PCR using primers NWMN_1067_−1144_F and NWMN_1067_+1542_R confirming the deletion of *flipR*. Loss of the excised plasmid was confirmed by plating onto TSA alone and TSA supplemented with chloramphenicol.

Primer name	Sequence (5′-3′)
NWMN_1067_-998_KpnI_F2	AAGCTGGGTACCCCATTGAATTAAATGCTCTAAAACGAC
NWMN_1067_+6_R	GTATGTTTTTTAATATTTCATAATAAGTTCTCCCTGTAAAATAAATTTG
NWMN_1067_+397_F	CTTATTATGAAATATTAAAAAACATACTGAATTAAATAGTTGTACGC
NWMN_1067_ +1425_SacI_R2	GAATTGGAGCTCGATAACCCTATATGGTTGAATCATGTTG
NWMN_1067_-313_EcoRI_F	ATCCGGGAATTCGGAGTGTTTGTCTATCCAACTTAGCAAAC
NWMN_1067_+467_PstI_R	GCTTGGCTGCAGGCACGCCAATACGTTAGCATTG
NWMN_1067_-1144_F	GTGACCCAGCTAATGATTAACGTTG
NWMN_1067_+1542_R	GGAGGTCGTGTCATGAATGTTTG

Table 1: Primers used in this study

Complementation of the flipR mutant

In order to complement the *flipR* deletion mutant, the *flipR* gene including 313 bp upstream of the start codon was amplified using primers NWMN_1067_−313_EcoRI_F and NWMN_1067_+467_PstI_R (Table 1) and cloned into the *Eco*RI and *Pst*I restriction sites of pOS1[32]. The complementing plasmid and the empty control plasmid were passaged through RN4220 and then transformed into *S. aureus* strain USA300 Δ*flipR*.

Assessment of in vitro complement activity

The assessment of *in vitro* complement activity was analysed using a complement screening kit (Wieslab COMP300). This enzyme based immunoassay was developed for the *in vitro* determination of complement dysfunctions in patients. The system relies on the specific activation of the three distinct complement

pathways (CP, MBL pathway and AP) through activators immobilized on the microtiter wells, using the deposition of the terminal MAC (C5-9) complex as readout. Buffers containing specific blockers to ensure the activation of the respective pathway were used to dilute the samples. For our purposes, serial concentrations (5 µM, 1 µM and 0.2 µM) of FLIPr in HBS buffer (20 mM HEPES, 150 mM NaCl pH 7.3) were added to human serum previously diluted as suggested by supplier. Positive control was constituted by diluted serum and HBS buffer only, while negative control was constituted by heat inactivated serum. Additional control is represented by HBS buffer pre-incubated with serum. The amount of complement activation correlates with the colour intensity measured as OD_{405} nm. The value for the positive control was defined as 100%; the value for negative control as 0%. All measured values were expressed as relative % of complement activation using the following formula: (sample value − negative control value)/(positive control value−negative control value) × 100. Student's t test was used for comparison of paired means of two groups. P values of 0.05 were considered significant.

Whole blood phagocytosis assay

S. aureus survival in presence of FLIPr was assessed through whole blood phagocytosis assay. For such purpose an overnight culture of *S. aureus* cells from USA 300 LAC strain in BHI, was diluted 1:40 and grown at 37 °C with shaking 180 RPM to $OD_{600} = 0.300$. The bacteria were then diluted in BHI and 50 µl of the bacterial suspension (2.5×10^5CFU) were added to 1 ml of fresh blood from healthy donors supplemented with anticoagulant lepirudin 50 mg/L (20 µl/ml of blood) and previously preincubated for 30 min at 37 °C with different amount of FLIPr (0.4-3 µM), or with FLIPr KO (Δ*flipR*), or the Δ*flipR* mutant harboring the empty control plasmid or with PBS. A portion of this culture was plated on BHI-agar to determine the input CFU. The blood samples were incubated with bacteria at 37 °C for 2 h with shaking 180 RPM. Aliquots were then incubated for 3 min on ice with a final concentration of 0.5% of saponin-PBS to lyse neutrophils. The number of viable bacteria was determined by serial tenfold dilutions in BHI and plating on BHI- agar plates. Colonies were counted after incubation of the plates at 37 °C for 18 h. Control was the blood sample preincubated with PBS. Normal freshly drawn human blood was obtained from healthy volunteers and informed consent was obtained from all participants. The methods described were carried out in accordance with the approved guidelines and experimental protocols were approved with the recommendations of the local ethical committee of the University of Pavia (permit 19/9/2013).

Bacterial supernatant analysis

The determination of FLIPr in bacterial supernatants has been evaluated by western blot analyses. *Staphylococcus aureus* Newman WT was grown overnight in TSB (17 g/l bacto tryptone, 3 g/l bacto soyone, 2.5 g/l glucose, 5 g/l NaCl, 2.5 g/l Dipotassium Hydrogen Phosphate) medium at 37 °C until it reached the OD_{600} = 11,7 (stationary phase) and cell-free supernatant was harvested by centrifugation and filter sterilized. For the western blot analyses, supernatant has been concentrated 40 times with Amicon CutOff 3 kDa and protein content quantify by BCA assay (Thermo Scientific). 5 µl of concentrated supernatant have been loaded into a 4–12% SDS-PAGE gel (Invitrogen) and western blot assay was performed using affinity purified monoclonal antibody against FLIPr produced in mouse and anti-mouse HRP 1:5000.

GNF Protein microarray construction and processing

The GNF protein microarrays were generated by using 2354 human recombinant proteins from the GNF library, which were produced as described previously[7]. Each protein of the library was spotted in duplicates in 24 blocks per array onto ultra-thin nitrocellulose coated glass slides (PATH slides; Grace Bio Labs) using a contact printer (MicroGrid II; Digilab). Printing was performed at room temperature and ambient relative humidity. Proteins were diluted ½ in arraying buffer (100 mM NaCl, 0.05% TritonX and 5% Glycerol in PBS) and printed between 10 amol to 75 fmol per 150 µm diameter spot. A Chrompure human IgG (Jackson IR 009-000-003) was printed at 0.4 fmol per spot several times on each single block and served as a printing control and to define the blocks. Eight empty blocks were available to print additional antigens and relevant controls such as biotinylated BSA. Since all secretomics proteins have a 6-His tag and approximately 1/3 have an additional mouse Fc-tag, the printing efficiency of the proteins and microarray quality was evaluated by probing the microarrays with a mouse anti-His (Sigma H1029) antibody followed by a detection using a mix of a Cy5 conjugated $F(ab')_2$ goat a-mIgG Fc specific (Jackson IR 115-176-071) and a Cy5 conjugated goat α-hIgG $F(ab')_2$ specific secondary antibody (Jackson IR 109-175-097). The last secondary antibody (Jackson IR 109-175-097) was systematically used in the assays to detect the human IgG control spots printed on the arrays in order to define the blocks. Bexsero® vaccine antigen NadA, was biotinylated using EZ-Link Sulfo-NHS-LC-Biotin (Thermo Scientific) following manufacturer's instruction. The mass of the proteins and degree of biotinylation was checked with Liquid chromatography coupled to mass spectrometry (LC-MS). The incubation of protein microarrays with NadA

was performed using an automated hybridization station (HS400; Tecan), programmed with an internal protocol. First, the protein microarrays were incubated with a PBS blocking solution containing 1% BSA and 0.1% Tween20 for 1 hour at 23 °C to reduce non-specific binding. Then, NadA, diluted in probing buffer (2.5% glycerol, 1% BSA, and 0.05% TritonX in PBS) at final concentrations of 150 nM and 1 µM, were incubated for 1 h at 23 °C. After a washing step with probing buffer, the microarrays were probed with Cy5-Streptavidin (Invitrogen SA1011) combined with Cy5-goat a-hIgG $F(ab')_2$ specific (Jackson IR 109-175-097) diluted in probing buffer at 7.5 µg/ml final concentration. Finally, after two washing steps using probing buffer and Milli-Q water, the microarrays were dried under a flow of nitrogen at 30 °C for 4 min. In parallel a control microarray slide probed with buffer and the mix of the detection antibodies was performed.

GNF Microarray imaging and data analysis

Microarray image acquisition was done using a fluorescence microarray scanner (GenePix Professional 4200 A; Molecular Devices) equipped with a red laser (635 nm) at a resolution of 10 µm/pixel and images were analyzed using the GenePix Pro v6.1 software (Molecular Devices). Data analysis was performed using in-house developed software. For each protein, the mean fluorescence intensity (MFI) of replicated spots was determined, after subtraction of the background value surrounding each spot. The MFI value of the control dots (biotinylated BSA) was arbitrary set as 100%. For each of the spotted protein, the obtained MFI was normalized and expressed as a percentage of the reference spots. Proteins with a high coefficient variation (CV) between the two replicates were discarded. All signals with MFI score equal or greater than 25% were considered as positive hits, excluding the ones found in the control microarray where the Cy5-Streptavidin alone was probed to determine its non-specific binding to the printed proteins.

NadA and NadA constructs cloning, expression, purification and characterization

The *nadA* gene fragments from *N. meningitidis* strain 2996 were cloned by PCR, using the PIPE (polymerase incomplete primer extension) method, as described previously[16]. The cloned fragments lacked the first 23 residues of NadA which encode a signal peptide for protein export. The fragments were inserted into a pET-21 vector (Novagen), enabling cytoplasmic expression of the NadA proteins with a C-terminal 6-His tag. The residue numbering employed refers to the full-length NadA protein, Uniprot code Q8KH85.

All NadA proteins were produced in *E. coli* BL21D3 (T1r) cells (Invitrogen) and were purified at room temperature (RT, 18–26 °C) using an AKTA purifier 10 system (GE Healthcare) by Ni-affinity chromatography (5 mL HiTrap Ni-NTA column) and by size-exclusion chromatography on a HiLoad (16/60) Superdex 75 column equilibrated in 20 mM Tris–HCl, 150 mM NaCl pH8.0. The quality of the final NadA samples was checked using 4–12% SDS–PAGE gradient gels in MES buffer and also by size-exclusion high-performance liquid chromatography (SE-HPLC), revealing a high level of purity (estimated to be >97% for all proteins) and a lack of any aggregated species. SE-HPLC was performed at RT on an analytical size exclusion TSK Super SW3000 column by loading 20 µl of each sample at a concentration of ~40 µM. Samples were eluted isocratically in 0.1 M NaH_2PO_4, 0.4 M $(NH_4)_2SO_4$ buffer at pH 6.0. Coupling SE-HPLC with Multi-angle laser light scattering (SE-HPLC/MALLS) NadA samples were analyzed for molecular size. Data analyses were carried out using Astra V software (Wyatt) to determine the weight-average molecular mass (MW) in Daltons and the polydispersity index (MW/Mn) for each oligomer present in solution.

BioLayer Interferometry (BLI)-based OCTET analysis

Octet QKe (ForteBio, Pall Science) was used for binding studies. SA (streptavidin) and AR2G (amine reactive 2nd generation) tips were obtained from ForteBio and were used respectively to immobilize biotinylated proteins and to covalently attach ligand protein using amine based chemistry. Immediately before analysis, tips were prewet in kinetic buffer.

For the FLIPr-C1q characterization, after 180 sec baseline in kinetic buffer (10 mM HEPES, 300 mM NaCl, 0,02% P-20 pH 7.4), the biosensor tips were activated for 300 sec using a freshly mixed solution of 200 mM EDC in 50 mM NHS further diluted 1:20 in dH_2O and the tips were then immersed in ligand solution for 600 sec loading (C1q 12.5 ug/ml in 10 mM NaH_2PO_4 pH 6.5 or FLIPr 50 ug/ml in 10 mM Na acetate pH 5). Excess reactive groups were blocked with 1 M ethanolamine pH 8.5 for 300 sec and a second 300 sec baseline in kinetic buffer was performed and kinetic was monitored.

For the NadA/LOX-1 characterization after 180 sec baseline in kinetic buffer (10 mM HEPES, 150 mM NaCl, 0,02% P-20 pH 7), AR2G tips were activated for 300 sec using a freshly mixed solution of 200 mM EDC in 50 mM NHS further diluted 1:20 in dH_2O. The tips were then immersed in ligand solution (LOX-1 at 12.5 µg/ml in acetate pH 5.5) for 600 sec. Excess reactive groups were blocked with 1 M ethanolamine

pH 8.5 for 300 sec and a second 300 sec baseline in kinetic buffer was performed and kinetic was monitored. For NadA constructs characterization, SA biosensor tips after 180 sec baseline in kinetic buffer, were directly immersed in ligand solution for 600 sec loading (biotinylated NadA, $NadA_{24–170}$ and $NadA_{91–342}$ at 25 µg/ml diluted kinetic buffer) and a second 300 sec baseline in kinetic buffer was performed and kinetic was monitored. Recombinant LOX-1 ectodomain produced in mammalian cells was purchased from R&D systems.

During the entire kinetic assay, the sample plate was kept shaking 1000 rpm. A column of biosensors where no ligand protein was loaded, was activated and quenched (where necessary) to be used as parallel reference control in association with the analyte titration; a ligand-loaded biosensor was also used in association with buffer as baseline.

Reference subtracted BLI response curves were used for the affinity constant determination. Inter-step correction and Y-alignment were used to minimize tip-dependent variability. Data were globally fitted in a 1:1 model using the Data Analysis Software v7.1 (Forte Bio).

Dot blot assays

$NadA_{24–170}$ (head&neck), $NadA_{91–342}$ (stalk) and NadA protein constructs (200 ng) were spotted and adsorbed onto nitrocellulose membrane strips. The strips were blocked in PBS containing 3% (w/v) milk and 0.1% Tween 20 (v/v), and then incubated with the mAbs 9F11, 1C9/A9 and 3C11/H7 at 1 µg/ml for 1 h at 37 °C, respectively. Membranes were washed with PBS containing 0.1% Tween 20 (v/v), (T-PBS), and then incubated with sheep anti-mouse horseradish peroxidase-conjugated IgG diluted 1:5000 in milk/T-PBS. Membranes were washed and signals were revealed with the SuperSignal WestPico Chemiluminescent Substrate Kit (Thermo Scientific Pierce, Waltham, MA, USA).

mAbs selection and binding competition

For competition experiments, a preliminary screening to select high-affinity anti-NadA mAbs was performed. Protein G biosensors tips were pre-wet in kinetic buffer (10 mM HEPES, 150 mM NaCl, 0,02% P-20 pH 7.4). After 180 sec baseline, tips were directly immersed in each mAb (diluted at 50 µg/ml in

kinetic buffer) for 600 sec. A second 300 sec baseline in kinetic buffer was performed. NadA was tested as analyte at 200 nM. Competition experiments were performed immobilizing LOX-1 as above. NadA was pre-incubated with an excess of mAb (1:3) overnight at 4 °C and the mix was used as analyte in the same assay conditions as above.

Dynamic Light Scattering (DLS) measurements

For DLS analysis DynaPro® Plate Reader II (WYATT Technology) with 96 Well Plates was used. NadA, LOX-1 and the complex mixed in a 1:1 molar ratio were diluted in HBS-P buffer in a final concentration of 5 µM. A cut off from 0, 1–100 nm was applied. Results are mean of 30 measurements per sample.

FACS binding experiments

To perform binding assay, LOX-1 transfected and non-transfected CHO cells were detached using trypsin (CDS, Sigma), harvested and suspended in F12-K medium supplemented with 10% FBS. Approximately 1×10^6 cells were incubated with 200 µg/ml NadA or PBS alone for 30 minutes at 4 °C. Cells were then incubated with 5 µg/ml of anti-NadA 9F11 mouse monoclonal antibody for 1 hour at 4 °C, and with Allophycocyanin (APC)-conjugated goat F(ab)2 anti-mouse Ig (diluted 1:100; Jackson ImmunoResearch Laboratories) for 30 minutes at 4 °C. Cells were stained with Live/Dead Aqua (Invitrogen) diluted 1:400 for 20 minutes in the dark and analyzed with a Canto II analyzer (Becton Dickinson, Pharmingen, San Diego, CA). Flow-cytometric analysis was performed using FlowJo software (Treestar Inc.).

Results

Two different microarray-based set-ups were applied to the discovery of novel host-pathogen interactions

The overall strategy for the microarray-based identification of new interactions between human and bacterial extracellular proteins is reported in Fig. 1. Two different microarray screening setups were designed for the two pathogens, trying to answer different biological questions. The first setup had the primary objective of acquiring a picture of the reciprocal interactions between staphylococcal and human extracellular proteins. A complete unbiased approach in this setup would have allowed the screening of 381,600 different interactions, i.e. 159 staphylococcal proteins tested against 2400 human proteins. To show the feasibility of the approach, a subset of the human library consisting of major components from the complement system and extracellular matrix was selected for expression and purification, since these protein classes represent the first line of interaction at the host-pathogen interface. The resulting 75 recombinant proteins were tested against the staphylococcal library, leading to the remarkable number of 11,925 different interactions screened. The second set-up had the main goal of identifying new soluble/cellular receptors for the meningococcal adhesin NadA. In an unbiased approach, the complete library was expressed and NadA screened against it.

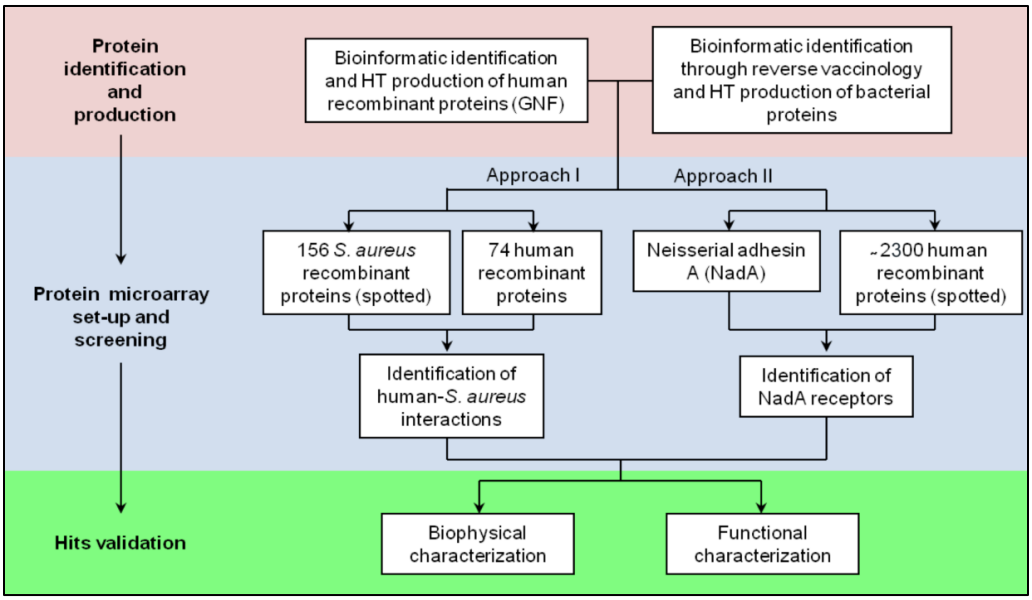

Conceptual organization of the workflow
We divided the work in three main steps: the protein identification and production, the protein microarray preparation and screening, and the hits validation. The two different approaches applied to S. aureus and to *N. meningitidis* are shown.

Protein microarray led to the identification of 17 interactions with high Mean Fluorescence Intensity (MFI) between S. aureus and human proteins

The protein microarray screening was performed testing 159 purified recombinant *S. aureus* proteins spotted onto nitrocellulose coated glass slides against 75 human recombinant proteins that include human complement factors and extracellular matrix proteins (Fig. 2a and Supplementary Table S1). The *S. aureus* proteins printed on the arrays represent surface and secreted factors selected *in silico* using a combined bioinformatics approach[17,18]. A total of 114 unique proteins were spotted, of which 104 were included as single constructs and 10 as multiple constructs for a total of 159 recombinant constructs (Fig. 2b and Supplementary Table S2). Supplementary Fig. S1 and supplementary Table S3 show the results obtained; out of 11766 possible binary interactions, 11168 (94.92%) resulted below the background threshold and were thereby considered as negative, while 598 (5.08%) resulted positive. Among these, 518/598 (4.40%) were ranked as low, 61/598 (0.52%) as medium and 19/598 (0.16%) as highly reactive (Supplementary Fig. S1, upper left panel) based on their MFI signals. Within the top 19 interactions (Supplementary Table S4), factor H binding protein (fHbp) variants 1 and 3 - which constituted the positive controls - were found when tested with human complement factor H. Among the tested human proteins, ficolin-2 showed medium/high binding signals with 80 out of the 159 bacterial proteins tested (Fig. 2c). Although we cannot exclude that a specific binding may occur between ficolin-2 and some staphylococcal proteins, this result seems to suggest that components other than the specific proteins spotted on the chip are recognized. In fact, ficolin-2 is known to bind to N-acetylglucosamine (GlcNAc) sugar residues[19] and our analysis may have been compromised in this case by the presence of residual GlcNAc-containing LPS in the staphylococcal recombinant proteins produced in *E. coli*. Similarly, since the detection system relies on the use of antibodies and several human proteins were fused to an Fc-tag, the putative hits of the staphylococcal protein A (SpA) were not considered for further validation, knowing its ability to bind immunoglobulins. The rest of the highly reactive hits were shared between the staphylococcal glycyl-glycine endopeptidase LytM (4 hits), the conserved staphylococcal antigen 1D (Csa1D) (1 hit), and the FPRL1 (formyl peptide receptor-like 1) inhibitory protein (FLIPr) (6 hits). LytM (Fig. 2d) showed high reactivity signals with the complement factor P (CFP) (MFI score of 95%), adiponectin protein (ADIPOQ) (MFI score of 67%), the complement component 1q subcomponent like 4 (C1QL4) (MFI score of 52%) and the matrix remodelling associated protein 8 (MXRA8) (MFI score of 50%). Csa1D was instead highly reactive with ficolin-1 (FCN1). FLIPr showed several interesting putative interactors (Fig. 2e): the intercellular adhesion molecule 5 (ICAM5) (MFI score of 89%), the heat stable enterotoxin receptor (GUCY2C) (MFI score of 84%), the complement component 1q subcomponent-like 4 (C1QL4) (MFI score of 76%), the matrix remodeling

associated protein 8 (MXRA8) (MFI score of 66%), the complement component 1q subcomponent B (C1QB) (MFI score of 61%) and the bone sialoprotein 2 (IBSP) (MFI score of 59%). Interestingly FLIPr showed signals of medium intensity also with the complement component 1q subcomponent A (C1QA - MFI 24%), the complement component 1q subcomponent-like 2 (C1QL2 - MFI 16%) and the complement component 1q subcomponent C (C1QC – MFI 13%). Most identified interactions are novel and require further validation since they involved loosely characterized proteins. Since the interaction between FLIPr and the human C1q subcomponents involved key players of the bacterial offense and host defense, this interaction was further validated at the biochemical and functional level.

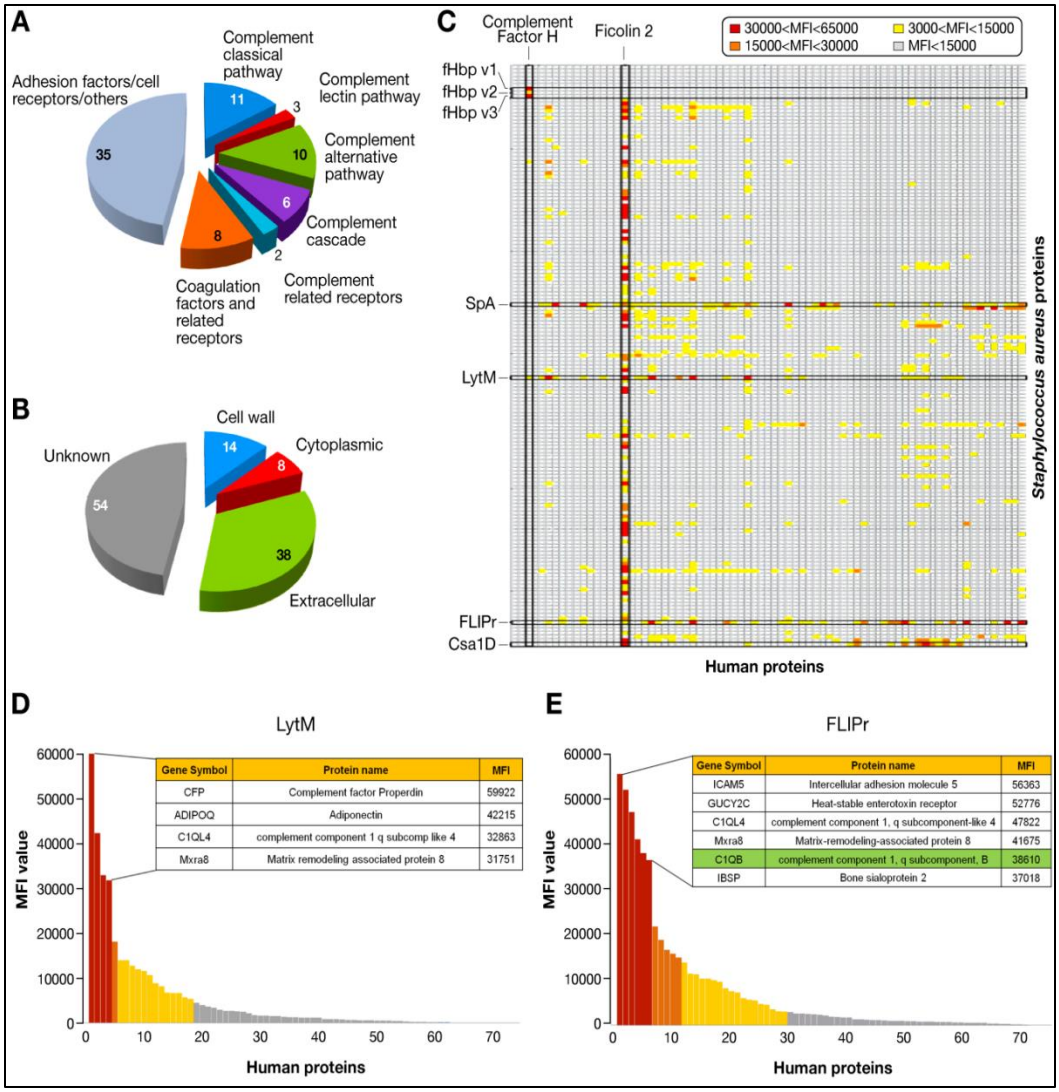

Protein microarray applied to *S. aureus*: design and results

(**a)** Classification of the 75 human proteins tested in the microarray screening based on their biological function and **(b)** of the *S. aureus* proteins spotted on the chip based on their predicted localization. **(c)** Schematic overview of the grid resulting from the screening. *S. aureus* proteins (lines) spotted on the chip were plotted against human proteins (columns) tested in overlay. Cells contain MFI value for each pair. Color code is used for visual information and to identify the three MFI cut-off thresholds (grey: MFI < 5%; yellow: 5% < MFI < 25%; orange: 25% < MFI < 50%; red: 50% < MFI < 100%. Human complement factor H and ficolin-2 and the bacterial fHbp v 1, 2 and 3 (neisserial proteins used as control), SpA, FLIPr and Csa1D are highlighted. **(d)**Plotting of MFIs of the 75 human proteins on the spotted LytM. Inset table shows MFI values, protein name and gene symbol of the 4 human proteins displaying fluorescence intensities above 50% MFI. **(e)** Plotting of MFIs of the 75 human proteins on the spotted FLIPr. Inset table shows MFI values, protein name and gene symbol of the first 20 human proteins. C1qB subcomponent is highlighted in green.

FLIPr binds in vitro the C1q subcomponents and the C1q complex purified from human plasma

To validate the FLIPr/C1q interaction the BLI (BioLayer Interferometry) technology was used. FLIPr protein was immobilized on the BLI biosensor and C1qA, C1qB and C1qC subunits, previously used in the screening, were tested as analytes in serial dilutions. The three subcomponents showed low nanomolar affinity for FLIPr (equilibrium dissociation constant, K_D, of 3.2 nM, 2.1 nM and 9.9 nM respectively–Fig. 3a–c). In biological conditions, however, the three C1qA, C1qB and C1qC subunits are super-organized to constitute the C1q complex. Binding experiments between FLIPr and the human C1q complex purified from human plasma were therefore performed. When immobilized, FLIPr showed picomolar affinity for the C1q complex (K_D = 62 pM–Fig. 3d). Conversely, when the C1q complex was immobilized, the measured affinity was in the high nanomolar range (K_D = 679 nM–Fig. 3e).

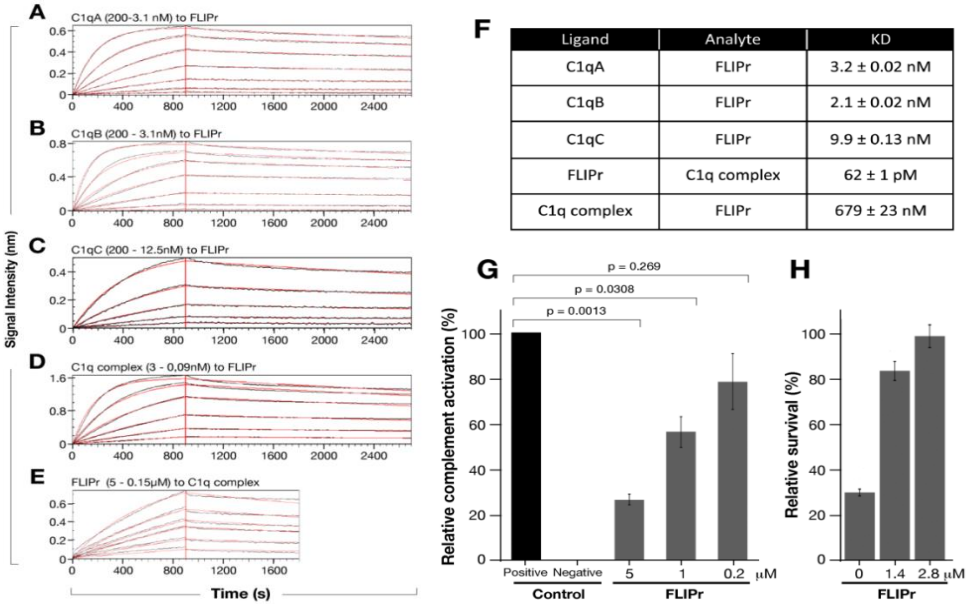

Biophysical and functional characterization of the FLIPr-C1q interaction
Bio-layer interferometry (BLI) blank subtracted sensograms of **(a)** C1qA (200-3.1 nM), **(b)** C1qB (200-3.1 nM) and **(c)** C1qC (200-12.5 nM) subcomponents tested on covalently immobilized FLIPr. **(d)** BLI blank subtracted sensograms of FLIPr (5-0.15 µM) on immobilized C1q complex and **(e)** of C1q complex (3-0.09 nM) on immobilized FLIPr. The amount of ligand associating with the analyte was measured in nanometres (nm). Association and dissociation curves were fitted in a 1:1 model. **(f)** Summary table of the measured affinity constants (KD). **(g)** Complement classical pathway influence by FLIPr in WiELISA assay. Relative % of complement activation is shown for each sample. Results are mean of three replicates. P values ≤ 0.05 were considered significant. **(h)** FLIPr-mediated dose dependent increase of *S. aureus* survival in whole blood assay. Relative survival was monitored through CFU count. **(i)** Survival in human blood of *S. aureus* USA 300 LAC wt, *flipR* deletion mutant (Δ*flipR*) and *flipR* deletion mutant complemented with empty (Δ*flipR* + pOS1) and with plasmid bearing the *flipR* insert (Δ*flipR* + pOS1-*flipR*). Results are mean of three replicates. P values ≤ 0.05 were considered significant.

FLIPr reduces classical complement pathway activation and increases S. aureus survival in whole human blood (WHB)

In order to clarify whether the binding of FLIPr to C1q could influence activation of the complement classical pathway, a WiELISA (Wieslab) complement system screening kit was used. The complement classical pathway was investigated, and different amounts of FLIPr were pre-incubated with human serum. FLIPr at 1 µM reduced the complement classical pathway activation to ~56% and to ~26% when used at 5 µM (Fig. 3 g). FLIPr expression in *S. aureus* bacterial supernatant was confirmed by western blot assay using anti-FLIPr antibodies (Supplementary Fig. S2). To improve the understanding in FLIPr contribution to bacterial pathogenesis, *S. aureus* survival in whole human blood (WHB) was monitored in presence and absence of FLIPr. WHB pre-incubation with FLIPr significantly increased *S. aureus* survival (Fig. 3 h): FLIPr at 1.4 µM and 2.8 µM lead to a *S. aureus* survival rate of respectively 80% and 100%. A *S. aureus* knock out (KO) mutant for FLIPr was generated in order to corroborate the survival assay in whole blood. Loss of FLIPr resulted in a significant reduction of bacterial viability in WHB relative to the wild-type strains. Conversely, introduction of a plasmid borne copy of *flipR* restored viability of the bacteria compared to either the Δ*flipR* mutant or the Δ*flipR* mutant harboring the empty control plasmid (Fig. 3i).

Screening of NadA by protein microarray revealed 8 novel putative human interactors

In order to identify human proteins interacting with the Neisserial adhesin NadA[12], a large-scale protein microarray screening was performed spotting 2354 human recombinant proteins from the GNF library. Biotinylated NadA was used at 150 nM and 1 µM, and interactions were detected using fluorescently labeled streptavidin. The obtained MFI was normalized for each of the spotted proteins and expressed as a percentage of the reference spots (biotinylated BSA). The results of the screening at 150 nM showed several putative human interactors (Fig. 4a). In particular, isoform 1 and 2 of the Vasoactive Intestinal Peptides (VIP) showed an MFI score of 153% and 60% respectively, and the Protein Tyrosine Phosphatase Receptor type Sigma isoform 4 (PTPRS) with an MFI of 64% were highlighted as strong hits. Two replicates of the low-density oxidized lipoprotein receptor 1 (LOX-1) showed an MFI score of 45% and 37% represented potentially relevant hits. These data were substantiated when NadA was tested at 1 µM. All five hits identified in the 150 nM screen were confirmed (Fig. 4b). In addition to these proteins, further putative hits were identified: the Stromal interaction molecule 1 precursor (STIM1), the Natriuretic Peptide Precursor C (NPPC), the sperm acrosome-associated protein 7 precursor (SPACA7) and the Interleukin 6

precursor (IL-6). Among all the identified hits, LOX-1 represented an interesting candidate for further validation processes since it is known to be involved in bacterial adhesion and invasion[20,21] and its deletion enhances bacterial clearance[22].

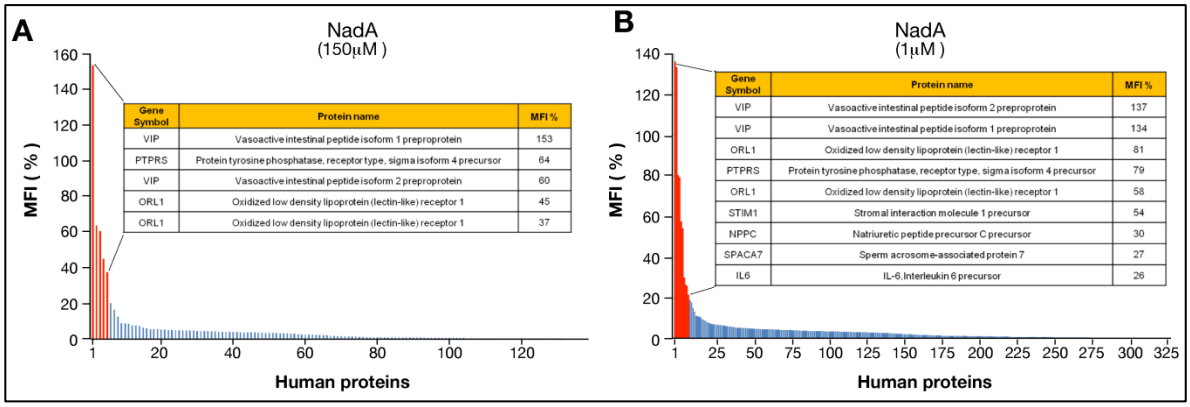

Screening for NadA interactors

(a) Plotting of MFIs relative percentage of spotted human proteins tested against NadA at 150 nM and **(b)** 1 µM. Red bars represent human proteins above the 25% cut-off threshold defining relevant interactions. Blue bars represent human proteins above the 4% cut-off threshold. Inset table shows gene symbol, protein name and MFI values of the relevant interactions.

LOX-1 binds to the N-terminal region of NadA

To validate and characterize the binding kinetics between NadA and LOX-1 BLI was used. LOX-1 recombinant protein was first immobilized onto the BLI biosensor, and NadA was used as analyte. The calculated K_D was approximately 5 nM (Fig. 5a). This value was also confirmed when the system was reverted (Fig. 5b). Dynamic light scattering (DLS) analysis was carried out to study the interaction in solution (Supplementary Fig. S3): the proteins were first analyzed alone, resulting in a hydrodynamic radius of 4.2 nm and 6.2 nm for LOX-1 and NadA, respectively. The two proteins were then mixed at a final concentration of 5 µM (each component) in a 1:1 molar ratio (trimeric NadA and dimeric LOX-1) prior to DLS analyses. As a result, a single peak with hydrodynamic radius of 8.9 nm and low polydispersity index, *i.e.* 13.4% was obtained. Nevertheless, the rod-shaped structure of both NadA and LOX-1 may have led to an overestimation of the hydrodynamic radii and therefore also to an overestimation of the protein MWs, thus hindering a precise determination of the size and stoichiometry of the complex. However, the low polydispersity and the absence of peaks corresponding to single protein radii or aggregates in the complex solution, is consistent with a 1:1 complex between one NadA trimer and one LOX-1 dimer.

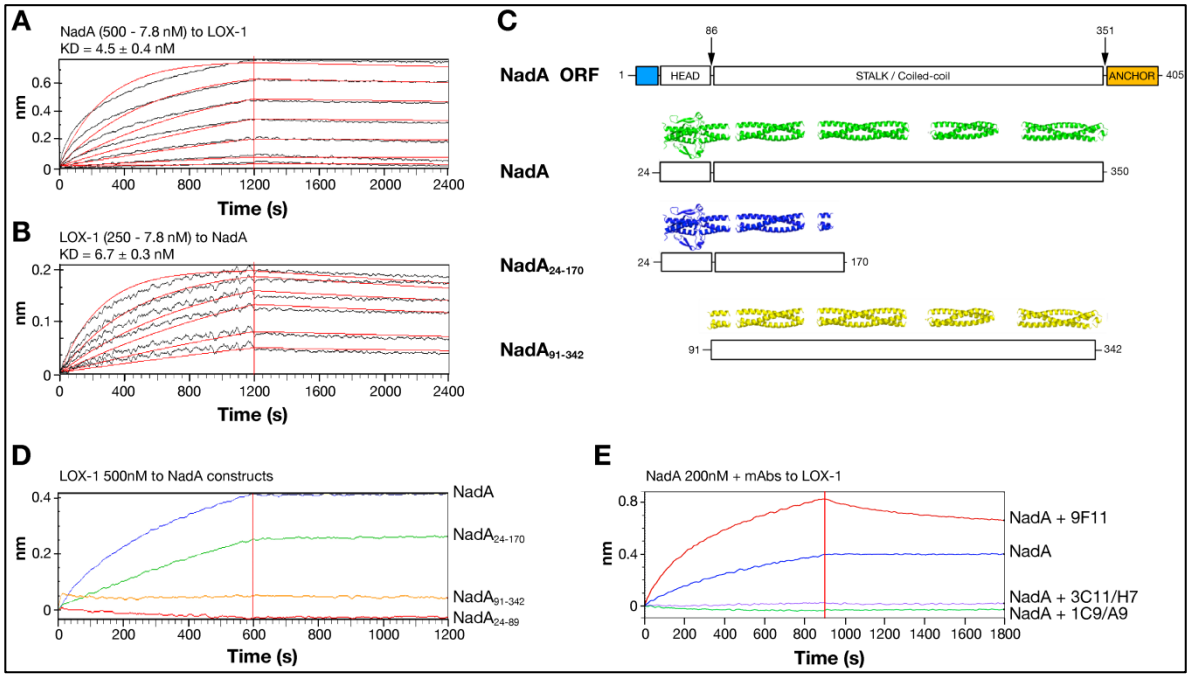

Biophysical characterization of the NadA/LOX-1 interaction.
(**a)** Blank subtracted sensograms of NadA (500 - 7.8 nM) tested on covalently immobilized LOX-1 and **(b)** of LOX-1 (250 - 7.8 nM) tested on biotinylated NadA immobilized on SA biosensors. Association and dissociation curves were fitted in a 1:1 model. **(c)** Schematic representation of the NadA constructs used to determine NadA binding site on LOX-1. NadA gene, NadA (green), $NadA_{24–170}$ (blue) and $NadA_{91–342}$(yellow) structure are shown. $NadA_{24–89}$ head construct is represented only as a cartoon (rectangles) since it is not trimeric and not folded. Signal peptide (light blue) and membrane anchor (orange) are shown in the cartoon. **(d)** Blank subtracted sensograms of LOX-1 (200 nM) on biotinylated NadA (blue), $NadA_{24–170}$(green), $NadA_{91–342}$ (yellow) and $NadA_{24–89}$ (red). **(e)** Binding competition between LOX-1 and anti-NadA mAbs. Binding between NadA and LOX-1 is shown (blue). mAb 9F11 mapping NadA stalk does not inhibit the binding with NadA (red). mAb 3C11/H7 (violet) and mAb 1C9/A9 (green) mapping on NadA head abrogated NadA binding on LOX-1.

To identify the binding region for LOX-1, the $NadA_{24–170}$ (head&neck), $NadA_{91–342}$ (stalk) and $NadA_{24–89}$ (head-only) constructs, designed based on the recently published crystal structure[16], were produced as his-tagged recombinant proteins (Fig. 5c). The $NadA_{24–170}$ and $NadA_{91–342}$ constructs were shown to be trimeric and well-folded according to size-exclusion high-performance liquid chromatography (SE-HPLC) with Multi-angle laser light scattering (MALLS), while the $NadA_{24–89}$ resulted monomeric and unfolded (Supplementary Fig. S4), also in accordance with differential scanning calorimetry (DSC) experiments reported previously[16]. BLI binding experiments revealed the retained capability of the $NadA_{24–170}$ construct to bind LOX-1. The binding was instead not observed for the $NadA_{91–342}$ and $NadA_{24–89}$ constructs (Fig. 5d). Binding competition experiments using BLI were also performed in order to understand the potential ability of anti-head monoclonal antibodies (mAbs) to inhibit the NadA/LOX-1 interaction. Anti-NadA mAbs were selected based on their binding site on NadA constructs using dot blot (Supplementary Fig. S5). BLI binding assay (Fig. 5e) showed a marked ability of mAbs (3C11/H7 and 1C9/A9) mapping to the

NadA head&neck region to inhibit the binding with LOX-1. By contrast the 9F11 mAb, which maps to the NadA stalk, did not inhibit the binding to LOX-1, confirming the NadA head&neck region as the one involved in LOX-1 binding.

NadA binds LOX-1 transfected CHO cells

To further validate the interaction between LOX-1 and NadA, binding assays on eukaryotic cell lines were performed. Western blot analysis confirmed that CHO (Chinese Hamster Ovary) cells do not constitutively express LOX-1 (data not shown). CHO cells were transiently transfected with a pEYFP-N1 vector expressing human LOX-1 and FACS analysis showed that transfected cells exposed the receptor on the cell surface (Fig. 6, bottom left panel). Non-transfected cells did not bind NadA (Fig. 6, upper right panel). NadA binding was observed selectively on the entire LOX-1 expressing cell population (Fig. 6, bottom right panel). These data are consistent with a specific interaction of NadA with human LOX-1 recapitulating in the cellular context the results obtained with protein array and BLI analysis.

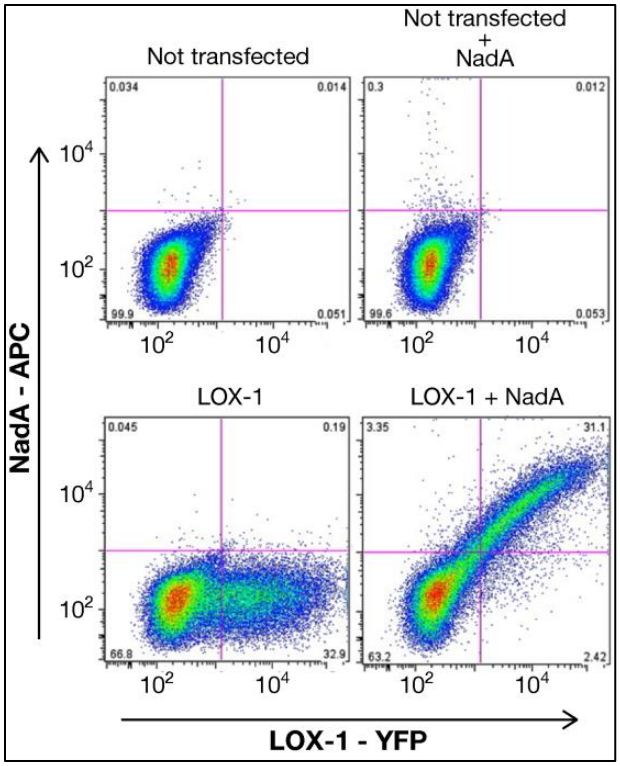

NadA binds CHO cells expressing hLOX-1.
FACS plots representative of LOX-1 (YFP) expression in CHO cells and cells able to bind NadA (APC). The gating strategy was designed to separate the cells of interest from large aggregates and debris [initial gate on forward scatter (FSC) versus side scatter (SSC) plot], deplete dead cells (Live/Dead Aqua staining) and doublets/aggregates (standard gates on both FSC-width and SSC-width) (data not shown). Simple gating by quadrants allowed defining the absolute percentages of cells positive for LOX-1 only (32%, bottom left) and double positive cells (30%, bottom right) representing the cells able to bind recombinant NadA. The upper right panel shows that not-transfected cells are not able to bind NadA. The upper left panel shows the non-transfected cells.

Discussion

S. aureus and *N. meningitidis* possess a wide variety of molecules specifically produced to adhere to and penetrate host tissues, evade the immune system and invade the host during pathogenesis. The main players in these processes are the host and bacterial extracellular proteomes. Recent studies pointed out the importance of a deeper understanding of the molecular mechanisms which underlie bacterial immune evasion and pathogenesis[23]. To this aim, we have applied a systematic large-scale protein microarray-based approach to identify novel host-pathogen interactions.

S. aureus is considered a master of complement evasion, with an impressive ability to persist within diverse microenvironments in the human body by using a number of secreted proteins that contribute to its pathogenesis. In order to discover novel interactions between the human and the *S. aureus* extracellular proteins, we screened 159 extracellular *S. aureus* proteins against 75 human extracellular components consisting of key effectors of the innate immune system as well as extracellular matrix proteins. The screening resulted in the identification of a novel target for a well-known *S. aureus* effector. We report for the first time the identification and biochemical/functional characterization of the interaction between FLIPr, a protein already described to be involved in *S. aureus* immune evasion process[24], and the subcomponents of human complement factor C1q.

When tested by label-free BLI technology, C1qA, C1qB and C1qC showed low nanomolar equilibrium dissociation constants with FLIPr, indicating a high affinity interaction with each of the subcomponents. Additional binding experiments were performed using the assembled C1q complex purified from human plasma, confirming that FLIPr is able to bind the assembled complex, and not only its single recombinant subcomponents. The measured affinity for the interaction between FLIPr and C1q complex was different depending on the binding orientation. The reason for the latter discrepancy was not investigated. It is conceivable that since the C1q complex likely possesses multiple binding sites for FLIPr, the apparently tighter binding when FLIPr is immobilized may be due to an avidity effect of the C1q complex, as previously shown for other bacterial C1q-binding proteins[25]. FLIPr is a staphylococcal virulence factor able to interfere with opsonophagocytosis by targeting the Fcγ receptor (FcγR) and formyl-peptide receptor (FPR) on phagocytes[24,26]. Our data show the human complement C1q complex as an additional target for this important protein; we show that FLIPr is able to interfere with the classical complement pathway activation in a cell-free complement assay in presence of human serum and to increase *S. aureus* survival in blood, while loss of FLIPr resulted in a significant reduction of bacterial viability in WHB relative to the

wild-type strains. This latter result may, in the first instance, be considered the result of a synergistic effect between the simultaneous inhibition of FcγR and FPR on phagocytes surface, and the inhibition of the complement mediated killing through C1q binding. Despite this, the phagocytosis inhibition exerted by FLIPr has been shown to dramatically decrease at near-physiological serum concentrations[24]. This effect might be described with a complement receptor-dependent phagocytosis, while only at low serum concentrations the process would be dependent on FcγR. Since the conditions we used presuppose physiological serum concentrations, we can exclude that the increased survival we see is dependent on decreased phagocytosis (dependent on FPR and Fcγ receptor). Rather, we think that the increased survival depends on complement perturbation and therefore on the interaction between FLIPr and C1q. What we hypothesize, combining the literature data and the data shown in this work, is a dual role of FLIPr during infection and pathogenesis; on one hand, in those environments at low serum concentrations like the interstitial tissue, through the binding of FcγR and FPR, FLIPr would allow to evade phagocytosis. On the other hand, in serum rich environments like the bloodstream, through the binding of C1q, FLIPr would instead allow to escape complement and complement receptor-mediated killing, but not phagocytosis. Moreover, an intracellular lifestyle at this last step may constitute a preferential mechanism for *S. aureus* survival and spreading.

As a further proof-of-concept of the experimental approach, a completely unbiased large-scale screening was carried out in order to identify novel human receptors for the Neisserial adhesin NadA by screening a library of 2354 human extracellular proteins spotted on slides. NadA is considered to be involved in the initial adhesion to epithelial cells[13], but may act also on different cell types, including monocytes/macrophages[27]. It has also been recently reported to bind human β1 integrins that are widely distributed in different human cells[15]. Interestingly, the microarray screening here described revealed new putative NadA receptors involved in endothelial permeabilisation and bacterial pathogenesis, *i.e.* the VIP peptides and the inducible oxidized LDL receptor LOX-1[21,22,23]. LOX-1, in particular, is known to be involved in the translocation of low-density lipoprotein vesicles and even bacteria across the endothelial barrier[20].

BLI binding experiments carried out using NadA stalk and head&neck constructs identified the latter as the major binding region. This data was also confirmed by competition experiments using anti-NadA mAbs. The mAbs targeting NadA head showed competition with LOX-1 for NadA binding. Furthermore, the binding test with the unfolded $NadA_{24–89}$ construct revealed that a structured head domain is required to accomplish the binding, suggesting a conformation-dependent protein-protein interaction. The binding

between LOX-1 and NadA was further corroborated by cellular binding assay in which the CHO cells transiently expressing LOX-1 were able to bind recombinant NadA.

The identification of the interaction between NadA and LOX-1 was reported here for the first time, and suggests an intriguing new role for the Bexsero® vaccine component NadA in meningococcus B pathogenesis. In fact, NadA has been described so far as having mainly epithelial targets, with a role in the colonization/invasion of the epithelial barrier. Here we report the identification of its first endothelial receptor, LOX-1, mainly reported as the receptor for oxidized low-lipoproteins and responsible for their internalization in endothelial cells. Recently, a specific interaction between the meningococcal pili type IV and host CD147 has been reported to be essential for meningococcal adhesion to human endothelial cells and colonization of human blood vessels[28], but other receptors might be necessary to allow bacterial invasion and pathogenesis. Meningococcus B might take advantage of the internalization mechanism exerted by LOX-1 to cross the blood-brain barrier, as also previously described for other pathogens[20,21,29]. Although further studies are necessary for a deeper understanding on NadA/LOX-1 role in endothelial crossing, our findings indicate that NadA is actually active far beyond the first meningococcal pathogenesis step and can have a crucial role at a later stage in the blood stream.

To our knowledge, this is the first time a microarray approach has been applied to the investigation of staphylococcal and meningococcal proteins targeting the human extracellular proteome. Moreover, this is the most extensive study carried out so far on protein-protein interactions at the host-pathogen interface for any human pathogen, including bacteria and parasites, raising the number of human proteins screened from a few tens up to more than 2300 that has driven the identification of novel host-pathogen interactions, providing novel insights on the molecular events that underlie *S. aureus* and *N. meningitidis* pathogenesis.

References

1. Bardoel B. W. & Strijp J. A. Molecular battle between host and bacterium: recognition in innate immunity. J Mol Recognit 24, 1077–1086 (2011). [PubMed]
2. Crosnier C. et al. . Basigin is a receptor essential for erythrocyte invasion by *Plasmodium falciparum*. Nature 480, 534–537 (2011). [PMC free article] [PubMed]
3. Bartholdson S. J. et al. . Semaphorin-7 A is an erythrocyte receptor for *P. falciparum* merozoite-specific TRAP homolog, MTRAP. PLoS Pathog 8, e1003031 (2012). [PMC free article] [PubMed]
4. Bartholdson S. J., Crosnier C., Bustamante L. Y., Rayner J. C. & Wright G. J. Identifying novel *Plasmodium falciparum* erythrocyte invasion receptors using systematic extracellular protein interaction screens. Cell Microbiol 15, 1304–1312 (2013). [PMC free article] [PubMed]
5. Galeotti C. L. et al. . Surface interactome in *Streptococcus pyogenes*. Mol Cell Proteomics 11, M111 015206 (2012). [PMC free article] [PubMed]
6. Margarit I. et al. . Capturing host-pathogen interactions by protein microarrays: identification of novel streptococcal proteins binding to human fibronectin, fibrinogen, and C4BP. FASEB J 23, 3100–3112 (2009). [PubMed]
7. Gonzalez R. et al. . Screening the mammalian extracellular proteome for regulators of embryonic human stem cell pluripotency. Proc Natl Acad Sci USA 107, 3552–3557 (2010). [PMC free article] [PubMed]
8. Peacock S. J., de Silva I. & Lowy F. D. What determines nasal carriage of *Staphylococcus aureus*? Trends Microbiol 9, 605–610 (2001). [PubMed]
9. Foster T. J., Geoghegan J. A., Ganesh V. K. & Hook M. Adhesion, invasion and evasion: the many functions of the surface proteins of *Staphylococcus aureus*. Nat Rev Microbiol 12, 49–62 (2014). [PubMed]
10. Kim H. K., Thammavongsa V., Schneewind O. & Missiakas D. Recurrent infections and immune evasion strategies of *Staphylococcus aureus*. Curr Opin Microbiol 15, 92–99 (2012). [PMC free article] [PubMed]
11. Serruto D., Bottomley M. J., Ram S., Giuliani M. M. & Rappuoli R. The new multicomponent vaccine against meningococcal serogroup B, 4CMenB: immunological, functional and structural characterization of the antigens. Vaccine 30 Suppl 2, B87–97 (2012). [PMC free article] [PubMed]

12. Magagnoli C. et al. . Structural organization of NadADelta(351–405), a recombinant MenB vaccine component, by its physico-chemical characterization at drug substance level. Vaccine 27, 2156–2170 (2009). [PubMed]
13. Capecchi B. et al. . *Neisseria meningitidis* NadA is a new invasin which promotes bacterial adhesion to and penetration into human epithelial cells. Mol Microbiol 55, 687–698 (2005). [PubMed]
14. Cecchini P. et al. . The soluble recombinant *Neisseria meningitidis* adhesin NadA(Delta351–405) stimulates human monocytes by binding to extracellular Hsp90. PLoS One 6, e25089 (2011). [PMC free article] [PubMed]
15. Nagele V. et al. . *Neisseria meningitidis* adhesin NadA targets beta1 integrins: functional similarity to *Yersinia* invasin. J Biol Chem 286, 20536–20546 (2011). [PMC free article] [PubMed]
16. Malito E. et al. . Structure of the meningococcal vaccine antigen NadA and epitope mapping of a bactericidal antibody. Proc Natl Acad Sci USA 111, 17128–17133 (2014). [PMC free article] [PubMed]
17. Bagnoli F. et al. . Vaccine composition formulated with a novel TLR7-dependent adjuvant induces high and broad protection against *Staphylococcus aureus*. Proc Natl Acad Sci USA 112, 3680–3685 (2015). [PMC free article] [PubMed]
18. Altindis E. et al. . Protectome analysis: a new selective bioinformatics tool for bacterial vaccine candidate discovery. Mol Cell Proteomics 14, 418–429 (2015). [PMC free article] [PubMed]
19. Kilpatrick D. C. & Chalmers J. D. Human L-ficolin (ficolin-2) and its clinical significance. J Biomed Biotechnol 2012, 138797 (2012). [PMC free article] [PubMed]
20. Shimaoka T. et al. . LOX-1 supports adhesion of Gram-positive and Gram-negative bacteria. J Immunol 166, 5108–5114 (2001). [PubMed]
21. Campbell L. A. et al. . *Chlamydia pneumoniae* binds to the lectin-like oxidized LDL receptor for infection of endothelial cells. Microbes Infect 14, 43–49 (2012). [PMC free article] [PubMed]
22. Wu Z. et al. . LOX-1 deletion improves neutrophil responses, enhances bacterial clearance, and reduces lung injury in a murine polymicrobial sepsis model. Infect Immun 79, 2865–2870 (2011). [PMC free article] [PubMed]
23. Laarman A., Milder F., van Strijp J. & Rooijakkers S. Complement inhibition by gram-positive pathogens: molecular mechanisms and therapeutic implications. J Mol Med (Berl) 88, 115–120 (2010). [PMC free article] [PubMed]

24. Stemerding A. M. et al. . *Staphylococcus aureus* formyl peptide receptor-like 1 inhibitor (FLIPr) and its homologue FLIPr-like are potent FcgammaR antagonists that inhibit IgG-mediated effector functions. J Immunol 191, 353–362 (2013). [PubMed]
25. Kang M. et al. . Collagen-binding microbial surface components recognizing adhesive matrix molecule (MSCRAMM) of Gram-positive bacteria inhibit complement activation via the classical pathway. J Biol Chem 288, 20520–20531 (2013). [PMC free article] [PubMed]
26. Prat C., Bestebroer J., de Haas C. J., van Strijp J. A. & van Kessel K. P. A new staphylococcal anti-inflammatory protein that antagonizes the formyl peptide receptor-like 1. J Immunol 177, 8017–8026 (2006). [PubMed]
27. Franzoso S. et al. . Human monocytes/macrophages are a target of *Neisseria meningitidis Adhesin A* (NadA). J Leukoc Biol 83, 1100–1110 (2008). [PubMed]
28. Bernard S. C. et al. . Pathogenic *Neisseria meningitidis* utilizes CD147 for vascular colonization. Nat Med 20, 725–731 (2014). [PubMed]
29. Honjo M. et al. . Lectin-like oxidized LDL receptor-1 is a cell-adhesion molecule involved in endotoxin-induced inflammation. Proc Natl Acad Sci USA 100, 1274–1279 (2003). [PMC free article] [PubMed]
30. Palumbo E. et al. . Antigen identification starting from the genome: a “Reverse Vaccinology” approach applied to MenB. Methods Mol Biol 799, 361–403 (2012). [PubMed]
31. Monk I. R., Shah I. M., Xu M., Tan M. W. & Foster T. J. Transforming the untransformable: application of direct transformation to manipulate genetically *Staphylococcus aureus* and *Staphylococcus epidermidis*. MBio 3 (2012). [PMC free article] [PubMed]

6.2 Material and methods

6.2.1 Cell culture

6.2.1.1 Blood-Brain Barrier hCMEC/D3 cell line

hCMEC/D3 cells, a brain endothelial cell line immortalized by transduction with hTERT and SV40 large T were obtained from Millipore (SCC066). Cells were grown on Collagen type I (Becton-Diskinson 354-236) coated flask in EBM-2 medium (Lonza) supplemented with 2.5% iFBS, 100 U/mL penicillin, 100 mg/mL streptomycin and 10mM HEPES, VEGF, IGF-1, EGF, FGF, ascorbate, hydrocortisone (EGM-2 BulletKit Lonza CC-3162/6) as recommended by the furnisher. Cells were maintained at 37°C in a controlled humidified atmosphere containing 5% CO_2.

6.2.1.2 Human Dermal Microvascular Endothelial Cells (HDMEC)

Primary Human Dermal Microvascular Endothelial Cells (HDMEC) were isolated from the dermis of juvenile foreskin and adult skin (different locations). Since the dermis contains blood and lymphatic capillaries, HDMEC comprise Blood and Lymphatic Microvascular Endothelial Cells. Both have a common origin and can be identified by several markers. HDMECs were purchased from Promocell and grown in endothelial cell growth medium MV (Promocell) supplemented with 10% iFBS, endothelial cell growth medium supplement mix (Promocell), 100 U/mL penicillin and 100 mg/mL streptomycin. Cells were maintained at 37°C in a controlled humidified atmosphere containing 5% CO_2.

6.2.1.3 EA.hy926

EA.hy926, an immortalized endothelial cell line, was obtained from ATCC (CRL-2922™) and cultured in Dulbecco's Modified Eagle's Medium (ATCC 30-2002) supplemented with 10% iFBS, 100 U/mL penicillin and 100 mg/mL streptomycin. Cells were maintained at 37°C in a controlled humidified atmosphere containing 5% CO_2.

6.2.2 Fluorescence-activated cell sorting (FACS) binding experiments

Binding assay was performed as previously described (Comanducci et al. 2002). Briefly, cells were non-enzymatically detached using cell dissociation solution (CDS, Sigma), harvested and suspended in RPMI-1640 (Gibco) medium supplemented with 1% iFBS. Approximately $3X10^5$ cells were mixed with 200 µg/mL rNadA or blocking solution (phosphate-buffered saline (PBS) + 1% iFBS) alone for time and temperature indicated in the graph. Cells were then incubated with primary antibodies for 1 h at 4°C, and with Alexa Fluor-labelled F(ab')2 for 30 min at 4°C. Cells were analysed with a FACS-Scan flow cytometre (Beckton-Dickinson). The mean fluorescence intensity (MFI) for each population was calculated using BD FACSDIVA™ software.

For inhibition of the binding experiments cells were incubated with different concentrations of anti-Lox1 antibody prior to rNadA incubation.

Antibodies used in the study: Polyclonal anti-Lox-1 antibody produced in rabbit (SAB1410858 Sigma); Mouse polyclonal serum against NadA (produced in house).

6.3 *Neisseria meningitidis* strains, growth conditions

Neisseria meningitidis 2C4.3 (C:22:NST:L3,7,9), a piliated capsulated Opa−Opc− variant of the serogroup C meningococcal strain 8013 (Nassif et al. 1993; Eugene et al. 2002), were cultured in Chocolate Agar Base (GC medium, Difco) medium at 37°C, 5% CO_2. When required, antibiotics were added at the following concentrations: Kanamycin (100 µg/mL), Erythromycin (2 µg/mL), Chloramphenicol (6 µg/mL).

The wild-type nadA, nadR and pilE locus were inactivated through transformation of chromosomal DNA with a previously described (Geoffroy et al. 2003) aphA3–insertionally inactivated endogenous gene derivative and selected with the corresponding antibiotics (ΔNadA – Kanamycin; ΔNadR – Kanamycin; ΔPilE – Erytromycin). For the ΔNadAΔNadR mutant, the Kanamycin resistance cassette within the NadA gene was replaced, thanks to the Gibson Assembly method (Gibson 2011; Gibson et al. 2009), with an Erytromycin resistance cassette prior to Nm transformation.

6.4 *N. meningitidis* adhesion assay

2.5 x10^5 HCMEC/D3 cells were seeded, in antibiotics-free complete medium, in a 24 well plate coated with 500 µL collagen (Rat Tail Collagen type I (Becton-Diskinson 354-236, stock at 3,4 mg/ml) at a 1:30 dilution in water for 30min at 37°C and were allowed to grow for 24 h. For adhesion analysis, bacteria were grown to OD 0.2 and each well was infected with 5x10^6 bacteria. Infection was carried out for 30 minutes at 37°C and 5% CO_2. The total number of cell-associated colony forming units (CFU) was determined after extensive washing of the cell monolayer followed by scraping the cells from the dish before plating dilutions.

6.5 Transmission Electron Microscopy Immunogold technique

The relative amount and surface distribution of the NadA molecules on wildtype and mutated *Neisseria meningitidis* 2C4.3 bacteria was assessed with Transmission Electron Microscopy Immunogold (IG-TEM) technique. The entire protocol was performed at room temperature. Almost 10 colonies from overnight cultures were dissolved into 100µL of PBS and 100µL of PFA added to fix bacteria. After 15 minutes of incubation, 5µL of bacterial suspension was directly loaded onto a nickel commercial 300-square mesh grid of carbon/formvar (Agar Scientific) and let dry for 5 min, while 10µL were plated on GC plate and incubated overnight at 37°C, 5% CO_2 to check bacteria inactivation. Soaked off the excess of the solution by Whatman® filter Paper No.1 (SIGMA-Aldrich), the grid was incubated with PBS-BSA 0.1% for 30 minutes to block the unspecific sites and stained with a mouse polyclonal serum against NadA (produced in house) for 1 hour. An anti-mouse secondary antibodyconjugated with 5nm gold particle was diluted according to manufacturer's instructions (Agar Scientific) in PBS-BSA 0.1% and used to detect the surface adhesin. The sample was then washed 5 times for 5 minutes each in PBS 1X and negatively stained using 2% of Uranyl Acetate in water solution for 45 seconds. The excess of the stain was soaked off and the grid left to air dry for 5 minutes. The images were acquired using a TECNAI-G2 Spirit TEM operating at 120 KV and equipped with a TVIPS Olympus Morada 2Kx4K CCD Camera, corresponding to a pixel size of 3.8 Å/pixel on the specimen.

6.6 Results

6.6.1 Lox-1 expression and NadA binding ability of human endothelial cells

In the work of Scietti (Scietti et al. 2016) we suggested an additional role for NadA at the host peripheral microvasculature and at the brain blood barrier (BBB) through the identification of an interaction between the soluble recombinant adhesin and the Lectin-like oxidized low-density lipoprotein receptor-1 (Lox-1). In spite of the strong biochemical evidence of the NadA/Lox-1 binding, the biological outcome of this interaction was not approached. In order to identify the most suitable model to study this interaction, cells were firstly screened in order to assess the surface expression of Lox-1. We used an anti-Lox-1 antibody to analyse Lox-1 surface expression on non permeabilized cells by FACS analysis, both in non-stimulated and TNFα stimulated conditions. Results of such analysis are shown in Fig. 1 and allow us to conclude that:

- HDMEC and hCMEC/D3 present a basal expression of the receptor increased following TNFα stimulation
- EA cells do not express the receptor neither is induced by TNFα

With the purpose of evaluating the ability to bind rNadA, non-stimulated and TNFα stimulated cells were incubated with the recombinant adhesin. Surprising the amount of rNadA cell-bounded was comparable between all three cell types, thus independent by the surface level of Lox-1. This result suggests the presence of additional interacting proteins at the cell surface (Fig.18).

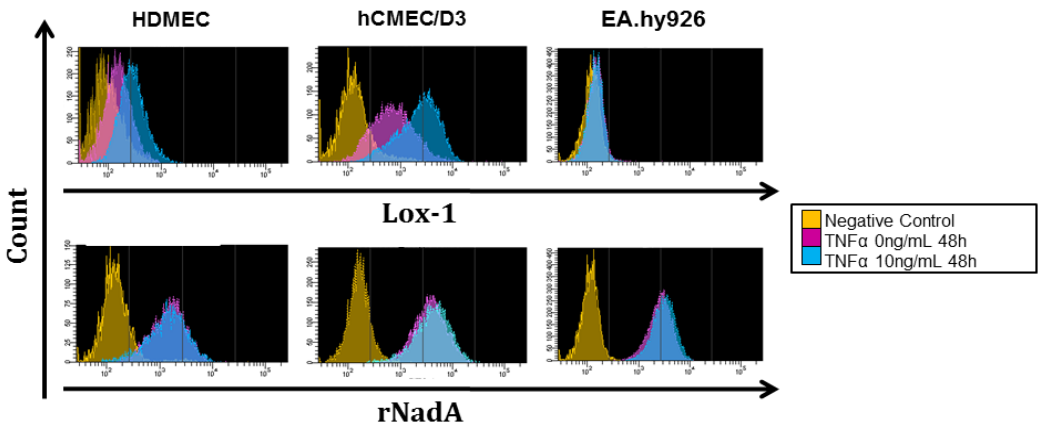

Fig. 18: Screening of Lox-1 expression and NadA binding ability of human endothelial cells. Three different human endothelial cells (HDMEC, hCMEC/D3 and EA.hy926) were cultured in medium alone (pink area) or with the addition of 10ng/mL TNFα (blue area). In the upper portion of the figure FACS plots represent the result of a surface staining against Lox-1; while in the lowest parts, of 30 minutes incubation with rNadA (200 µg/mL) at 37°C followed by staining with anti-NadA antibodies.

6.6.2 Characterization of rNadA binding to human endothelial cells

We investigated the temperature dependence and kinetics of NadA binding to human endothelial cells using Blood-Brain Barrier hCMEC/D3 cells as model. Non-permeabilized cells were incubated with rNadA and, after washing, the bound fraction was revealed by FACS analysis with anti-NadA antibody. At first this analysis was performed after 30 minutes of incubation at different temperatures. The result is shown in Fig. 19A. The rNadA binding to hCMEC/D3 cells is temperature dependent, giving the highest value at 37°C while dropping to about 60% at 25°C. Lowering the incubation temperatures at 4°C resulted in a signal comparable to the background (independent IgG used as control).

Setting incubation temperature at 37°C, we then analysed the kinetics of rNadA binding (Fig. 19B). The maximum level of rNadA surface bound was observed at 1 hour and decreased at longer incubation times. The binding kinetics, thus, is similar to what observed on epithelial cells (see section 4.1)

To verify if rNadA binding occurred through the endothelial receptor Lox-1, we pre-incubated cells with specific anti-Lox1 antibodies at different concentrations prior addition of rNadA. Although the rNadA binding was reduced, especially at higher antibodies concentrations, it was not completely abolished suggesting the presence of additional rNadA interactor (Fig. 19C). This result is consistent with the observation above that NadA is still able to bind Lox-1 non-expressing endothelial cells.

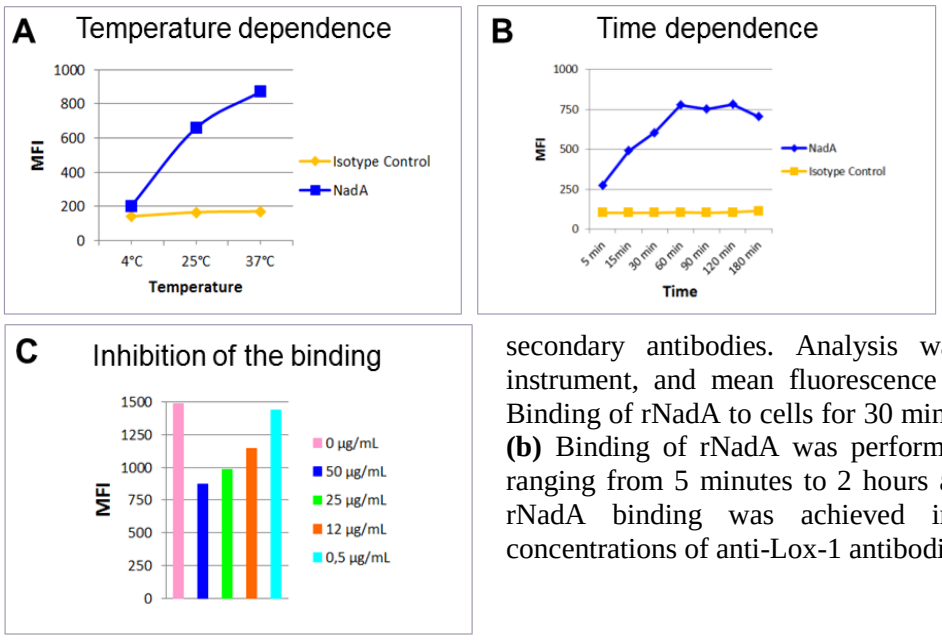

Figure 19: rNadA binds hCMEC/D3 cells in a time- and temperature dependent manner. A&B. hCMEC/D3 cells were incubated with 200 µg/mL rNadA and then washed with PBS – 1% FBS. Binding was detected using anti-NadA antibodies and Allophycocyanin conjugated secondary antibodies. Analysis was performed with FACS aria instrument, and mean fluorescence intensity is reported (MFI). **(a)** Binding of rNadA to cells for 30 minutes at the indicated temperatures **(b)** Binding of rNadA was performed at 37°C for a period of time ranging from 5 minutes to 2 hours as indicated. **(c)** Inhibition of the rNadA binding was achieved incubating cells with different concentrations of anti-Lox-1 antibodies prior to rNadA incubation.

6.6.3 The role of NadA in adhesion of N. meningitidis to endothelial cells

In order to assess the NadA contribution to *N. meningitidis* adhesion to endothelial cells, infection experiments on hCMEC/D3 cells were conducted. After 30 minutes of incubation with bacteria, cells were extensively washed and the total number of cell-associated colony forming units (CFU) was determined by scraping the cells from the dish and plating dilutions. Results, shown in Fig. 20, revealed no difference in adhesion between wild type and ΔNadA bacteria, while, bacteria overexpressing NadA (ΔNadR mutants), adhere about 3,5 fold more. The same experiment was repeated with not piliated mutants. As expected, Tfp resulted as the master factor driving adhesion to endothelial cells, however NadA overexpressing mutants still adhere about 3,5 fold more compared to the wild type or ΔNadA. Taken together, this data suggest a role of NadA in the bacterial colonization of endothelial cells, likely cooperating with Tfp.

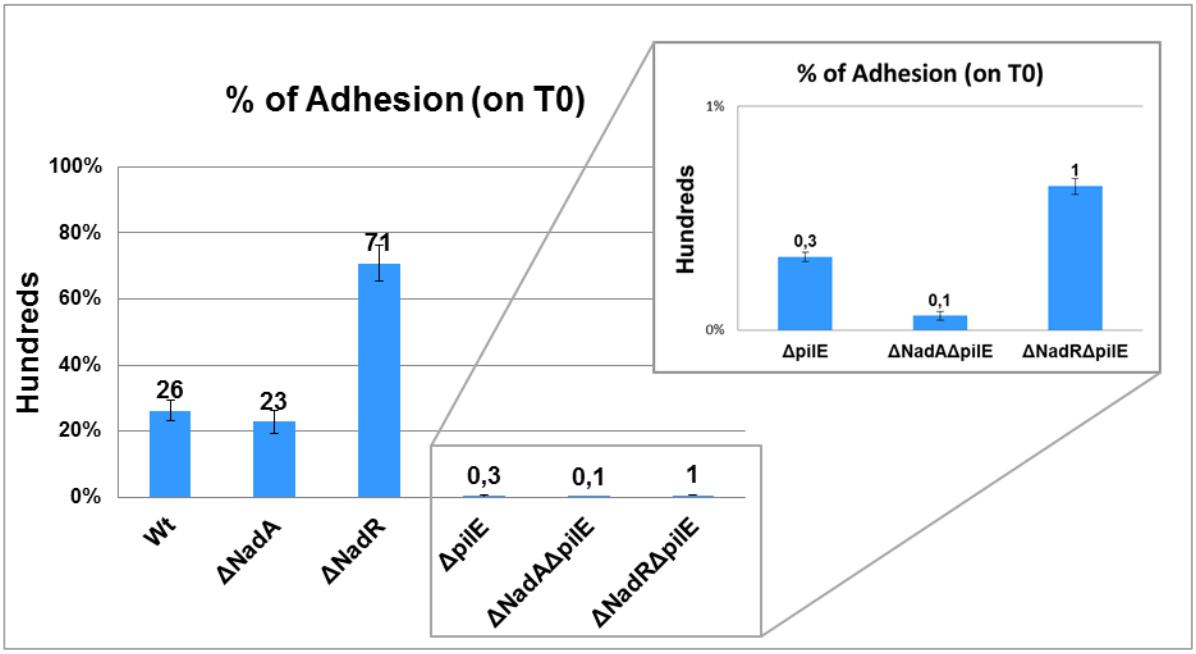

Fig. 20: Role of NadA in the adhesion of meningococcus to endothelial cells. (a) Association of wild-type and mutated *N. meningitidis* 2C4.3 to hCMEC/D3 cells after 30 minutes of incubation (MOI 100). The number of associated bacteria is expressed as percentage of adhesion on inoculated bacteria. Values represent the mean ± standard deviation of one out of three experiments performed in triplicate.

In the previous experiment, the adhesion of the wild type and ΔNadA bacteria provided similar results in adhesion and we sought to explore deeper this point. We speculated that NadA could have been present at very low level on the surface of wild type *N. meningitidis 2C4.3* making no much difference with KO strain. It is known that *nadA* gene expression is induced by appropriate niche-specific signals, via the

transcriptional regulator NadR, that could not be present when bacteria are grown in laboratory medium (Fagnocchi et al. 2013; Metruccio et al. 2009). To assess this point, IG-TEM of the three mentioned bacteria was performed. As it can be seen in figure 3, the wild type and ΔNadA bacteria did not show much difference in NadA expression (Fig. 21 panel A and B respectively) whereas the overexpressing mutant showed a consistent presence of the adhesin on the surface (Fig. 21 panel C).

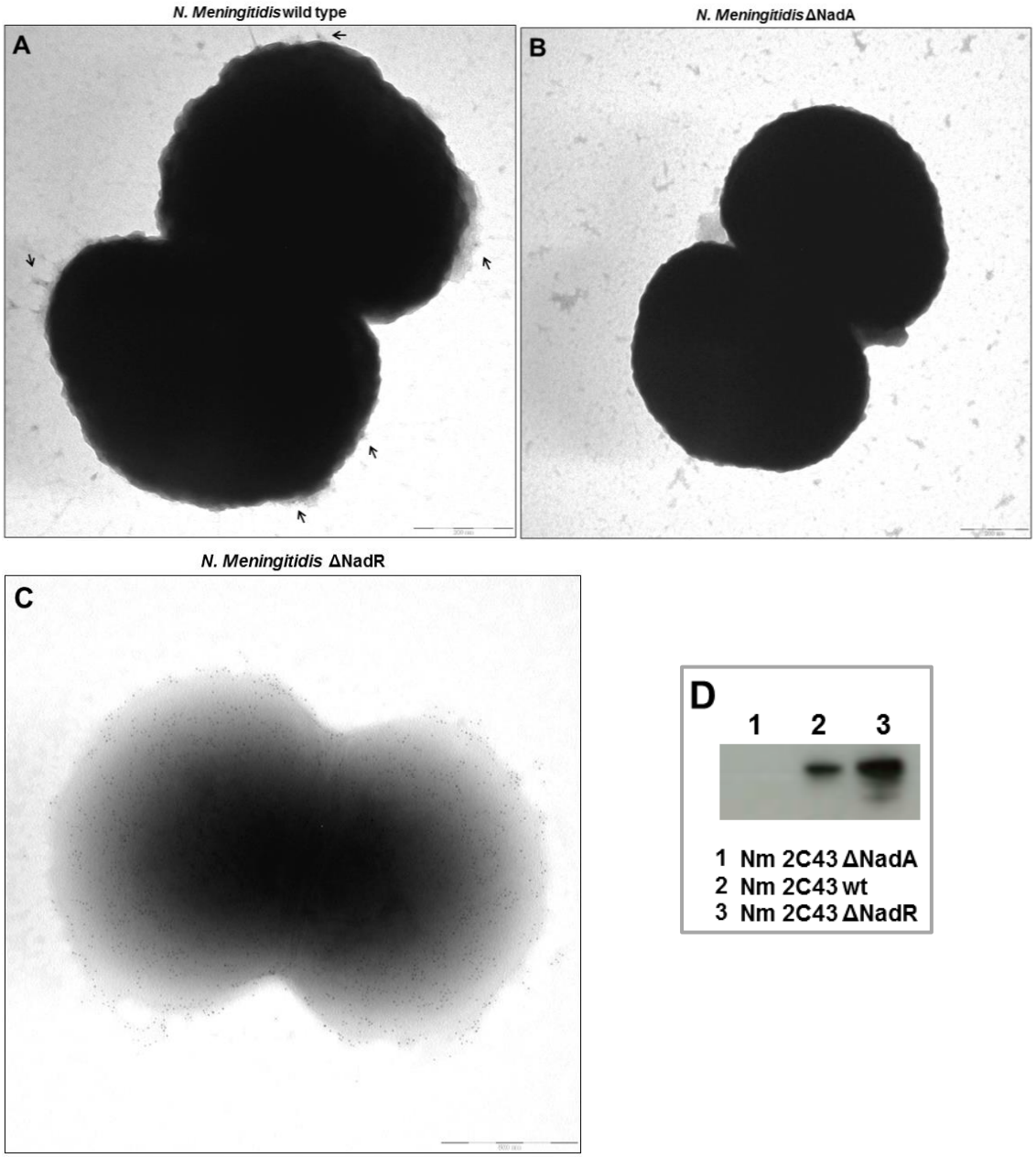

Fig. 21: Transmission Electron Microscopy Immunogold on *N. meningitidis* 2C4.3. Micrographs of the immunogold assay to detect the surface expression of NadA on **(a)** wild type, **(b)** ΔNadA and **(c)** ΔNadR bacteria. **(d)** Western blot analysis against NadA of bacteria lysate.

7 Discussion and conclusion

The overall goal of my PhD thesis is the understanding of the molecular basis exploited by *Neisseria meningitidis* Adhesin A to contribute in the complex pathophysiology of *N. meningitidis.*

NadA represents a good model to study the mechanisms underlying the host-pathogen interaction because:

- It is an important virulence factor included among the key recombinant antigens of Bexsero®, the first *N. meningitidis* serogroup B vaccine;
- Identified as an adhesin, it shows additional features at least on epithelial cells where we demonstrated its involvement in cellular internalization (Montanari et al. 2012; Bozza et al. 2014);
- It shows the peculiar characteristic of maintaining the quaternary structure as soluble recombinant product;
- It is expressed and correctly localized in heterologous bacteria (among which *E. Coli*) inducing a NadA-driven cell attachment and internalization.

Knowledge of the NadA function is not as accurate as its immunological potential. From the early reports, NadA was shown to target human epithelial cells promoting adhesion (Capecchi et al. 2005; Comanducci et al. 2002). Later on our group demonstrated a direct interaction of the external molecular chaperone Hsp90 as important to direct NadA-driven epithelial intracellular trafficking (Montanari et al. 2012).

During the first part of my PhD, I participated to a project focus on the understanding of the mechanism exploited by NadA to enter human epithelial cells, thus a lane to traverse the epithelial barrier (Bozza et al. 2014). Our experiments indicate that the soluble recombinant NadA is able to enter into Chang epithelial cells thanks to a PI3K-dependent endocytosis process regulated by ARF6. The extracellular secreted pool of Hsp90 is involved in the intracellular trafficking so much so that cell treatments with Hsp90 inhibitors lead to intracellular accumulation of rNadA. In addition, thanks to hydrogen–deuterium exchange (HDX)-MS analysis performed with rNadA in complex with Hsp90, we identified peptides located in the NadA Head domain as crucial for the interaction.

Our data indicate that, in non-polarized Chang epithelial cells, the adhesin avoid the lysosome pathway hijacking the recycling endosome and it is usually recycled back to the surface throughout Rab11 positive vesicles. Using polarized cells, Barrile *et al.*, reported that meningococcus is able to subvert the host cell architecture and intracellular trafficking system as a strategy to overcome the nasopharyngeal barrier without affecting the monolayer integrity (Barrile et al. 2015). As described, we have generated KO and over-expressing NadA *N. meningitidis* and we plan to test these strains on polarized epithelial cells in order to elucidate the contribution of this adhesin in the bacteria crossing towards the bloodstream.

In order to understand deeper the molecular mechanisms exploited by NadA to enter host cells and as logical pursuing of the studies described above, I started a project aimed to identify NadA receptors. Apart from interacting with human epithelial cells, in fact, NadA was also found to target human monocytes inducing the production of pro-inflammatory cytokines and chemotactic factors, as well as the inhibition of apoptosis leading to macrophages differentiation (Franzoso et al. 2008). I approached this target by performing an unbiased large-scale screening of two libraries, a first one including about 2500 and a second of more than 6000 human surface protein spotted on a microarray. With this method a discrete number of putative NadA interactors were identified and the effective binding was confirmed for 4 of them with different techniques. One of the identified proteins (Lectin-like oxidized low-density lipoprotein receptor-1 or Lox-1) is a receptor predominantly express on endothelial cells while the other three are mainly expressed on cells of myeloid origin and better characterized on monocytes/macrophages. Unfortunately none of the candidates is expressed by epithelial cells and the identity of the NadA receptor on this cell type is still missing.

Although spending part of my time on Lox-1 recognition by NadA (see below), in the second part of my PhD I focused my attention to the characterization of the NadA binding to monocytes in order to elucidate the contribution of this *N. meningitidis* antigen in this step of the bacteria pathogenesis. As anticipated, the protein microarray identified three different monocytic receptors involved in the NadA binding:

a) Sialic acid-binding immunoglobulin-type lectins receptor 5 (Siglec 5)
b) Sialic acid-binding immunoglobulin-type lectins receptor 14 (Siglec 14)
c) Low affinity immunoglobulin gamma Fc region receptor II-a (FcγR2A).

Siglec 5 and Siglec 14 are described to be paired receptors (Ali et al. 2014); the high sequence similarity of their first two immunoglobulin domains allow them to respond to the same ligands, while, the opposite immunoreceptor tyrosine-based motif in the tails, provide a balance of signalling inside the cell (Ali et al. 2014). Siglec 5 has already been described (Jones, Virji, and Crocker 2003) to bind the terminal capping structure displayed on the lipopolysaccharide (LPS) of *N. meningitidis*. Here we report evidence of a novel interaction with a Nm surface protein suggesting a model in which meningococcus sialic acid acts as tethering factor whereas NadA establish a stronger adhesive interaction. It will be interesting to establish whether the NadA-mediate binding results in an internalization or induce a colonization niche analogous at what observed for endothelial cells (Coureuil et al. 2014). Also the FcγR2A, thanks to its immunoreceptor tyrosine-based activation motif (ITAM) motif in the intracellular domain, is involved in the same signalling pathway suggesting a complex scenario in which bacteria, through the NadA antigen, exploit multiple and alternative way to target host monocytes.

The putative interactions were further corroborated by cellular binding assays in which non-permissive CHO-K1 cells were able to bind rNadA after transient expression of the receptors. These data were confirmed by the ability of polyclonal anti-receptor antibodies to abrogate the binding. In order to characterize the interactions from a biochemical point of view, BLI binding experiments allowed the identification of a strong affinity, in the range of nanomolarity, between rNadA and Siglec 5 and Siglec 14. Furthermore, this technology allowed us to define the Head portion of NadA as responsible for the binding with Siglecs receptors. To locate more precisely the NadA residues involved in the interaction, hydrogen–deuterium exchange (HDX)-MS was performed with rNadA in complex with Siglec 5, and two non-consecutive peptides, located in the NadA head, were identified as crucial. Interestingly, the region identified is overlapping with the epitopes recognized by murine monoclonal bactericidal antibody 33E8 (Malito et al. 2014) and the NadA binding site with Hsp90. This latter interaction was found to be protective towards NadA-mediated meningococcus adhesion and invasion to epithelial cells, indicating this region of the adhesin as a crucial one required for specific recognition of host species. The full picture has still to be completed by establishing the affinity constants and the NadA region involved in the interaction with FcγR2A.

Functional validation of the binding in a “natural” cellular context was achieved taking advantage of THP-1 monocytic cells. Confocal analysis revealed a strong co-localization of signals between rNadA and both

receptors. Surprisingly, a co-localization between the two receptors was achieved also in absence of the recombinant adhesin suggesting the proximity of the two proteins, likely within the same lipid raft at the cellular surface. Inhibition of the binding by FACS experiments combined with a temperature dependence analysis, allowed us to visualize and separate the binding to the different receptors suggesting that the binding between NadA and Siglec 5 & 14 is influenced by temperature (as on epithelial and endothelial cells) while no dependence is observed for the binding to FcγR2A.

Recently, we suggested an additional role for NadA at the host peripheral microvasculature and at the brain blood barrier through the identification of the interaction with the Lectin-like oxidized low-density lipoprotein receptor-1 (Lox-1), a multifunctional endothelial receptor described to bind a broad spectrum of physiological ligands including oxLDL and bacteria (Scietti et al. 2016). In this work we confirm the interaction with binding assays on transfected eukaryotic cells and by biophysical and functional studies. The affinity constant is in the low nanomolar range, indicating a very strong binding with the NadA head domain identified by competition with anti-NadA murine monoclonal antibodies.

In spite of the strong biochemical evidence of the NadA/Lox-1 binding, the biological outcome of this interaction has not been approached. In order to fill this gap, I spent three months of my PhD at X. Nassif laboratory in Paris that represent the leading group engaged in studying the endothelial colonization by meningococcus. Here, I had the possibility to screen different endothelial cell models. Surprisingly, the amount of rNadA cell-bounded was strong and comparable between all tested cells, and it was not influenced by the surface level of Lox-1. These data, although identifying the ability of NadA to bind human endothelial cells, suggest the presence of additional interacting proteins at the cell surface. Blood-Brain Barrier hCMEC/D3 cell line was selected as the best model to proceed with the characterization and we revealed a strong temperature dependence of the NadA binding similar to what observed on epithelial cells as well as human monocytes. Specific anti-Lox-1 antibodies, although lowering the level of NadA bound to cells, were not able to abolish the interaction with the endothelia providing additional data in support of the presence of additional receptors.

Assays with wild type and mutated *N. meningitidis* confirmed the role of NadA in the adhesion of the bacteria to endothelial cells even if the primary and predominant interaction is mediated by Tfp. Further

studies are ongoing in order to better characterize the role and cooperation of this two meningococcus components in this step of the bacteria pathogenesis.

N. meningitidis is able to cross the epithelium of the upper respiratory tract, survive in the blood and be transported to the endothelium of the blood-brain barrier where adhesion and colonization generate the dramatic consequence of the invasive meningitis. All considered, NadA is able to interact with all three cell types involved in the bacterium cycle of infection suggesting unknown and multifaceted roles for this protein in the complex multi-step mechanism of MenB pathogenesis. Dissecting the biological meaning of the interactions between NadA and host cells will provide new insight on the bacteria pathogenesis and will help in the generation of tools to fight a devastating disease that, according to the World Health Organization, provoke 1.2 million cases and 135,000 related deaths a year.

8 References

Ali, S. R., J. J. Fong, A. F. Carlin, T. D. Busch, R. Linden, T. Angata, T. Areschoug, M. Parast, N. Varki, J. Murray, V. Nizet, and A. Varki. 2014. 'Siglec-5 and Siglec-14 are polymorphic paired receptors that modulate neutrophil and amnion signaling responses to group B Streptococcus', *J Exp Med*, 211: 1231-42.

Angata, T., T. Hayakawa, M. Yamanaka, A. Varki, and M. Nakamura. 2006. 'Discovery of Siglec-14, a novel sialic acid receptor undergoing concerted evolution with Siglec-5 in primates', *FASEB J*, 20: 1964-73.

Angata, T., T. Ishii, T. Motegi, R. Oka, R. E. Taylor, P. C. Soto, Y. C. Chang, I. Secundino, C. X. Gao, K. Ohtsubo, S. Kitazume, V. Nizet, A. Varki, A. Gemma, K. Kida, and N. Taniguchi. 2013. 'Loss of Siglec-14 reduces the risk of chronic obstructive pulmonary disease exacerbation', *Cell Mol Life Sci*, 70: 3199-210.

Arase, H., E. S. Mocarski, A. E. Campbell, A. B. Hill, and L. L. Lanier. 2002. 'Direct recognition of cytomegalovirus by activating and inhibitory NK cell receptors', *Science*, 296: 1323-6.

Bai, X., J. Findlow, and R. Borrow. 2011. 'Recombinant protein meningococcal serogroup B vaccine combined with outer membrane vesicles', *Expert Opin Biol Ther*, 11: 969-85.

Bambini, S., M. De Chiara, A. Muzzi, M. Mora, J. Lucidarme, C. Brehony, R. Borrow, V. Masignani, M. Comanducci, M. C. Maiden, R. Rappuoli, M. Pizza, and K. A. Jolley. 2014. 'Neisseria adhesin A variation and revised nomenclature scheme', *Clin Vaccine Immunol*, 21: 966-71.

Bambini, S., A. Muzzi, P. Olcen, R. Rappuoli, M. Pizza, and M. Comanducci. 2009. 'Distribution and genetic variability of three vaccine components in a panel of strains representative of the diversity of serogroup B meningococcus', *Vaccine*, 27: 2794-803.

Barrile, R., M. Kasendra, S. Rossi-Paccani, M. Merola, M. Pizza, C. Baldari, M. Soriani, and B. Arico. 2015. 'Neisseria meningitidis subverts the polarized organization and intracellular trafficking of host cells to cross the epithelial barrier', *Cell Microbiol*, 17: 1365-75.

Bentley, S. D., G. S. Vernikos, L. A. Snyder, C. Churcher, C. Arrowsmith, T. Chillingworth, A. Cronin, P. H. Davis, N. E. Holroyd, K. Jagels, M. Maddison, S. Moule, E. Rabbinowitsch, S. Sharp, L. Unwin, S. Whitehead, M. A. Quail, M. Achtman, B. Barrell, N. J. Saunders, and J. Parkhill. 2007. 'Meningococcal genetic variation mechanisms viewed through comparative analysis of serogroup C strain FAM18', *PLoS Genet*, 3: e23.

Bernard, S. C., N. Simpson, O. Join-Lambert, C. Federici, M. P. Laran-Chich, N. Maissa, H. Bouzinba-Segard, P. C. Morand, F. Chretien, S. Taouji, E. Chevet, S. Janel, F. Lafont, M. Coureuil, A. Segura, F. Niedergang, S. Marullo, P. O. Couraud, X. Nassif, and S. Bourdoulous. 2014. 'Pathogenic Neisseria meningitidis utilizes CD147 for vascular colonization', *Nat Med*, 20: 725-31.

Blacklow, R. S., and L. Warren. 1962. 'Biosynthesis of sialic acids by Neisseria meningitidis', *J Biol Chem*, 237: 3520-6.

Blixt, O., B. E. Collins, I. M. van den Nieuwenhof, P. R. Crocker, and J. C. Paulson. 2003. 'Sialoside specificity of the siglec family assessed using novel multivalent probes: identification of potent inhibitors of myelin-associated glycoprotein', *J Biol Chem*, 278: 31007-19.

Boisier, P., P. Nicolas, S. Djibo, M. K. Taha, I. Jeanne, H. B. Mainassara, B. Tenebray, K. K. Kairo, D. Giorgini, and S. Chanteau. 2007. 'Meningococcal meningitis: unprecedented incidence of serogroup X-related cases in 2006 in Niger', *Clin Infect Dis*, 44: 657-63.

Bowe, F., E. C. Lavelle, E. A. McNeela, C. Hale, S. Clare, B. Arico, M. M. Giuliani, A. Rae, A. Huett, R. Rappuoli, G. Dougan, and K. H. Mills. 2004. 'Mucosal vaccination against serogroup B meningococci:

induction of bactericidal antibodies and cellular immunity following intranasal immunization with NadA of Neisseria meningitidis and mutants of Escherichia coli heat-labile enterotoxin', *Infect Immun*, 72: 4052-60.

Bozza, G., M. Capitani, P. Montanari, B. Benucci, M. Biancucci, V. Nardi-Dei, E. Caproni, R. Barrile, B. Picciani, S. Savino, B. Arico, R. Rappuoli, M. Pizza, A. Luini, M. Sallese, and M. Merola. 2014. 'Role of ARF6, Rab11 and external Hsp90 in the trafficking and recycling of recombinant-soluble Neisseria meningitidis adhesin A (rNadA) in human epithelial cells', *PLoS One*, 9: e110047.

Bradley, C. J., N. J. Griffiths, H. A. Rowe, R. S. Heyderman, and M. Virji. 2005. 'Critical determinants of the interactions of capsule-expressing Neisseria meningitidis with host cells: the role of receptor density in increased cellular targeting via the outer membrane Opa proteins', *Cell Microbiol*, 7: 1490-503.

Branham, S. E. 1953. 'Serological relationships among meningococci', *Bacteriol Rev*, 17: 175-88.

Callaghan, M. J., K. A. Jolley, and M. C. Maiden. 2006. 'Opacity-associated adhesin repertoire in hyperinvasive Neisseria meningitidis', *Infect Immun*, 74: 5085-94.

Cao, H., B. de Bono, K. Belov, E. S. Wong, J. Trowsdale, and A. D. Barrow. 2009. 'Comparative genomics indicates the mammalian CD33rSiglec locus evolved by an ancient large-scale inverse duplication and suggests all Siglecs share a common ancestral region', *Immunogenetics*, 61: 401-17.

Capecchi, B., J. Adu-Bobie, F. Di Marcello, L. Ciucchi, V. Masignani, A. Taddei, R. Rappuoli, M. Pizza, and B. Arico. 2005. 'Neisseria meningitidis NadA is a new invasin which promotes bacterial adhesion to and penetration into human epithelial cells', *Mol Microbiol*, 55: 687-98.

Carlin, A. F., S. Uchiyama, Y. C. Chang, A. L. Lewis, V. Nizet, and A. Varki. 2009. 'Molecular mimicry of host sialylated glycans allows a bacterial pathogen to engage neutrophil Siglec-9 and dampen the innate immune response', *Blood*, 113: 3333-6.

Casey, L. C. 2000. 'Immunologic response to infection and its role in septic shock', *Crit Care Clin*, 16: 193-213.

Casey, L. C., R. A. Balk, and R. C. Bone. 1993. 'Plasma cytokine and endotoxin levels correlate with survival in patients with the sepsis syndrome', *Ann Intern Med*, 119: 771-8.

Chang, Y. C., and V. Nizet. 2014. 'The interplay between Siglecs and sialylated pathogens', *Glycobiology*, 24: 818-25.

Chang, Y. C., J. Olson, F. C. Beasley, C. Tung, J. Zhang, P. R. Crocker, A. Varki, and V. Nizet. 2014. 'Group B Streptococcus engages an inhibitory Siglec through sialic acid mimicry to blunt innate immune and inflammatory responses in vivo', *PLoS Pathog*, 10: e1003846.

Ciabattini, A., B. Giomarelli, R. Parigi, D. Chiavolini, E. Pettini, B. Arico, M. M. Giuliani, L. Santini, D. Medaglini, and G. Pozzi. 2008. 'Intranasal immunization of mice with recombinant Streptococcus gordonii expressing NadA of Neisseria meningitidis induces systemic bactericidal antibodies and local IgA', *Vaccine*, 26: 4244-50.

Comanducci, M., S. Bambini, B. Brunelli, J. Adu-Bobie, B. Arico, B. Capecchi, M. M. Giuliani, V. Masignani, L. Santini, S. Savino, D. M. Granoff, D. A. Caugant, M. Pizza, R. Rappuoli, and M. Mora. 2002. 'NadA, a novel vaccine candidate of Neisseria meningitidis', *J Exp Med*, 195: 1445-54.

Comanducci, M., S. Bambini, D. A. Caugant, M. Mora, B. Brunelli, B. Capecchi, L. Ciucchi, R. Rappuoli, and M. Pizza. 2004. 'NadA diversity and carriage in Neisseria meningitidis', *Infect Immun*, 72: 4217-23.

Coureuil, M., S. Bourdoulous, S. Marullo, and X. Nassif. 2014. 'Invasive meningococcal disease: a disease of the endothelial cells', *Trends Mol Med*, 20: 571-8.

Coureuil, M., H. Lecuyer, M. G. Scott, C. Boularan, H. Enslen, M. Soyer, G. Mikaty, S. Bourdoulous, X. Nassif, and S. Marullo. 2010. 'Meningococcus Hijacks a beta2-adrenoceptor/beta-Arrestin pathway to cross brain microvasculature endothelium', *Cell*, 143: 1149-60.

Coureuil, M., and S. Marullo. 2011. '[beta(2) adrenergic receptor and beta-arrestins: the meningococcal instruments to breach meninges]', *Med Sci (Paris)*, 27: 365-7.

Craig, L., N. Volkmann, A. S. Arvai, M. E. Pique, M. Yeager, E. H. Egelman, and J. A. Tainer. 2006. 'Type IV pilus structure by cryo-electron microscopy and crystallography: implications for pilus assembly and functions', *Mol Cell*, 23: 651-62.

Criss, A. K., and H. S. Seifert. 2012. 'A bacterial siren song: intimate interactions between Neisseria and neutrophils', *Nat Rev Microbiol*, 10: 178-90.

Crocker, P. R. 2002. 'Siglecs: sialic-acid-binding immunoglobulin-like lectins in cell-cell interactions and signalling', *Curr Opin Struct Biol*, 12: 609-15.

Crocker, P. R., S. Mucklow, V. Bouckson, A. McWilliam, A. C. Willis, S. Gordon, G. Milon, S. Kelm, and P. Bradfield. 1994. 'Sialoadhesin, a macrophage sialic acid binding receptor for haemopoietic cells with 17 immunoglobulin-like domains', *EMBO J*, 13: 4490-503.

Crocker, P. R., J. C. Paulson, and A. Varki. 2007. 'Siglecs and their roles in the immune system', *Nat Rev Immunol*, 7: 255-66.

Crocker, P. R., and A. Varki. 2001. 'Siglecs, sialic acids and innate immunity', *Trends Immunol*, 22: 337-42.

Crosnier, C., L. Y. Bustamante, S. J. Bartholdson, A. K. Bei, M. Theron, M. Uchikawa, S. Mboup, O. Ndir, D. P. Kwiatkowski, M. T. Duraisingh, J. C. Rayner, and G. J. Wright. 2011. 'Basigin is a receptor essential for erythrocyte invasion by Plasmodium falciparum', *Nature*, 480: 534-7.

Danielson, L.; Mann, E. 1806. 'A history of a singular and very noted disease, which lately made its appearance in Medfield', *Med Agricultural Reg*, 1.

Dull, P. M., J. Abdelwahab, C. T. Sacchi, M. Becker, C. A. Noble, G. A. Barnett, R. M. Kaiser, L. W. Mayer, A. M. Whitney, S. Schmink, G. W. Ajello, J. Dolan-Livengood, D. S. Stephens, M. S. Cetron, T. Popovic, and N. E. Rosenstein. 2005. 'Neisseria meningitidis serogroup W-135 carriage among US travelers to the 2001 Hajj', *J Infect Dis*, 191: 33-9.

Estabrook, M. M., J. M. Griffiss, and G. A. Jarvis. 1997. 'Sialylation of Neisseria meningitidis lipooligosaccharide inhibits serum bactericidal activity by masking lacto-N-neotetraose', *Infect Immun*, 65: 4436-44.

Eugene, E., I. Hoffmann, C. Pujol, P. O. Couraud, S. Bourdoulous, and X. Nassif. 2002. 'Microvilli-like structures are associated with the internalization of virulent capsulated Neisseria meningitidis into vascular endothelial cells', *J Cell Sci*, 115: 1231-41.

Fagnocchi, L., A. Biolchi, F. Ferlicca, G. Boccadifuoco, B. Brunelli, S. Brier, N. Norais, E. Chiarot, G. Bensi, J. S. Kroll, M. Pizza, J. Donnelly, M. M. Giuliani, and I. Delany. 2013. 'Transcriptional regulation of the nadA gene in Neisseria meningitidis impacts the prediction of coverage of a multicomponent meningococcal serogroup B vaccine', *Infect Immun*, 81: 560-9.

Figueroa, J. E., and P. Densen. 1991. 'Infectious diseases associated with complement deficiencies', *Clin Microbiol Rev*, 4: 359-95.

Finne, J., M. Leinonen, and P. H. Makela. 1983. 'Antigenic similarities between brain components and bacteria causing meningitis. Implications for vaccine development and pathogenesis', *Lancet*, 2: 355-7.

Folsch, H. 2008. 'Regulation of membrane trafficking in polarized epithelial cells', *Curr Opin Cell Biol*, 20: 208-13.

Franzoso, S., C. Mazzon, M. Sztukowska, P. Cecchini, T. Kasic, B. Capecchi, R. Tavano, and E. Papini. 2008. 'Human monocytes/macrophages are a target of Neisseria meningitidis Adhesin A (NadA)', *J Leukoc Biol*, 83: 1100-10.

Frasch, C. E., W. D. Zollinger, and J. T. Poolman. 1985. 'Serotype antigens of Neisseria meningitidis and a proposed scheme for designation of serotypes', *Rev Infect Dis*, 7: 504-10.

Freeman, S. D., S. Kelm, E. K. Barber, and P. R. Crocker. 1995. 'Characterization of CD33 as a new member of the sialoadhesin family of cellular interaction molecules', *Blood*, 85: 2005-12.

Frosch, M., C. Weisgerber, and T. F. Meyer. 1989. 'Molecular characterization and expression in Escherichia coli of the gene complex encoding the polysaccharide capsule of Neisseria meningitidis group B', *Proc Natl Acad Sci U S A*, 86: 1669-73.

Gagneux, S. P., A. Hodgson, T. A. Smith, T. Wirth, I. Ehrhard, G. Morelli, B. Genton, F. N. Binka, M. Achtman, and G. Pluschke. 2002. 'Prospective study of a serogroup X Neisseria meningitidis outbreak in northern Ghana', *J Infect Dis*, 185: 618-26.

Geoffroy, M. C., S. Floquet, A. Metais, X. Nassif, and V. Pelicic. 2003. 'Large-scale analysis of the meningococcus genome by gene disruption: resistance to complement-mediated lysis', *Genome Res*, 13: 391-8.

Gibson, A., C. E. Futter, S. Maxwell, E. H. Allchin, M. Shipman, J. P. Kraehenbuhl, D. Domingo, G. Odorizzi, I. S. Trowbridge, and C. R. Hopkins. 1998. 'Sorting mechanisms regulating membrane protein traffic in the apical transcytotic pathway of polarized MDCK cells', *J Cell Biol*, 143: 81-94.

Gibson, D. G. 2011. 'Enzymatic assembly of overlapping DNA fragments', *Methods Enzymol*, 498: 349-61.

Gibson, D. G., L. Young, R. Y. Chuang, J. C. Venter, C. A. Hutchison, 3rd, and H. O. Smith. 2009. 'Enzymatic assembly of DNA molecules up to several hundred kilobases', *Nat Methods*, 6: 343-5.

Giuliani, M. M., J. Adu-Bobie, M. Comanducci, B. Arico, S. Savino, L. Santini, B. Brunelli, S. Bambini, A. Biolchi, B. Capecchi, E. Cartocci, L. Ciucchi, F. Di Marcello, F. Ferlicca, B. Galli, E. Luzzi, V. Masignani, D. Serruto, D. Veggi, M. Contorni, M. Morandi, A. Bartalesi, V. Cinotti, D. Mannucci, F. Titta, E. Ovidi, J. A. Welsch, D. Granoff, R. Rappuoli, and M. Pizza. 2006. 'A universal vaccine for serogroup B meningococcus', *Proc Natl Acad Sci U S A*, 103: 10834-9.

Glover, J. A. 1918. 'The Cerebro-Spinal Fever Epidemic of 1917 at X Depot', *J Hyg (Lond)*, 17: 350-65.

Goldschneider, I., E. C. Gotschlich, and M. S. Artenstein. 1969a. 'Human immunity to the meningococcus. I. The role of humoral antibodies', *J Exp Med*, 129: 1307-26.

———. 1969b. 'Human immunity to the meningococcus. II. Development of natural immunity', *J Exp Med*, 129: 1327-48.

Gonzalez, R., L. L. Jennings, M. Knuth, A. P. Orth, H. E. Klock, W. Ou, J. Feuerhelm, M. V. Hull, E. Koesema, Y. Wang, J. Zhang, C. Wu, C. Y. Cho, A. I. Su, S. Batalov, H. Chen, K. Johnson, B. Laffitte, D. G. Nguyen, E. Y. Snyder, P. G. Schultz, J. L. Harris, and S. A. Lesley. 2010. 'Screening the mammalian extracellular proteome for regulators of embryonic human stem cell pluripotency', *Proc Natl Acad Sci U S A*, 107: 3552-7.

Greenwood, B. 1999. 'Manson Lecture. Meningococcal meningitis in Africa', *Trans R Soc Trop Med Hyg*, 93: 341-53.

Hager-Braun, C., and K. B. Tomer. 2005. 'Determination of protein-derived epitopes by mass spectrometry', *Expert Rev Proteomics*, 2: 745-56.

Hanasaki, K., A. Varki, and L. D. Powell. 1995. 'CD22-mediated cell adhesion to cytokine-activated human endothelial cells. Positive and negative regulation by alpha 2-6-sialylation of cellular glycoproteins', *J Biol Chem*, 270: 7533-42.

Hart, C. A., and L. E. Cuevas. 1997. 'Meningococcal disease in Africa', *Ann Trop Med Parasitol*, 91: 777-85.

Hibbs, M. L., L. Bonadonna, B. M. Scott, I. F. McKenzie, and P. M. Hogarth. 1988. 'Molecular cloning of a human immunoglobulin G Fc receptor', *Proc Natl Acad Sci U S A*, 85: 2240-4.

Hill, D. J., N. J. Griffiths, E. Borodina, and M. Virji. 2010. 'Cellular and molecular biology of Neisseria meningitidis colonization and invasive disease', *Clin Sci (Lond)*, 118: 547-64.

Hobb, R. I., Y. L. Tzeng, B. P. Choudhury, R. W. Carlson, and D. S. Stephens. 2010. 'Requirement of NMB0065 for connecting assembly and export of sialic acid capsular polysaccharides in Neisseria meningitidis', *Microbes Infect*, 12: 476-87.

Hulett, M. D., and P. M. Hogarth. 1994. 'Molecular basis of Fc receptor function', *Adv Immunol*, 57: 1-127.

Hung, M. C., and M. Christodoulides. 2013. 'The biology of Neisseria adhesins', *Biology (Basel)*, 2: 1054-109.

Jackson, L. A., A. Schuchat, M. W. Reeves, and J. D. Wenger. 1995. 'Serogroup C meningococcal outbreaks in the United States. An emerging threat', *JAMA*, 273: 383-9.

Jones, C., M. Virji, and P. R. Crocker. 2003. 'Recognition of sialylated meningococcal lipopolysaccharide by siglecs expressed on myeloid cells leads to enhanced bacterial uptake', *Mol Microbiol*, 49: 1213-25.

Kahler, C. M., L. E. Martin, G. C. Shih, M. M. Rahman, R. W. Carlson, and D. S. Stephens. 1998. 'The (alpha2-->8)-linked polysialic acid capsule and lipooligosaccharide structure both contribute to the ability of serogroup B Neisseria meningitidis to resist the bactericidal activity of normal human serum', *Infect Immun*, 66: 5939-47.

Kahler, C. M., and D. S. Stephens. 1998. 'Genetic basis for biosynthesis, structure, and function of meningococcal lipooligosaccharide (endotoxin)', *Crit Rev Microbiol*, 24: 281-334.

Kallstrom, H., M. K. Liszewski, J. P. Atkinson, and A. B. Jonsson. 1997. 'Membrane cofactor protein (MCP or CD46) is a cellular pilus receptor for pathogenic Neisseria', *Mol Microbiol*, 25: 639-47.

Kazmierczak, B. I., K. Mostov, and J. N. Engel. 2001. 'Interaction of bacterial pathogens with polarized epithelium', *Annu Rev Microbiol*, 55: 407-35.

Kiefer, F. 1896. 'Zur differential Diagnose des Erregers der epidemischen Cerebrospinal meningitis und der Gonorrhoea', *Berl Klin Wochenschr*, 33: 628.

Kirchner, M., D. Heuer, and T. F. Meyer. 2005. 'CD46-independent binding of neisserial type IV pili and the major pilus adhesin, PilC, to human epithelial cells', *Infect Immun*, 73: 3072-82.

Lecuyer, H., X. Nassif, and M. Coureuil. 2012. 'Two strikingly different signaling pathways are induced by meningococcal type IV pili on endothelial and epithelial cells', *Infect Immun*, 80: 175-86.

Lewis, L. A., and S. Ram. 2014. 'Meningococcal disease and the complement system', *Virulence*, 5: 98-126.

Litt, D. J., S. Savino, A. Beddek, M. Comanducci, C. Sandiford, J. Stevens, M. Levin, C. Ison, M. Pizza, R. Rappuoli, and J. S. Kroll. 2004. 'Putative vaccine antigens from Neisseria meningitidis recognized by serum antibodies of young children convalescing after meningococcal disease', *J Infect Dis*, 190: 1488-97.

Lucidarme, J., M. Comanducci, J. Findlow, S. J. Gray, E. B. Kaczmarski, M. Guiver, P. J. Vallely, P. Oster, M. Pizza, S. Bambini, A. Muzzi, and R. Borrow. 2010. 'Characterization of fHbp, nhba (gna2132), nadA, porA, and sequence type in group B meningococcal case isolates collected in England and Wales during January 2008 and potential coverage of an investigational group B meningococcal vaccine', *Clin Vaccine Immunol*, 17: 919-29.

Macauley, M. S., P. R. Crocker, and J. C. Paulson. 2014. 'Siglec-mediated regulation of immune cell function in disease', *Nat Rev Immunol*, 14: 653-66.

Maiden, M. C., J. A. Bygraves, E. Feil, G. Morelli, J. E. Russell, R. Urwin, Q. Zhang, J. Zhou, K. Zurth, D. A. Caugant, I. M. Feavers, M. Achtman, and B. G. Spratt. 1998. 'Multilocus sequence typing: a

portable approach to the identification of clones within populations of pathogenic microorganisms', *Proc Natl Acad Sci U S A*, 95: 3140-5.

Malagolini, N., M. Chiricolo, M. Marini, and F. Dall'Olio. 2009. 'Exposure of alpha2,6-sialylated lactosaminic chains marks apoptotic and necrotic death in different cell types', *Glycobiology*, 19: 172-81.

Malito, E., M. Biancucci, A. Faleri, I. Ferlenghi, M. Scarselli, G. Maruggi, P. Lo Surdo, D. Veggi, A. Liguori, L. Santini, I. Bertoldi, R. Petracca, S. Marchi, G. Romagnoli, E. Cartocci, I. Vercellino, S. Savino, G. Spraggon, N. Norais, M. Pizza, R. Rappuoli, V. Masignani, and M. J. Bottomley. 2014. 'Structure of the meningococcal vaccine antigen NadA and epitope mapping of a bactericidal antibody', *Proc Natl Acad Sci U S A*, 111: 17128-33.

Materu, S., H. S. Cox, P. Isaakidis, B. Baruani, T. Ogaro, and D. A. Caugant. 2007. 'Serogroup X in meningococcal disease, Western Kenya', *Emerg Infect Dis*, 13: 944-5.

Medzhitov, R., and C. Janeway, Jr. 2000. 'Innate immunity', *N Engl J Med*, 343: 338-44.

Meesmann, H. M., E. M. Fehr, S. Kierschke, M. Herrmann, R. Bilyy, P. Heyder, N. Blank, S. Krienke, H. M. Lorenz, and M. Schiller. 2010. 'Decrease of sialic acid residues as an eat-me signal on the surface of apoptotic lymphocytes', *J Cell Sci*, 123: 3347-56.

Merz, A. J., C. A. Enns, and M. So. 1999. 'Type IV pili of pathogenic Neisseriae elicit cortical plaque formation in epithelial cells', *Mol Microbiol*, 32: 1316-32.

Merz, A. J., and M. So. 2000. 'Interactions of pathogenic neisseriae with epithelial cell membranes', *Annu Rev Cell Dev Biol*, 16: 423-57.

Metruccio, M. M., E. Pigozzi, D. Roncarati, F. Berlanda Scorza, N. Norais, S. A. Hill, V. Scarlato, and I. Delany. 2009. 'A novel phase variation mechanism in the meningococcus driven by a ligand-responsive repressor and differential spacing of distal promoter elements', *PLoS Pathog*, 5: e1000710.

Montanari, P., G. Bozza, B. Capecchi, E. Caproni, R. Barrile, N. Norais, M. Capitani, M. Sallese, P. Cecchini, L. Ciucchi, Z. Gao, R. Rappuoli, M. Pizza, B. Arico, and M. Merola. 2012. 'Human heat shock protein (Hsp) 90 interferes with Neisseria meningitidis adhesin A (NadA)-mediated adhesion and invasion', *Cell Microbiol*, 14: 368-85.

Nassif, X., J. Lowy, P. Stenberg, P. O'Gaora, A. Ganji, and M. So. 1993. 'Antigenic variation of pilin regulates adhesion of Neisseria meningitidis to human epithelial cells', *Mol Microbiol*, 8: 719-25.

Nikaido, H. 1999. 'Microdermatology: cell surface in the interaction of microbes with the external world', *J Bacteriol*, 181: 4-8.

Nimmerjahn, F., and J. V. Ravetch. 2008. 'Fcgamma receptors as regulators of immune responses', *Nat Rev Immunol*, 8: 34-47.

Okuma, K., Y. Matsuura, H. Tatsuo, Y. Inagaki, M. Nakamura, N. Yamamoto, and Y. Yanagi. 2001. 'Analysis of the molecules involved in human T-cell leukaemia virus type 1 entry by a vesicular stomatitis virus pseudotype bearing its envelope glycoproteins', *J Gen Virol*, 82: 821-30.

Pangburn, M. K., V. P. Ferreira, and C. Cortes. 2008. 'Discrimination between host and pathogens by the complement system', *Vaccine*, 26 Suppl 8: I15-21.

Parkhill, J., M. Achtman, K. D. James, S. D. Bentley, C. Churcher, S. R. Klee, G. Morelli, D. Basham, D. Brown, T. Chillingworth, R. M. Davies, P. Davis, K. Devlin, T. Feltwell, N. Hamlin, S. Holroyd, K. Jagels, S. Leather, S. Moule, K. Mungall, M. A. Quail, M. A. Rajandream, K. M. Rutherford, M. Simmonds, J. Skelton, S. Whitehead, B. G. Spratt, and B. G. Barrell. 2000. 'Complete DNA sequence of a serogroup A strain of Neisseria meningitidis Z2491', *Nature*, 404: 502-6.

Pillai, S., I. A. Netravali, A. Cariappa, and H. Mattoo. 2012. 'Siglecs and immune regulation', *Annu Rev Immunol*, 30: 357-92.

Pincetic, A., S. Bournazos, D. J. DiLillo, J. Maamary, T. T. Wang, R. Dahan, B. M. Fiebiger, and J. V. Ravetch. 2014. 'Type I and type II Fc receptors regulate innate and adaptive immunity', *Nat Immunol*, 15: 707-16.

Pinner, R. W., P. A. Spellman, and D. S. Stephens. 1991. 'Evidence for functionally distinct pili expressed by Neisseria meningitidis', *Infect Immun*, 59: 3169-75.

Pizza, M., V. Scarlato, V. Masignani, M. M. Giuliani, B. Arico, M. Comanducci, G. T. Jennings, L. Baldi, E. Bartolini, B. Capecchi, C. L. Galeotti, E. Luzzi, R. Manetti, E. Marchetti, M. Mora, S. Nuti, G. Ratti, L. Santini, S. Savino, M. Scarselli, E. Storni, P. Zuo, M. Broeker, E. Hundt, B. Knapp, E. Blair, T. Mason, H. Tettelin, D. W. Hood, A. C. Jeffries, N. J. Saunders, D. M. Granoff, J. C. Venter, E. R. Moxon, G. Grandi, and R. Rappuoli. 2000. 'Identification of vaccine candidates against serogroup B meningococcus by whole-genome sequencing', *Science*, 287: 1816-20.

Plant, L., J. Sundqvist, S. Zughaier, L. Lovkvist, D. S. Stephens, and A. B. Jonsson. 2006. 'Lipooligosaccharide structure contributes to multiple steps in the virulence of Neisseria meningitidis', *Infect Immun*, 74: 1360-7.

Proft, T., and E. N. Baker. 2009. 'Pili in Gram-negative and Gram-positive bacteria - structure, assembly and their role in disease', *Cell Mol Life Sci*, 66: 613-35.

Pujol, C., E. Eugene, L. de Saint Martin, and X. Nassif. 1997. 'Interaction of Neisseria meningitidis with a polarized monolayer of epithelial cells', *Infect Immun*, 65: 4836-42.

Rahman, M. M., V. S. Kolli, C. M. Kahler, G. Shih, D. S. Stephens, and R. W. Carlson. 2000. 'The membrane phospholipids of Neisseria meningitidis and Neisseria gonorrhoeae as characterized by fast atom bombardment mass spectrometry', *Microbiology*, 146 (Pt 8): 1901-11.

Rapoport, E. M., Y. B. Sapot'ko, G. V. Pazynina, V. K. Bojenko, and N. V. Bovin. 2005. 'Sialoside-binding macrophage lectins in phagocytosis of apoptotic bodies', *Biochemistry (Mosc)*, 70: 330-8.

Ravetch, J. V., and S. Bolland. 2001. 'IgG Fc receptors', *Annu Rev Immunol*, 19: 275-90.

Razi, N., and A. Varki. 1998. 'Masking and unmasking of the sialic acid-binding lectin activity of CD22 (Siglec-2) on B lymphocytes', *Proc Natl Acad Sci U S A*, 95: 7469-74.

Read, R. C., A. Fox, K. Miller, T. Gray, N. Jones, R. Borrows, D. M. Jones, and R. G. Finch. 1995. 'Experimental infection of human nasal mucosal explants with Neisseria meningitidis', *J Med Microbiol*, 42: 353-61.

Riordan, F. A., O. Marzouk, A. P. Thomson, J. A. Sills, and C. A. Hart. 1996. 'Proinflammatory and anti-inflammatory cytokines in meningococcal disease', *Arch Dis Child*, 75: 453-4.

Rosenstein, N. E., B. A. Perkins, D. S. Stephens, L. Lefkowitz, M. L. Cartter, R. Danila, P. Cieslak, K. A. Shutt, T. Popovic, A. Schuchat, L. H. Harrison, and A. L. Reingold. 1999. 'The changing epidemiology of meningococcal disease in the United States, 1992-1996', *J Infect Dis*, 180: 1894-901.

Rosenstein, N. E., B. A. Perkins, D. S. Stephens, T. Popovic, and J. M. Hughes. 2001. 'Meningococcal disease', *N Engl J Med*, 344: 1378-88.

Schneider, M. C., R. M. Exley, S. Ram, R. B. Sim, and C. M. Tang. 2007. 'Interactions between Neisseria meningitidis and the complement system', *Trends Microbiol*, 15: 233-40.

Schoen, C., J. Blom, H. Claus, A. Schramm-Gluck, P. Brandt, T. Muller, A. Goesmann, B. Joseph, S. Konietzny, O. Kurzai, C. Schmitt, T. Friedrich, B. Linke, U. Vogel, and M. Frosch. 2008. 'Whole-genome comparison of disease and carriage strains provides insights into virulence evolution in Neisseria meningitidis', *Proc Natl Acad Sci U S A*, 105: 3473-8.

Scietti, L., K. Sampieri, I. Pinzuti, E. Bartolini, B. Benucci, A. Liguori, A. F. Haag, P. Lo Surdo, W. Pansegrau, V. Nardi-Dei, L. Santini, S. Arora, X. Leber, S. Rindi, S. Savino, P. Costantino, D. Maione, M. Merola, P. Speziale, M. J. Bottomley, F. Bagnoli, V. Masignani, M. Pizza, M. Scharenberg, J. M. Schlaeppi, M. Nissum, and S. Liberatori. 2016. 'Exploring host-pathogen interactions through genome wide protein microarray analysis', *Sci Rep*, 6: 27996.

Seib, K. L., D. Serruto, F. Oriente, I. Delany, J. Adu-Bobie, D. Veggi, B. Arico, R. Rappuoli, and M. Pizza. 2009. 'Factor H-binding protein is important for meningococcal survival in human whole blood and serum and in the presence of the antimicrobial peptide LL-37', *Infect Immun*, 77: 292-9.

Serruto, D., T. Spadafina, L. Ciucchi, L. A. Lewis, S. Ram, M. Tontini, L. Santini, A. Biolchi, K. L. Seib, M. M. Giuliani, J. J. Donnelly, F. Berti, S. Savino, M. Scarselli, P. Costantino, J. S. Kroll, C. O'Dwyer, J. Qiu, A. G. Plaut, R. Moxon, R. Rappuoli, M. Pizza, and B. Arico. 2010. 'Neisseria meningitidis GNA2132, a heparin-binding protein that induces protective immunity in humans', *Proc Natl Acad Sci U S A*, 107: 3770-5.

Sgroi, D., A. Varki, S. Braesch-Andersen, and I. Stamenkovic. 1993. 'CD22, a B cell-specific immunoglobulin superfamily member, is a sialic acid-binding lectin', *J Biol Chem*, 268: 7011-8.

Slaterus, K. W. 1961. 'Serological typing of meningococci by means of micro-precipitation', *Antonie Van Leeuwenhoek*, 27: 305-15.

Smith, H. R., J. W. Heusel, I. K. Mehta, S. Kim, B. G. Dorner, O. V. Naidenko, K. Iizuka, H. Furukawa, D. L. Beckman, J. T. Pingel, A. A. Scalzo, D. H. Fremont, and W. M. Yokoyama. 2002. 'Recognition of a virus-encoded ligand by a natural killer cell activation receptor', *Proc Natl Acad Sci U S A*, 99: 8826-31.

Snape, M. D., and A. J. Pollard. 2005. 'Meningococcal polysaccharide-protein conjugate vaccines', *Lancet Infect Dis*, 5: 21-30.

Stephens, D. S., B. Greenwood, and P. Brandtzaeg. 2007. 'Epidemic meningitis, meningococcaemia, and Neisseria meningitidis', *Lancet*, 369: 2196-210.

Stephens, D. S., and Z. A. McGee. 1981. 'Attachment of Neisseria meningitidis to human mucosal surfaces: influence of pili and type of receptor cell', *J Infect Dis*, 143: 525-32.

Su, E. L., and M. D. Snape. 2011. 'A combination recombinant protein and outer membrane vesicle vaccine against serogroup B meningococcal disease', *Expert Rev Vaccines*, 10: 575-88.

Sutherland, T. C., P. Quattroni, R. M. Exley, and C. M. Tang. 2010. 'Transcellular passage of Neisseria meningitidis across a polarized respiratory epithelium', *Infect Immun*, 78: 3832-47.

Takai, T. 2002. 'Roles of Fc receptors in autoimmunity', *Nat Rev Immunol*, 2: 580-92.

Tettelin, H., N. J. Saunders, J. Heidelberg, A. C. Jeffries, K. E. Nelson, J. A. Eisen, K. A. Ketchum, D. W. Hood, J. F. Peden, R. J. Dodson, W. C. Nelson, M. L. Gwinn, R. DeBoy, J. D. Peterson, E. K. Hickey, D. H. Haft, S. L. Salzberg, O. White, R. D. Fleischmann, B. A. Dougherty, T. Mason, A. Ciecko, D. S. Parksey, E. Blair, H. Cittone, E. B. Clark, M. D. Cotton, T. R. Utterback, H. Khouri, H. Qin, J. Vamathevan, J. Gill, V. Scarlato, V. Masignani, M. Pizza, G. Grandi, L. Sun, H. O. Smith, C. M. Fraser, E. R. Moxon, R. Rappuoli, and J. C. Venter. 2000. 'Complete genome sequence of Neisseria meningitidis serogroup B strain MC58', *Science*, 287: 1809-15.

Tobiason, D. M., and H. S. Seifert. 2001. 'Inverse relationship between pilus-mediated gonococcal adherence and surface expression of the pilus receptor, CD46', *Microbiology*, 147: 2333-40.

Trivedi, K., C. M. Tang, and R. M. Exley. 2011. 'Mechanisms of meningococcal colonisation', *Trends Microbiol*, 19: 456-63.

Uria, M. J., Q. Zhang, Y. Li, A. Chan, R. M. Exley, B. Gollan, H. Chan, I. Feavers, A. Yarwood, R. Abad, R. Borrow, R. A. Fleck, B. Mulloy, J. A. Vazquez, and C. M. Tang. 2008. 'A generic mechanism in

Neisseria meningitidis for enhanced resistance against bactericidal antibodies', *J Exp Med*, 205: 1423-34.

van de Winkel, J. G., and P. J. Capel. 1993. 'Human IgG Fc receptor heterogeneity: molecular aspects and clinical implications', *Immunol Today*, 14: 215-21.

van Deuren, M., P. Brandtzaeg, and J. W. van der Meer. 2000. 'Update on meningococcal disease with emphasis on pathogenesis and clinical management', *Clin Microbiol Rev*, 13: 144-66, table of contents.

Varki, A. 1997. 'Sialic acids as ligands in recognition phenomena', *FASEB J*, 11: 248-55.

Varki, A., and T. Angata. 2006. 'Siglecs--the major subfamily of I-type lectins', *Glycobiology*, 16: 1R-27R.

Vernikos, G., and D. Medini. 2014. 'Bexsero(R) chronicle', *Pathog Glob Health*, 108: 305-16.

Vieusseux, M. 1805. 'Mémoire sur la maladie qui a régné à Genéve au printemps de 1805', *J Med Clin Pharm*, 11: 163–82.

Virji, M., D. Evans, A. Hadfield, F. Grunert, A. M. Teixeira, and S. M. Watt. 1999. 'Critical determinants of host receptor targeting by Neisseria meningitidis and Neisseria gonorrhoeae: identification of Opa adhesiotopes on the N-domain of CD66 molecules', *Mol Microbiol*, 34: 538-51.

Virji, M., K. Makepeace, D. J. Ferguson, M. Achtman, J. Sarkari, and E. R. Moxon. 1992. 'Expression of the Opc protein correlates with invasion of epithelial and endothelial cells by Neisseria meningitidis', *Mol Microbiol*, 6: 2785-95.

Virji, M., S. M. Watt, S. Barker, K. Makepeace, and R. Doyonnas. 1996. 'The N-domain of the human CD66a adhesion molecule is a target for Opa proteins of Neisseria meningitidis and Neisseria gonorrhoeae', *Mol Microbiol*, 22: 929-39.

Waage, A., P. Brandtzaeg, A. Halstensen, P. Kierulf, and T. Espevik. 1989. 'The complex pattern of cytokines in serum from patients with meningococcal septic shock. Association between interleukin 6, interleukin 1, and fatal outcome', *J Exp Med*, 169: 333-8.

Warmerdam, P. A., N. M. Nabben, S. A. van de Graaf, J. G. van de Winkel, and P. J. Capel. 1993. 'The human low affinity immunoglobulin G Fc receptor IIC gene is a result of an unequal crossover event', *J Biol Chem*, 268: 7346-9.

Warmerdam, P. A., J. G. van de Winkel, E. J. Gosselin, and P. J. Capel. 1990. 'Molecular basis for a polymorphism of human Fc gamma receptor II (CD32)', *J Exp Med*, 172: 19-25.

Weichselbaum, A. 1887. ' Ueber die Aetiologie der akuten Meningitis cerebrospinalis', *Fortschr Med*, 5: 573–83. 620–6.

Weis, D. D., J. R. Engen, and I. J. Kass. 2006. 'Semi-automated data processing of hydrogen exchange mass spectra using HX-Express', *J Am Soc Mass Spectrom*, 17: 1700-3.

Yamanaka, M., Y. Kato, T. Angata, and H. Narimatsu. 2009. 'Deletion polymorphism of SIGLEC14 and its functional implications', *Glycobiology*, 19: 841-6.

Zimmer, S. M., and D. S. Stephens. 2006. 'Serogroup B meningococcal vaccines', *Curr Opin Investig Drugs*, 7: 733-9.